DETAILED CHEMICAL KINETIC MODELING; IS THERE LIFE AFTER GRI-MECH 3.0?

Henry J. Curran

National University of Ireland, Galway, Ireland

Introduction

Throughout the 1990s, the Gas Research Institute (GRI) sponsored a research program that focused on the development of an optimized detailed chemical reaction mechanism capable of the best representation of natural gas flames and ignition[1]. Altogether, there were three releases of the mechanism, GRI-Mech 1.1, 2.11, and GRI-Mech 3.0. This mechanism was optimized for methane and natural gas as fuel in the temperature range 1000—2500 K, in the pressure range 10 Torr to 10 atm, and at equivalence ratios from 0.1 to 5 for premixed systems.

GRI-Mech 3.0 includes all steps thought to be important for describing natural gas ignition and flame propagation (including NO formation and reduction) using rate parameters that reflect current understanding of elementary reaction rate theory. Some aspects of natural gas combustion chemistry are not described by GRI-Mech 3.0. These include soot formation and the chemistry involved in selective non-catalytic reduction of NO. The latter may be important in natural gas reburning at lower temperatures[1].

Even though GRI-Mech does include reactions for species pertinent to natural gas combustion (e.g. ethane, propane, methanol, ethylene and acetylene), GRI recommend that the mechanism should not be used to simulate these pure fuels since the optimization did not include targets relevant to them.

Despite, these drawbacks, the GRI program was very successful, being the first of its kind to make the mechanism readily available over the Internet. Unfortunately, in February 2000 support for this work was discontinued.

The purpose of the current study is to develop a detailed chemical kinetic mechanism in a similar manner to the methodology employed in the GRI study. To date, a mechanism has been developed to reproduce fuel oxidation over a wide range of conditions for hydrogen, carbon monoxide, methane, and associated oxygenated species such as methanol, formaldehyde and acetaldehyde. It is our aim to further extend the study to create a reliable chemical kinetic mechanism to describe the oxidation of fuels up to C_3 hydrocarbon species and larger.

Hydrogen

Since hydrogen is a major component of all hydrocarbon fuels, the hydrogen submechanism is an essential foundation mechanism. To that end we have developed and validated a detailed H_2 mechanism[2] in the temperature range 298 to 2700 K, in the pressure range 0.05 to 20 atm, and at equivalence ratios from 0.2 to 6. To present the full range of data validated is beyond the scope of this paper. Two sets of data are chosen to illustrate the mechanism performance.

Mueller et al[3] studied moderately lean to moderately rich H_2/O_2 mixtures diluted in nitrogen in the temperature range 880—935 K and in the pressure range 0.30—15.7 atm. Figure 1 illustrates experimental (points) versus model-predicted (lines) profiles for hydrogen oxidation at different reactor temperatures. Overall, excellent agreement is observed between the model and experiment.

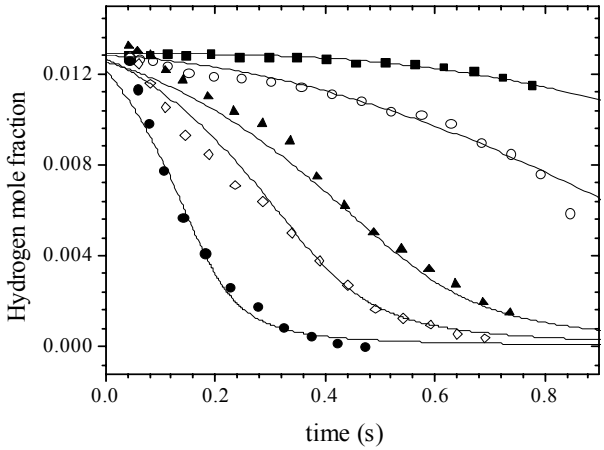

Figure 1. Comparison of experimental flow reactor[3] hydrogen concentration (points) and simulations (lines) versus residence time at 1.3% H_2, 2.2% O_2, P=6.5 atm. ■ 884 K, ○ 889 K, ▲ 906 K, ◊ 914 K, ● 934 K.

Moreover, Tse et al.[4] measured mass burning velocities for H_2/O_2/He mixtures in the equivalence ratio range $0.5 \leq \phi \leq 3.5$, at 1, 5, 10, 15 and 20 atm, at an initial temperature of 298 K. It was reported that flames became increasingly unstable at elevated pressures, and thus true, stretch-free flame speeds became more difficult to measure. For the 10—20 atm data, the oxygen to fuel ratio was reduced to suppress diffusional-thermal instability and delay hydrodynamic instability. Using helium as the diluent also helped minimize instability up to 20 atm by reducing the Lewis number of the flame and retarding the formation of flame cells.

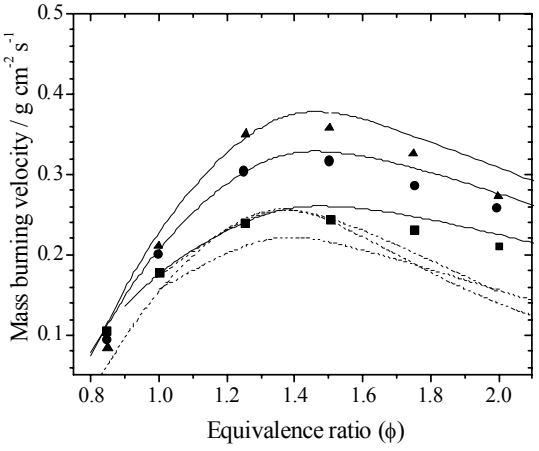

Figure 2. Comparison of experimental[4] (points) versus model predicted (lines) mass burning velocities for H_2/O_2/He flames as a function of equivalence ratio. O2:He = 1:11.5, ■ 10 atm, ○ 15 atm, ▲ 20 atm. Solid lines are current mechanism prediction, dotted lines GRI-Mech 3.0.

[1] Smith, G. P., Golden, D. M., Frenklach, M., Moriarty, N. W., Eiteneer, B., Goldenberg, M., Bowman, T., Hanson, R. K., Song, S., Gardiner, Jr., W. C., Lissianski, V.V., and Qin, Z., http://www.me.berkeley.edu/gri_mech/

[2] O'Conaire, M., Curran, H. J., Simmie, J. M., Pitz, W. J., Westbrook, C. K., submitted to *Intl. J. Chem. Kin*et. Nov. 2003.

[3] Mueller, M. A.; Yetter, R. A.; Dryer, F. L.; *Intl. J. Chem. Kinet.* **31**:113--125 (1999).

[4] Tse, S. D., Zhu, D. L., Law, C.K., *Proc. Combust. Inst.***28**:1793—1800 (2000).

Methane

Methane is the main component of natural gas and being the simplest stable C_1 species, its oxidation mechanism forms the foundation for all other hydrocarbon mechanisms. Several experimental shock tube studies have been simulated over the temperature range $700 \leq T \leq 2400$ K, in the pressure range 0.3—260 atm and in the equivalence ratio range $0.4 \leq \phi \leq 6.0$. Flame speed measurements between 1 and 5 atm in the equivalence ratio range $0.4 \leq \phi \leq 1.8$ have also been simulated. Both of these data sets, particularly those recorded at high pressure, are of particular importance in validating a kinetic mechanism, as internal combustion engines operate at elevated pressures and temperatures and rates of fuel oxidation are critical to efficient system operation.

Petersen et al.[5] conducted an analytical study to supplement extreme shock tube measurements of CH_4/O_2 ignition at elevated pressures (4—26 MPa), high dilution (fuel plus oxidizer ≤ 30%), intermediate temperatures (1040—1500 K), and equivalence ratios as high as 6.

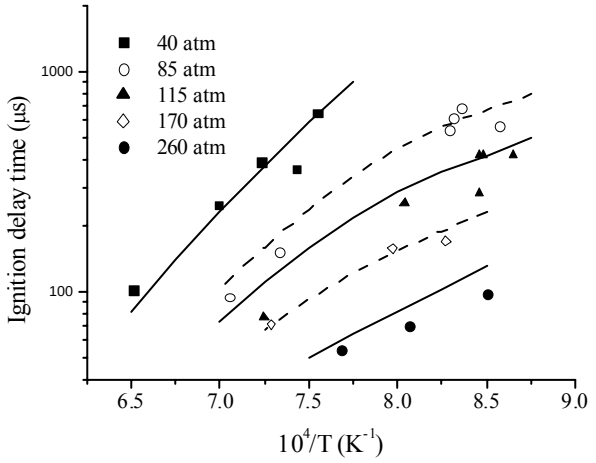

Figure 3. Comparison of experimental[5] (points) versus model predicted (lines) shock tube ignition delay times at 20% CH_4, 13.3% O_2, 66.7% Ar, ϕ = 3.0.

Figure 3 depicts experimental[5] and model predicted ignition delay times as a function of inverse temperature. It is observed that both the experimental data and the mechanism prediction show a decrease in activation energy at temperatures below approximately 1175 K. This is due to intermediate temperature chemistry where the $CH_3O_2 + CH_3 = CH_3O + CH_3O$ reaction is important. The Petersen study highlights the need to include the CH_3O_2 radical species and reactions in a reaction mechanism in order to correctly simulate methane oxidation chemistry under high-pressure, intermediate temperature conditions; conditions which prevail in high pressure natural gas combustors. The CH_3O_2 radical species and reactions are not included in GRI-Mech 3.0.

Methanol

Methanol is a component species in the natural gas submechanism, and has been validated using Princeton flow reactor data[6] in the temperature range 781—1043 K, in the equivalence ratio range $0.051 \leq \phi \leq 2.59$ and at pressures of 1, 2.5, 10, and 15 atm. Figure 4 depicts a comparison of the model-predicted intermediate profiles against the experimental data. Overall, the mechanism is able to reproduce the experimental data quite accurately.

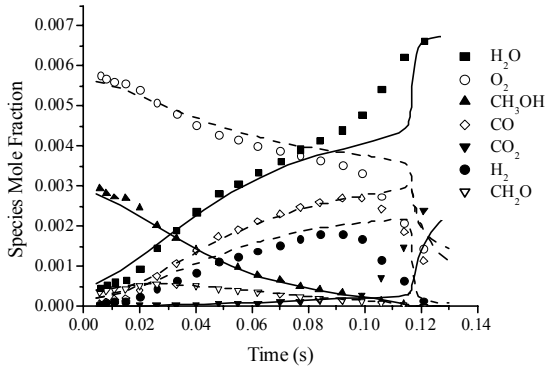

Figure 4. Comparison of experimental[6] (points) versus model predicted (lines) flow reactor species mole fractions for CH_3OH oxidation. 1010 ppm CH_3OH, ϕ = 0.86, P = 1.0 atm, T_i = 1043 K. τ_{offset} = -0.065 s.

In addition, experiments performed by Bowman[7] behind reflected shock waves in the temperature range 1545--2180~K, at reflected shock pressures of 1.5, 3, 3.5 and 4.5 bar and in the equivalence ratio range $0.75 \leq \phi \leq 6.0$, were also used to validate the mechanism. Figure 5 shows the influence of oxygen concentration on ignition delay time. Increasing the oxygen concentration from 1% to 4% results in a marked increase in the reaction rate—a positive shift in ignition delay time occurs as the oxygen content is increased at constant temperature. This trend is also well reproduced by the detailed mechanism.

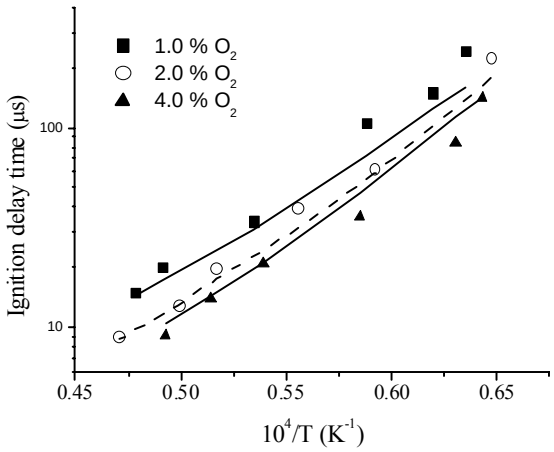

Figure 5. Comparison of experimental[7] (points) versus model predicted (lines) shock tube ignition delay times. 1.0% CH_3OH in Ar, P ≈ 3.0 bar.

[5] Petersen, E.L., Davidson, D.F., Hanson, R.K. *J. Prop. Power* (1999) **15**:82—91.

[6] Held,T.J., Dryer, F. L., *Int. J. Chem. Kinet.* **30**: 805—830 (1998).

[7] Bowman, C. T., *Combust. Flame* **25**: 343—354 (1975).

Efficient lumping technique for the automatic generation of n-heptane and iso-octane oxidation mechanism

S. S. Ahmed, G. Moréac, T. Zeuch and F. Mauss

Division of Combustion Physics, Lund University of Technology, P.O. Box 118

SE-22100 LUND, Sweden

Introduction

The future demands of engine development are to have highly efficient engines with almost no emissions. It is a global trend for the automotive industry to look forward in this area, mainly due to fact that the demands of energy consumption are increasing more and more and almost 90% of this came from the fossil fuels, which are becoming obsolete from their natural resources. New sources of energy and highly fuel-efficient existing conventional engines with low emissions are the demands of future. Low fuel consumption and increased efficiency is desirable both due to considerations of pollutant emissions (CO_2 production is contributing to the greenhouse effect) and economy (cost effectiveness). This all leads to the continuation in developing a better understanding of the combustion process, specially the oxidation process of large hydrocarbon fuels such as n-heptane and iso-octane over a wide range of engine operating conditions. These primary reference fuels (PRF) oxidation mechanisms are quite complex and large in terms of species and reactions such as 1033 species and 8476 reactions for example. An urgent need is there to reduce the size and complexity of the mechanism in order to implement this mechanism in the three dimensional computational fluid dynamics codes which are used to study different engine parameters and combustion processes and yet having the same reliability and results as the detailed ones. This could be done by generating a semi-detailed mechanism first and then its simplification by lumping process and further on by necessity analysis. Some previous works have been done on lumping procedures by Ranzi et al.[1] and Fournet et al.[2]

Mechanism

This work has been done to generate a semi-detailed mechanism for n-heptane and iso-octane oxidation mixture. The construction of the mechanism is systematically in accordance with Curran et al.[3] using the reaction classes and rate constants suggested by the authors as a reference. Intermediate reactions, considered of low importance for the timing of ignition, are simplified substantially by optimizing it. The mechanism contains the pathways involve the fuel species, iso-octane and n-heptane, and also the lower alkene sub-mechanisms of C_7, C_6 and C_5 species (where the C_4 and below is the part of the base mechanism[4]). The detailed mechanism contains 241 species and 1905 reactions. Lumping procedure has been applied on n-heptane mechanism which reduces the mechanism size to 223 species and 1869 reactions including iso-octane sub-mechanism. In the present mechanism all the reaction paths which are known to be pertinent from both high and low temperatures are included in order to cover the full range of temperature and pressure. To reduce the mechanism size in order to make it faster and fewer complexes, its reduction has been done first by lumping technique and further on by necessity analysis. Lumping is the procedure of substituting different species of similar molecular structure into one species called "lumped species". The new lumped species is related not only to the original species concentrations but also on the important parameters. Necessity analysis is the process to calculate the contribution of reaction steps to the production rate of necessary species and hence eliminate the non-important reactions. The mechanism is used in study the effect of elevated pressure and temperature of the n-heptane and iso-octane oxidation mixture in engine for different operating conditions.

The calculations have been performed for the 1st and 2nd ignition delay times using the constant volume flow model and then also Homogenous Charge Compression Ignition (HCCI) engine model in- house ignition code,[5] for both detailed and lumped mechanisms.

Lumping Procedure. The species of similar molecular structure and position of H-abstraction from secondary sites are lumped together. This is because the rate parameters and thermodynamic data vary slightly between different structures of the similar ring size species. At first four species of similar ring size 5, are lumped together to form new lumped species. The rate constants were calculated for each lumped species reactions individually for both forward and backward reactions. The concentration of new lumped species is then balanced by dividing the backward rate constants as shown in equation (1) for each individual reaction with the number of species lumped together which is four in this case. Similar approach has been made to lump the other species of the same ring sizes and molecular structure and further on in other reaction types of the mechanism as well. **Figure 1** is showing the concentration profiles of the lumped species against the four added species. **Figure 2** is showing the product species before and after lumping.

$$\frac{d[5r-HEOOH]}{dt} = \sum\left([2-C_7H_{15}O_2]+2\times[3-C_7H_{15}O_2]\right)k_{1f} + [4-C_7H_{15}O_2]k_{2f} - \left([5r-HEOOH]k^*_{1b}/4 + [5r-HEOOH]k^*_{2b}/4\right) \quad \rightarrow eq(1)$$

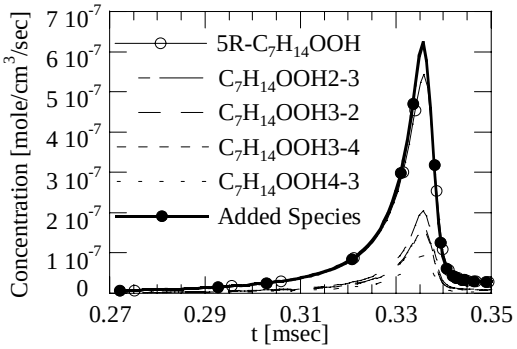

Figure 1 Concentration of new lumped species 5R-C7H14OOH is plotted by shifting the ignition delay time 0.034 sec to have better view against the added concentration of four species at initial pressure set to 40 bar, phi is 1.0 and initial temperature is 800 K.

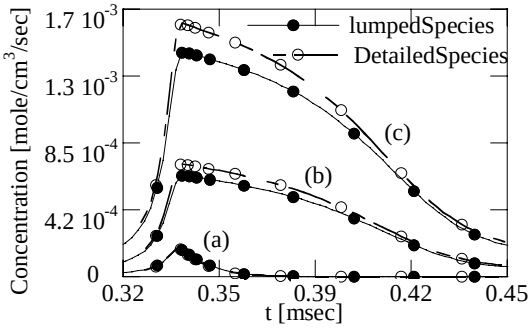

Figure 2 Concentration profile of a product species N-$C_4CH_9COCH_2$ (a), N-C_4H_9CHO (b) and N-C_3H_7CHO (c) before and after lumping at initial temperature of 800 K.

Validation

The lumped reaction model and the semi-detailed n-heptane and iso-octane mixture oxidation mechanism have been first validated against the shock tube experimental data from Fieweger et al.[6]and Ciezki et al.[7] Calculated and experimental ignition delay times have been compared at low and high temperatures. In the negative temperature regime, where the ignition occurs as a two-stage process, we compare in addition the timing of the occurrence of the low temperature oxidation. The mechanism was validated for fuel lean and rich conditions, a range of octane numbers and pressures from 13 bar to 40 bar. The initial temperature range from 700 to 1300 K is set for all the cases. Fuel-air equivalence ratio (ϕ) is equal to 0.5, 1.0 and 2.0, and Research Octane Number (RON) is 0, 20, 40, 60, 80, and 100. In general, there is a good agreement between the semi-detailed mechanism calculations and experimental ignition delay timings and then lump mechanism calculation fits well with the detailed one. Result for RON 0, ϕ=1 and P=40 atm is shown in the **Figure 3** as an example. This verifies the efficiency of the lumping technique.

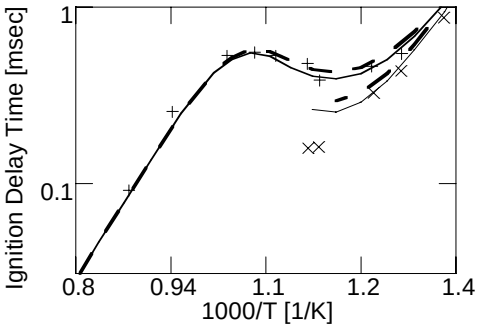

Figure 3 Ignition delay time for n-heptane at P=40 atm and ϕ=1.0. Experimental data (symbols). Calculated data (lines). 1st Ignition (×), 2nd Ignition (+). Detailed mechanism straight line. Lumped mechanism dashed lines.

The mechanism has been further validated against HCCI engine experiments using the same computer program[5], which was used for the constant volume calculations. For these calculations a zero-dimensional engine model was applied. The model compresses the gas to auto-ignition, using temperature and pressure at a certain crank angle position obtained from engine experiments as initial conditions.

The calculated data from the ignition code is validated against the experimental data, which was provided by Christensen et al.[8] The engine experiments were performed in a Volvo TD100 engine modified to run on one cylinder and with a secondary piston in the cylinder head giving the opportunity to vary the compression ratio. Iso-octane and n-heptane were mixed to achieve various octane numbers. The fuel was supplied via port injection. The charge temperature was varied between 30 and 130 °C. The compression ratio was adjusted between 21.4 and 10.8 in order to have an optimal point of ignition in each case. The validation of the detailed mechanism was performed for different cases of RON. Air-fuel equivalence ratio was set to 3.0 for all the cases and the engine speed were 1000 rpm. The initial pressure at inlet valve closing (IVC) for the calculations was consequently set to the measured cylinder pressure minus 0.1 bar, the wall temperature was chosen to be 490 K and EGR (5% residual gas) for all the cases. The semi-detailed mechanism calculation and the measured cylinder pressure for the RON 83 case is shown in **Figure 4**, at initial temperature of 330 K (at IVC), there is a good agreement between the detailed mechanism and the experiments; it can be seen in cylinder pressure trace and then it is a good agreement between detailed and lumped mechanism calculations. Ignition occurs at the same Crack Angle Degree (CAD) as experiment. The maximum pressure from the calculation is a bit high as compared to the experiment due to the assumption of homogeneity of the model[5], but altogether it follows the experimental data quite well especially in the low temperature region.

Conclusions

A semi-detailed reaction mechanism of n-heptane and iso-octane oxidation with special focus on optimizing it to the ignition delay timings of the shock tube experimental data from Fieweger et al.[6] and HCCI engine conditions has been presented. The mechanism was constructed using a reaction type concept as used for the automatic generation of mechanism. The size of the mechanism is limited by making use of lumping. This is very simple and straight forward approach which works very efficiently to generate automatically lumped mechanism, which has the same, performance as the detailed mechanism. The developed mechanism has been validated against the experimental data from shock tube and HCCI engine experiments. The ignition delay is well predicted for the shock tube experiments, at low and high temperatures and at low and high octane numbers. In the negative temperature regime the occurrence of low temperature reactions is well predicted. For the HCCI engine experiments there has been a significantly good agreement between model predictions and experimental data and in all the cases there is a good agreement between the lumped and detailed mechanism calculations. This work provides a detailed kinetic oxidation mechanism for mixture of n-heptane and iso-octane containing a reasonable low number of species and reactions, which provides a good base for further reduction of the mechanism, using sensitivity, reaction flow, lumping and necessity analysis.

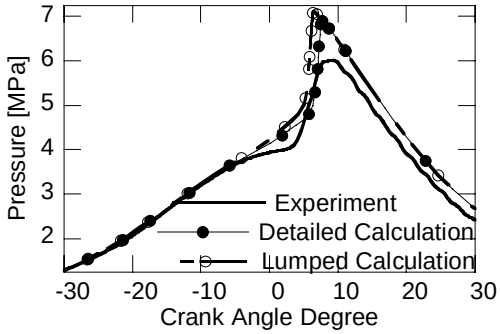

Figure 4 Cylinder pressure for RON83 at initial temperature of 359K

References

(1) Ranzi, E., Faravello, T., Gaffuri, P., and Sogaro, A. *Combustion and Flame*, **1995**, *102*: p. 179-192.

(2) Fournet, R., Warth, V., Glaude, P.A., Côme, G.M., Battin-LeClerc, F., and Scacchi, G. *International Journal of Chemical Kinetics.* **2000,** *32 (1)*: p. 36-51.

(3) Curran, H.J., Gaffuri, P., Pitz, W.J., and Westbrook, C.K. *Combustion and Flame*, **1998**, *114*: p. 149-177.

(4) Zeuch, T., Thesis Dissertation, Universität Göttingen, Germany, **2003.**

(5) Amnéus, P., Thesis Dissertation. Division of Combustion Physics Lund Institute of Technology, Sweden, **2002.**

(6) Fieweger, K., Blumenthal, R. and Adomeit, G. *Combustion and Flame*, **1997**, *109*: p. 599-619.

(7) Ciezki, K. and Adomeit, G. *Combustion and Flame*, **1993**, *93*: p. 421-433.

(8) Christensen, M., Hultqvist, A. and Johansson, B. **1999,** *SAE* 1999-01-3679.

AUTOMATIC OPTIMIZATION OF DETAILED KINETIC MECHANISM FOR HCCI-ENGINE SIMULATION

Bellanca[1], R., Mauss[1], F. and Wang[2], H.

1) Division of Combustion Physics, Lund University, 2) Mechanical Engineering, University of Delaware

Introduction

In recent years detailed kinetic models have been developed and validated for both auto ignition and laminar combustion processes. The range of validity of these models is limited by the range of physical parameters covered by the available experimental data. At high pressure, for example, shock tube data for the validation of ignition delay times are available for the investigated fuels with air-fuel equivalence ratios smaller than 2.0. Homogeneous Charge Compression Ignition (HCCI) engines are known to be operated with fuel-air equivalence ratios greater than 2.0, or with high rates of Exhaust Gas Recirculation (EGR). These conditions are not within the range of validity of the available kinetic models, and a re-optimization of the models is necessary.

Optimization

The optimization of reaction models has been automated in the past. The development of the GRI-Mech has been done using a semi-automated procedure[1], based on sensitivity analysis for the selection of reactions suitable for optimization and response surfaces method for the search of the best reaction coefficients. In this work a similar procedure has been applied to optimize a gasoline fuel reference mechanism consisting of 1905 reactions and 241 species as developed by Zeuch[2] for the base mechanism (C1-C4) and Ahmed, Blurock and Mauss[3] for larger hydrocarbons following the rules specified by Curran and Westbrook for automatic mechanism generation[4]. This model was used to simulate autoignition in a HCCI engine, using a homogeneous reactor model.

The optimization technique is based on the parameterization of model responses in terms of model parameters by simple algebraic expressions. The ignition delay time, deduced from the pressure profile as the crank angle corresponding to the maximum gradient, was used as optimization target (response). The pre-exponential factors in the reaction's rate Arrhenius expression were chosen as optimization parameters. Second order polynomial expressions were used to map the solution. The interpolation polynomial coefficients were obtained by computer experiments arranged in a fractional factorial design.

Simulations. The HCCI-process was modeled as a compressed homogeneous reactor[5]. The EGR was modeled, by running five consecutive engine cycles from Inlet Valve Closing (IVC) at -167 Crank Angle Degree (CAD) to Exhaust Valve Opening (EVO) at 167 CAD. The calculated gas composition at EVO was mixed with the fresh gas composition at IVC. Computations have been carried out on a PC with CPU time requirements of few minutes for each simulation and few hours for a complete optimization process. The entire procedure was performed inside a graphical user interface environment[6]. A sensitivity analysis of the temperature on the Arrhenius coefficients of all reactions included in the kinetic model was performed. The frequency factors of the most sensitive reactions were used as optimization parameters. The selection procedure is visualized in Figure 1. The colors in the graphic indicate the sensitivity level (red, yellow, green, blue, and shades of blue) of the reactions for the cases considered in the calculation.

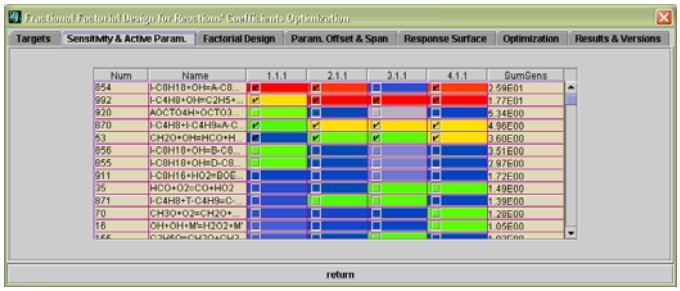

Figure 1 Screen Snapshot of the Optimization Section of the Graphical User Interface. Selection of Active Optimization Parameters for Each Target.

Experiments.

The data, needed for the optimization procedure, particularly the ignition delay times, were obtained from experiments conducted at Lund Institute of Technology on a modified Volvo TD100 engine with variable compression ratio and port injection mixes of iso-octane/n-heptane7. A fuel ratio of 0.333 and inlet pressure of 0.9 bars were used. As showed in

Table **1**, a combination of three different inlet temperatures and fuel mixtures was considered, for a total of nine cases. In Table 2 the engines parameters are reported.

Table 1 Simulations Initial Conditions for: Inlet Temperature, Fuel Mixture and Compression Ratio

N	T[K]	Fuel (I-C8H18/N-C7H16) %	CR
1	330	100 - 0	21.45
2	359	100 - 0	19.94
3	407	100 - 0	17.04
4	330	83 - 17	16.68
5	359	83 - 17	15.70
6	407	83 - 17	14.86
7	330	51 - 49	13.24
8	359	51 - 49	12.17
9	407	51 - 49	10.84

Table 2 Engine Parameters

Displaced Volume	1.602e-3 [m3]
Bore	0.12065 [m]
Stroke	0.14 [m]
Rod	0.26 [m]
Speed	1000 [m/s]
Wall Temperature	490 [K]
Start / End DCA	-167 / 167
EGR_Amont	0.05 [%]
EGR Cycles	5

Results and Discussion

In the framework of this preprint we selected four cases to demonstrate the functionality of the optimization tool (cases 1,2,3 and 6). This gave a reduced system of four targets to be optimized with respect to four reaction rate parameters. The corresponding reactions, their original coefficient and the optimization span, are reported in **Table 3**.

Table 3 Optimized Reactions

N	Name	Original	Optimized	Δ
53	CH2O+OH=HCO+H2O	3.4E9	2.0E9	2
854	I-C8H18+OH=A-C8H17+H2O	1.5E10	1.25E10	2
992	I-C4H8+OH=C2H5+CH3CHO	1.0E14	5.0E13	2
870	I-C4H8+I-C4H9=A-C8H17	8.5E10	9.9E10	2

The pressure profiles for the experimental data compared with those obtained with both the original and optimized model are shown in figure 1-4. For all cases the agreement of the ignition timing with the experiment got improved after the optimization. Shortcomings caused by the simple reactor model, such as to high pressure after ignition, or to short combustion duration can not be improved. The optimization of case 3 is not as good as for the other cases. However, for this case other sensitive reactions (level green in Figure 1) were found. Further optimization runs are prepared that will include these reactions as optimization parameter.

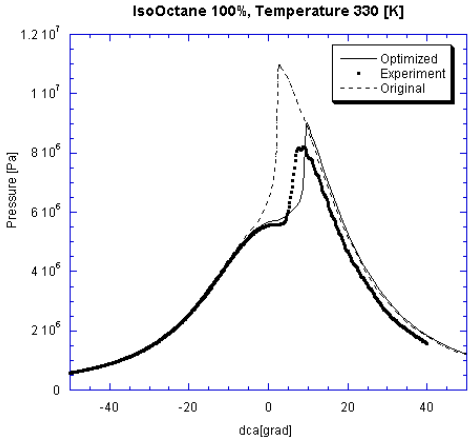

Figure 2 Pressure Profile vs. Crank Angle Degree for case 1.

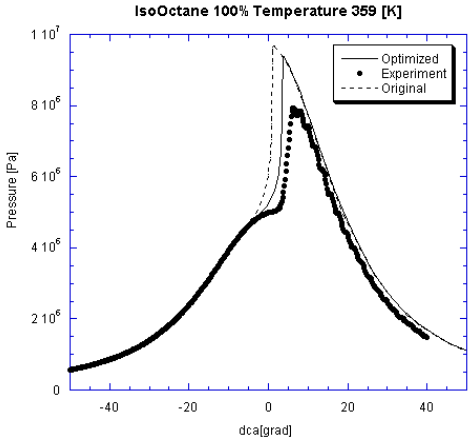

Figure 3 Pressure Profile vs. Crank Angle Degree for case 2.

Conclusion

An automatic optimization procedure, based on the solution mapping method, was used to optimize a detailed reaction mechanism for mixtures of n-heptane and iso-octane fuels at varying octane numbers under fuel lean conditions. This was done for HCCI-engine cases, by using a simple compressed reactor model. The optimization target, the maximum pressure rise, was taken from engine experiments. It was shown, that the agreement of mechanism and experiment can be significantly improved, while the effort needed for the procedure is reasonable. Further calculations will be performed, including more engine cases and additional optimization parameters.

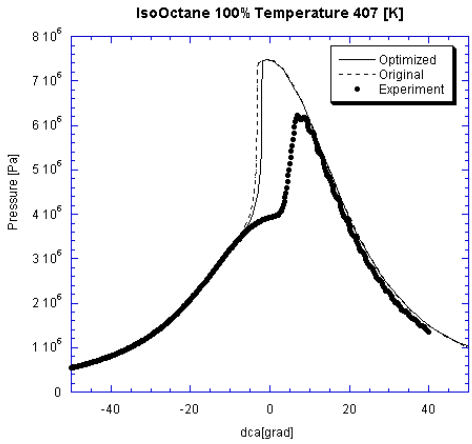

Figure 4 Pressure Profile vs. Crank Angle Degree for case 3.

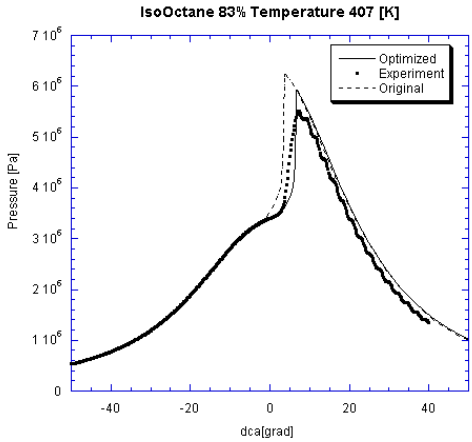

Figure 5 Pressure Profile vs. Crank Angle Degree for case 4.

References

[1] Frenklach, M.; Hai, W.; and Rabinowitz M.J. – Prog. Energy Combustion. Sci., 1992, 18, pp 47-73

[2] T. Zeuch, Thesis Dissertation, Universität Göttingen, Germany, 2003

[3] Ahmed, S.S., Blurock, E., and Mauss, F. - Proceedings of Scandinavian-Nordic and Italian Section of the Combustion Institute. 2003, 3.4, 1-4.

[4] Curran, H.J., Gaffuri, P., Pitz, W.J., and Westbrook, C.K. A comprehensive modelling study of n-heptane oxidation. Combustion and Flame, 1998, 114: p. 149-177

[5] Mauss F.; and Bellanca R. In "Ignition Code for the calculation of instationary combustion processes" Internal Report, Division of Combustion Physics, Lund University.

[6] Bellanca R. In "http:// forbrf.lth.se /chem. /blueBellMouseNew /intro.htm"

[7] Christensen M., Hultqvist A. and Johansson B. - SAE 1999, 01, 3679

THE DEVELOPMENT AND USE OF RATE-CONSTRAINED CHEMICAL EQUILBRIUM WITH HCCI COMBUSTION MODELING

Scott B. Fiveland
Engine Research
Caterpillar, Inc.

Chris Rutland
Engine Research Center, University of Wisconsin-Madison

Caterpillar, Inc.
Technical Center – F
P.O. Box 1875
Peoria, Il 61656-1875

Introduction

Homogeneous Charge Compression Ignition (HCCI) engines are essentially a combination of conventional spark ignited (SI) and compression ignited (CI) engines. As in a conventional SI engine, a homogeneous air-fuel mixture is achieved either in the inlet system or early during the compression stroke (direct injection). As in the diesel combustion process, ignition is achieved by compressing the mixture until it auto-ignites. Thus, the energy release event is dominated by the kinetic timescales. Accurate modeling requires the coupling of a detailed chemical kinetic description to the proper fluid-dynamic resolution (1).

The evolution of chemical reaction can, in principle, be solved accurately if a chemical mechanism for the conversion of fuel to products is available. The solution of practical chemical kinetic systems requires numerical methodologies that resolve the chemical process, down to the highest frequency mode, while maintaining numerical stability. As a result, the numerical solution of chemical kinetics problems is very computationally expensive because the process is occurring on multiple timescales, as some radical species are being formed and depleted rapidly while other species exhibit a slow evolution (such as H_2O or CO_2). The presence of a range of timescales is known as stiffness (13). Stiff kinetic systems require a large number of time-steps, thus making the numerical solution time-consuming. Current computing capability makes it possible to simulate homogeneous chemically reacting systems, but detailed chemical kinetic calculations coupled with computational fluid dynamic (CFD) simulations of chemically reacting flows are still unrealistic as the basis for a parametric simulation tool (1).

The solution of the kinetic system, even when using the most efficient solver, may be too computationally expensive. Therefore, the modeler must sacrifice some details within the kinetic scheme to improve the solution speed. Many techniques have been developed to generate reduced mechanisms such as quasi-steady state analysis (QSSA) (9), intrinsic low dimensional manifolds (ILDM) (10), partial equilibrium assumption (PEA), (8), computational singular perturbation (CSP) (5), sensitivity analysis (17), integral and local reaction flow analysis (17), time-scale analysis (15), and computer augmented reduced mechanism (CARM), (16). The application of these tools sets out to eliminate both species and reactions. The disadvantage of these reduction approaches is that the reduced mechanism is valid only for a very limited range of thermodynamic conditions. If the combustor conditions, such as pressure, temperature, or equivalence ratio (i.e. load range) increase or decrease outside the applicable range, the reduction procedure must be repeated and a new reduced equation set developed.

Several techniques exist to speed the solution of the chemistry while not reducing the chemical kinetic mechanism information, and hence the accuracy of the system. The common ones are rate-constrained chemical equilibrium (RCCE) and *in-situ* adaptive tabulation (ISAT) (7). The RCCE method was first proposed by Keck (4) and extensively developed by Metghalchi and co-workers (3). This work focuses on the extension of the RCCE method to model HCCI ignition events with the introduction of automatic constraint generation.

Rate Constrained Chemical Equilibrium – Overview

The general basis of the RCCE idea is that the chemical composition is constrained from equilibrium, at any time, due to slowly evolving constraints that are imposed in the system. The system evolves in time through a series of quasi-equilibrium states. The physical premise for the idea is that only equations describing the slowly evolving constraints need to be integrated. Much of the discussion in this section follows Hamiroune *et al.* (3). The RCCE approach is based on the following stated assumptions:

1. A complex chemically reacting system can be described by a relatively small number of degrees of freedom.
2. These degrees of freedom are constraints imposed on the system by slowly evolving reactions.
3. Other reactions are fast enough that they can equilibrate the system subject to the constraints imposed by the slow reactions.
4. The system thus progresses to chemical equilibrium through a series of quasi-equilibrium states.

RCCE Mathematical Formulation

The time-dependant constraints are a linear combination of species given by:

$$C_j = \sum_{i=1}^{ns} a_{ij} N_i , \tag{1}$$

where C_j is the molar concentration of constraint j and a_{ij} the number of moles of species i in constraint j. Once the differentiated form of equation (1) has been integrated, the constrained equilibrium composition may be determined with the method of element potentials using Lagrange undetermined multipliers as outlined by Keck (4) and Reynolds (13). We refer to this method as RCCE-A. Using this method, once the Lagrange multipliers are determined, the species compositions are found by:

$$N_i = Q_i \exp\left(-\sum_{j=1}^{nc} a_{ij}\gamma_j \right),\ Q_i = \frac{p_0 V}{RT}\exp\left(-\mu_i\right) \tag{2}$$

where γ_j is the undetermined multiplier conjugate to constraint j and μ_i is the Gibbs free energy of species i. Keck (4) points out that the computation of the constrained equilibrium at each time-step may be expensive because of the iterative procedure involved in determining the Lagrange multipliers. He presents an alternative method of solving for the constrained equilibrium composition. We refer to this alternative method as RCCE-B and discuss it below. All RCCE calculations in this work use the RCCE-B method (11).
Rather than directly integrate the constraints and then solve equation (2) for the species, rate equations for the Lagrange multipliers may be

derived with some manipulations. The equations for the rate of change of the Lagrange multipliers are given as follows:

$$\sum_{n=1}^{nc} C_{jn}\dot{\gamma}_n - C_{jT}\frac{\dot{T}}{T} - C_{jV}\frac{\dot{V}}{V} + \sum_{i=1}^{ns} a_{ij}\dot{\omega}_i = 0\,, \quad (3)$$

where $C_{jn} = \sum_{i=1}^{ns} a_{ij}a_{in}N_i$, $C_{jT} = \sum_{i=1}^{ns} a_{ij}\frac{E_i}{RT}N_i$, and

$$C_{jV} = \sum_{i=1}^{ns} a_{ij}N_i\,.$$

In the case where the temperature is not constant, an additional equation for the temperature (or energy) must be solved and this is given as:

$$\sum_{i=1}^{ns}\sum_{n=1}^{nc} E_i a_{in}N_i\dot{\gamma}_n - \sum_{i=1}^{ns} C_{iE}N_i\frac{\dot{T}}{T} - \sum_{i=1}^{ns} E_i N_i\frac{\dot{V}}{V} + \dot{E} = 0\,, \quad (4)$$

where $C_{iE} = \left(c_{v,i}T + \frac{E_i^2}{RT}\right)$ and E is the internal energy of the system. The rate of energy change in the system is described using the energy equation with the appropriate source and sink terms for work and heat transfer (11). Once the values of the Lagrange multipliers are determined by numerically integrating equations (3) and (4), the constrained equilibrium composition may be determined without any iteration. The equations are integrated using an implicit stiff ODE solver based on a backward differencing formulae (BDF) method (2).

Constraints - Overview

The constraints that have been used in works using the RCCE method were based on constraints generated through physical intuition (3,6). The most common constraints are conservation of elements. In this study, the system has four elements – C, H, O, and N and these are four "fixed" constraints, i.e. they do not depend on time. Time-dependant constraints include constraints on:

1. Total number of moles due to slow three body reactions,
2. Moles of ions due to slow radical reactions,
3. Moles of CO_2 due to slow oxidation of CO ,
4. Moles of fuel,
5. Moles of fuel radical,
6. Moles of oxygen, and
7. Moles of formaldehyde radical.

Results & Discussion

In understanding the RCCE method, it is instructive to look at the values of the constraint potentials as the constraints evolve over time. Figure 1 shows the constraint potentials for two "fixed" constraints, elemental nitrogen and elemental hydrogen, and two time-dependant constraints, total moles and free valences. The potentials for the time-dependant constraints reach a value of 0 as the system reaches equilibrium while the potentials for the fixed constraints reach their equilibrium values. This is because, at equilibrium, the system is constrained only by the elemental constraints and thus the potentials for the other constraints must be zero. It may be useful to note that an elemental constraint potential represents the contribution of the element to the chemical potential of a species that contains that element.

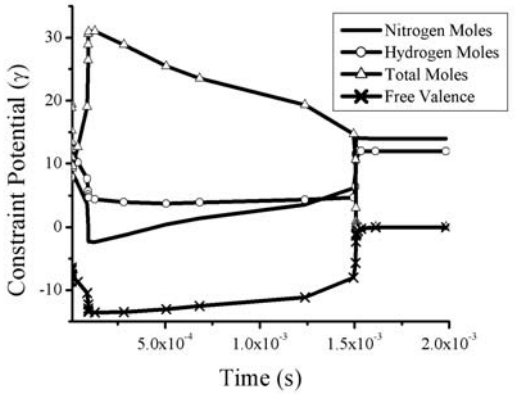

Figure 1. Evolution of Constraint Potentials vs. time

The constraints used in this study were based on constraints used by Gao and Methghalchi (6). In the work by Rao et al.(11), the RCCE method was compared to the detailed kinetic integration for lean and rich conditions through a range of gas temperatures.

Comparison of RCCE with Experiments

The comparison of the RCCE method with HCCI experiments for the 2% mass fraction burned point obtained in the Volvo TD-100 is shown in figure 2 for a methane-air blend. The reader is referred to Rao et. al. for a review of the experimental setup. This fuel study was a subset of a two-component fuel study (11) For this particular case study, the engine was operated under naturally aspirated conditions at an equivalence ratio of 0.3, an intake manifold temperature that ranged from 175C to 162C, and an engine speed of 1000 RPM. The compression ratio in the engine tests was reported at 19.8. It is shown in the figure that the RCCE method does a reasonably good job of predicting the trend with decreasing manifold temperature. For example, at a manifold temperature 171C the model exhibits a 2 CA-deg error when predicting the 2% mass fraction burned point. The RCCE prediction is closer to the experimental observation if the standard deviation (shown as error bars) in the experimental quantities is considered. It is noted that observed error could be a result of inaccuracies within the HCCI thermal description, the GRI kinetics mechanism or the assumed constraint matrix applied to the RCCE method.

Automatic Constraint Generation

The use of this method for larger chain hydrocarbon molecules will depend on the ability to efficiently develop the constraint matrix (3, 18). Yousefian has presented an algorithm for the selection of constraints. The algorithm is based on using equilibrium relations for fast reactions, since the RCCE method implicitly assumes that all fast reactions are in equilibrium. Recently, work by Rao et al. has developed/demonstrated an automatic constraint methodology for use with a hydrogen-air combustion scenario (12). Specifically, their work used a novel partial equilibrium criterion with the constraint generation scheme proposed by Yousefian (18).

In order to validate the RCCE solution, induction times for H_2-O_2-Ar mixtures were computed using the RCCE method against shock tube experiments (12). The experiment was performed at a pressure of 5 atm. with a composition comprising 8 mole percent H2 and two mole percent O2 in Ar. The initial temperature was varied from 964 K to 1075 K. The computations were carried out assuming constant volume and adiabatic combustion. An example of a

comparison between the detailed solution and the RCCE method for a hydrogen-air mixture is shown in figure 3..

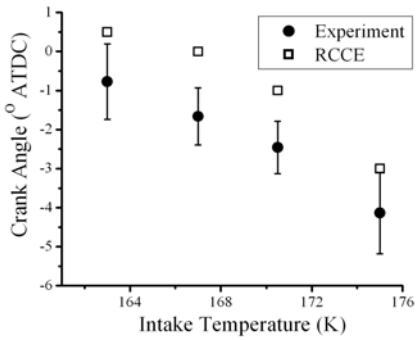

Figure 2: Methane-air simulation vs. experimental 2% mass burned point. 1000rpm, equivalence ratio (0.3), an intake pressure of 1 bar,

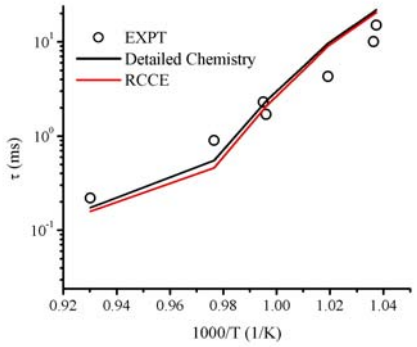

Figure 3: Comparison of computed and measured induction times for H_2-O_2-Ar mixtures

Conclusions

The RCCE method has been successfully applied to describe the time-evolution of hydrogen and methane-air combustion in constant and variable volume environments. Good agreement between RCCE and detailed chemistry calculations is obtained for a variety of initial conditions in various environments. Temperature and species profiles are predicted well by the RCCE method, as are induction times and ignition delay times for methane-air mixtures. CPU time usage is reduced for RCCE calculations as compared to calculations utilizing detailed chemical kinetics. There is potential for further reduction in computational cost by improving the numerical characteristics of the system and improvement in the accuracy of the method through improved selection of constraints. The RCCE method is used to simulate HCCI combustion of methane in a Volvo engine and good agreement against experimental data for burn durations is obtained. More work is needed to developed a robust automatic constraint generation method.

References

(1) Assanis, D.N., Lavoie, G.A., and Fiveland, S.B., Chapter 6, Overview of HCCI Modeling Approaches, *Homogeneous Charge Compression Ignition (HCCI) Engines Key Research and Development Issues,* SAE 2003.

1. (2) Brown, P. N., Hindmarsh, A. C. and L. R. Petzold (1994), *Using Krylov methods in the solution of large-scale differential-algebraic systems*, SIAM Journal of Scientific Computing, **15**: 1467-1488
2. (3) Hamiroune D, Bishnu P., Metghalchi M., and Keck J.C. (1998), "Rate-controlled Constrained-Equilibrium method using constraint potentials", Combustion Theory and Modeling, **2**:81-94
3. (4) Keck J.C. and Gillespie D. (1971), *Combustion and Flame*, **17**:237
4. (5) Lam S.H. and Goussis D. A. (1994), "The CSP Method of Simplifying Kinetics", *International Journal of Chemical Kinetics,* 26:461-486
5. (6) Gao Y. and Methghalchi M. (2002), Personal Communication
6. (7) Maas U.A. and Pope S.B. (1992), "Simplifying Chemical Kinetics: Intrinsic Low-Dimensional Manifolds in Composition Space", *Combustion and Flame*, **88**:239-264.
7. (8) Mott, David (1999), "New Quasi-Steady-State and Partial Equilibrium Methods for Integrating Chemically Reacting Systems", *Ph.D. Thesis*, Department of Aerospace Engineering and Scientific Computing, University of Michigan
8. (9) Peters, N. (1985), *Lecture Notes in Physics* Springer, Berlin, pg. 90–241.
9. (10) Pope S.B. (1997), "Computationally Efficient Implementation of Combustion Chemistry using In Situ Adaptive Tabulation," Combustion Theory and Modeling, **1**:41-63.
10. (11) Rao, S., Rutland C.J., and Fiveland S.B. (2003) "A Computationally Efficient Method for the Solution of Methane-air Chemical Kinetics with Application to HCCI Combustion," Submitted to SAE World Congress, 2003.
11. (12) Rao, S., Rutland, C.J., and Fiveland, S.B., Reduced Chemistry Modeling –A new method for identifying reactions in partial equilibrium, 16th AIAA Computational Fluid Dynamics Conference, Session: High Speed and Chemically Reacting Flows, 2003.
12. (13) Reynolds W.C. (1986), "The Element Potential Method for Chemical Equilibrium Analysis – Implementation in the Interactive Program STANJAN, Version 3", *Department of Mechanical Engineering*, Stanford University
13. (14) Shampine, L.F. (1985), "Measuring Stiffness", *Applied Numerical Mathematics*, 1:107-119.
14. (15) Soyhan, H. S., et al., (2000), "Automatic reduction of detailed chemical reaction mechanisms for autoignition under SI engine conditions," SAE Paper No. 2000-01-1895.
15. (16) Sung, C. J., Law, C. K., and Chen, J.-Y., "Further Validation of an Augmented Reduced Mechanism for Methane Oxidation: Comparison of Global Parameters and Detailed Structure," *Combust. Sci. Tech.,* 156, pp. 201-220 (2000).
16. (17) Warnatz J., Mass U., Dibble R.W. (1999), *Combustion Physical and Chemical Fundamentals, Modeling and Simulation, Experiments, Pollutant Formation*, Springer, pg. 97.
17. (18) Yousefian V. (1998), "A Rate-Controlled Constrained-Equilibrium Thermochemistry Algorithm for Complex Reacting Systems", *Combustion and Flame*, 115:66-80

SURFACE REACTIVITY AS A MANY BODY MULTISCALE PROBLEM

Ashish B. Mhadeshwar, Jeffrey Ludwig, Abhijit Chatterjee, and Dionisios G. Vlachos

Department of Chemical Engineering
and Center for Catalytic Science and Technology
University of Delaware
Newark, DE 19716-3110

In this talk, we will demonstrate that surface reactivity even of the simplest heterogeneous reactions is a many body problem. The disparity in length and time scales encountered in these processes is tremendous. Phenomena at the fluid-surface interface, at quantum and molecular length and time scales, range from Å to several nanometers and render classical continuum equations, often referred to as mean field equations, inapplicable. Examples of such phenomena include intermolecular forces, nucleation, spinodal decomposition, and quantum reaction effects. On the other hand, reactors are often in the meter length scale with a residence time of seconds to minutes. Application of quantum calculations and molecular simulations, such as Monte Carlo or molecular dynamics, to the entire spectrum of scales is currently impractical.

In this talk, we describe hierarchical multiscale simulations for modeling such reaction systems from first principles. The unity bond index, quadratic exponential potential (UBI-QEP) or bond-order conservation (BOC) of Shustorovich and co-workers is employed as an efficient, semi-empirical means of predicting activation energies of large reaction mechanisms of catalytic reactors with input from experiments or density functional theory. Transition state theory is employed to estimate pre-exponentials, which in conjunction with the energetics, provide an initial set of reaction rate constants for each local arrangement (class) of adsorbates. Density functional theory (DFT) is used to refine the input to the semi-empirical technique and/or to assess self-consistency of the important reaction steps identified via sensitivity analysis Refinement of such reaction rate constants is possible using suitable experimental data and efficient optimization tools. These data are then used as input in lattice Monte Carlo simulations. The latter simulations solve directly a master equation as a Markov process and are properly coupled with continuum, reactor scale simulations. Application of this approach to understanding the chemistry in partial oxidation of methane on Pt and ammonia decomposition on Ru will be presented and contrasted to experiments.

While MC simulations can capture nanometer spatial inhomogeneities, they are too intensive for larger scales. Novel coarse-grained Monte Carlo simulations will be presented and demonstrated to be an important step toward meeting the length scales gap.

The Importance of Gas Phase Kinetics Within the Anode Channel of a Solid Oxide Fuel Cell (SOFC)

Chad Sheng and Anthony M. Dean

Chemical Engineering Department
Colorado School of Mines
Golden, CO 80401

Introduction

A complete SOFC model is very complex, requiring descriptions of kinetics in multiple phases and coupling these kinetics to multiple transport processes. [1] Chemical reactions within the SOFC occur in three regions: in the anode channel (gas-phase kinetics), on the surface of the porous anode (heterogeneous catalysis) and at the three-phase boundary layer between the anode and electrolyte (electrochemical catalysis). Thus the homogeneous and heterogeneous kinetics have the potential to substantially change the nature of the species that ultimately undergo electrochemical oxidation. It is essential to account for such kinetic modifications to properly characterize SOFC operation and predict the overall efficiency.

As a first step toward characterizing the complex kinetics, we want to make sure that we properly understand the gas-phase hydrocarbon chemistry. The effect of gas phase reactions of methane in SOFCs has previously been reported. [2] There it was shown that the electrochemical production of H_2O and CO_2 did indeed significantly impact the predictions regarding deposit formation. In this work we extend this approach to butane, which is significantly more reactive than methane and thus more representative of a range of hydrocarbon fuels.

Experimental

The experiments used n-butane as the fuel over a temperature range of 550 – 800ºC, with a nominal five second residence time through a tubular flow reactor operating at an ambient (high-altitude) pressure of ~0.8 atm. The reactor used in these experiments was a 24 cm length x 6 mm ID (12mm OD) quartz tube, which was housed within a 14.5 cm length single-zone clamshell 2.5 cm ID electric tube furnace. The product stream flowed through a water trap, and the de-humidified product stream then flowed to a Hewlett-Packard 5890 Series II+ gas chromatograph. Axial temperature profiles were measured and used in the plug flow model.

Three different fuel mixtures were used: neat n-butane (100% n-butane), a 50:50 n-butane:N_2 mixture and a 50:50 n-butane:H_2O(g) mixture. The neat n-butane case is intended to simulate the situation near the entrance of the anode channel where little CO_2 and H_2O would be present. Likewise the nC_4/H_2O mixture represents a mixture further down the channel where the products of the electrochemical reaction would be coming into the fuel stream. The nC_4/N_2 mixture was used to account for the effect of simple dilution with an inert in contrast to dilution with steam, which could possibly be a reactant.

Reaction Mechanism

The reaction mechanism that was utilized in this study consists of 291 species and 2498 elementary reactions. It is an extension of a previous mechanism[3], which included formation of C_4 hydrocarbon species. The extensions include substantially more molecular weight growth chemistry, especially involving propargyl radical pathways, and explicit inclusion of certain C_6 hydrocarbon species, including n-hexane, cyclohexane, and 2,3-dimethyl butane. The current mechanism is similar to the one recently used by Walters, *et al*.[2] in their analysis of methane kinetics under SOFC conditions.

Comparison to Model Predictions

Butane Conversion The ratio of the predicted final/initial mole fraction of butane is compared to that observed for the neat and nC_4/N_2 mixture cases in Fig. 1.

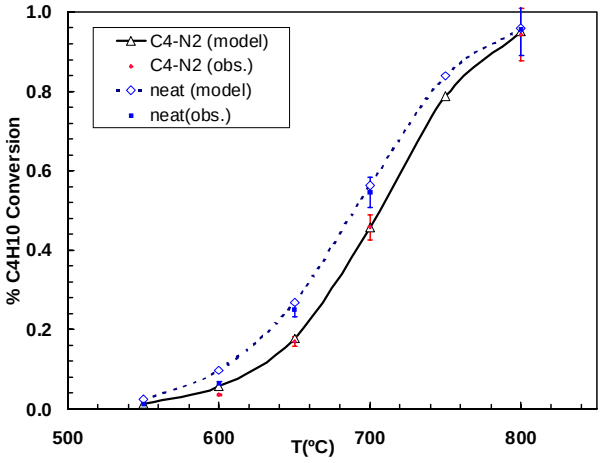

Figure 1. Comparison of predicted butane conversion to that observed for the neat butane case and for the 50% butane/50% nitrogen mixture.

The modeling predictions are in excellent agreement with the observations for both the neat and the nC_4/N_2 fuel mixture cases. The predictions clearly capture the observed temperature dependence for both the neat and nitrogen fuel mixture cases. From both the model predictions and the observed experimental data, it is also clear that the conversion for the neat n-butane case is higher than the nC_4/N_2 case. This difference is simply due to dilution in the nC_4/N_2 mixture. This good agreement, achieved without any modifications to the gas-phase kinetic mechanism, was very encouraging and suggests that the model can account for conversion of light hydrocarbons fuels under SOFC conditions.

Product Selectivity Four major products are observed: methane, ethane, ethylene, and propylene. The predicted selectivities are in reasonable agreement with those observed. For methane, the observed selectivity ranges from ~32% at 600ºC to ~38% at 800ºC, while the model predictions range from 32% to 35%. The propylene selectivity is observed to decrease with increasing temperature, from ~34% at 600ºC to ~13% at 800ºC. The predictions vary from ~32% at 600ºC to ~20% at 800ºC, not dropping off quite so rapidly with temperature as observed. The observed ethylene selectivity increases sharply from ~21% at 600ºC to ~42% at 800ºC. The predictions follow this reasonably well, ranging from ~19% at 600ºC to ~34% at 800ºC. This underprediction of the ethylene yield at 800ºC is reflected in an overprediction of the ethane yield. It was observed to vary from ~12% at 600ºC to ~5% at 800ºC, while the predictions yielded ~16% at 600ºC to ~10% at 800ºC. Thus one problem with the current model is the inability to precisely account for the distribution within the C_2 branch (ethane and ethylene) and with the C_1-C_3 branch (methane and propylene). Note that the predictions for the total C_2 branch are very consistent with the observations and properly account for the increase with temperature. Similarly, the sum of the methane and propylene selectivities show good agreement between predictions

and that observed, including the decrease in overall selectivity with temperature.

Deposit Formation One of the major concerns with the use of hydrocarbon fuels in solid oxide fuel cells is the propensity for deposit formation. In our experiments, qualitative observations of deposit formation were made by examining the quartz reactor after running a specific mixture through the reactor for 4 hours. We observed no apparent deposit formation within the reactor for any of the mixtures at 650ºC or lower temperatures. As the reactor temperature was increased to 700°C, an obvious deposit film was observed on the inner walls of the quartz reactor with the neat butane mixture. The deposit film was noticeably less dense for the nC_4/N_2 mixture, and barely evident for the nC_4/H_2O mixture. The first inference from these qualitative observations is that dilution does play a role in minimizing deposit formation. This is to be expected, since the lower concentration of reactive species would be expected to decrease the rate of molecular weight growth leading to deposits. The marked difference in the nitrogen and steam mixtures suggests that the steam is either actively participating in inhibition of molecular weight growth or that it is participating in some type of gasification of the deposit. All three mixtures show significant deposit formation at 800ºC.

To compare to the model, we considered all species in the model predictions above C_4 (denoted as C_5^+) as potential deposit precursors. The predicted C_5^+ mole fraction is a very strong function of temperature as illustrated in Fig. 2. It is encouraging to note that the predicted rapid increase in deposit precursors near 700ºC is consistent with the experimental observations.

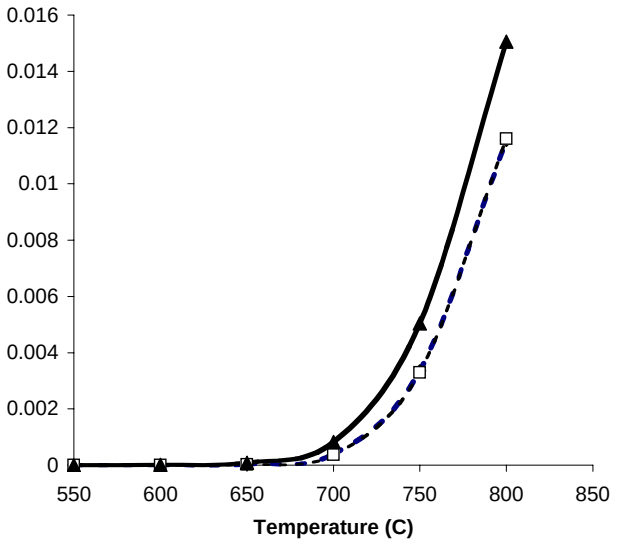

Figure 2. Predicted effect of temperature on the mole fraction of C5+ species.

The predicted C_5^+ values for the steam and nitrogen dilution cases are virtually identical. This is consistent with our observation that any gas-phase reactions of steam are very slow under these conditions, and thus steam is simply acting as a diluent, just like nitrogen. This is in contrast to the experimental observations that steam diminished deposit formation. This effect is probably due to heterogeneous reactions. The ratio of C_5^+ predicted for the neat butane case to that of the diluted mixtures decreases from approximately five at 550ºC to only slightly greater than unity at 800ºC. Thus at the higher temperatures, the predictions suggest that the inhibition of deposit formation by dilution is much less effective.

Kinetics Overview

The results from a sensitivity analysis indicate that, although the system consists of ~2500 reactions, there are only 10 reactions that dominate the formation or consumption of the five major species. These reactions suggest that butane pyrolysis can be described in terms of a simple Rice-Herzfeld mechanism. After initiation by breaking the C-C bonds in butane, the radicals formed abstract from the parent butane to form $n\text{-}C_4H_9$ and $s\text{-}C_4H_9$ radicals. The primary radicals lead to the C_2 products via beta-scission, while beta-scission of the secondary radicals lead to the C_1 and C_3 products. Thus the selectivity to these two product pairs can be traced to the selectivity of forming the two radicals in abstraction from the parent. An interesting complication is that the propylene product has an easily abstractable hydrogen, and the formation of allyl acts to inhibit conversion by modifying the nature of the free radical pool. This same allyl radical was also shown to be responsible for the small amounts of molecular weight growth observed since it can add to ethylene, forming cyclopentene. This pathway is accelerated since it is chemically-activated, and the initially energized linear adduct can directly form the cyclic species prior to collisional stabilization.

Conclusion

The butane pyrolysis experiments demonstrate that substantial gas-phase chemistry does occur under SOFC conditions, and that this must be accounted for when predicting fuel cell efficiency. These data were compared to predictions using a plug-flow model that incorporated the experimentally measured temperature profile along the reactor. Comparisons of the model predictions to the experimental data show that the model, without any modifications, captures the observed strong temperature dependence of n-butane conversion and is also able to capture the changes in product selectivity with temperature for the neat butane and the diluted butane mixtures. The model also properly predicts the observed onset of deposit formation near 700ºC. Both conversion and selectivity are shown to be sensitive to only a very small subset of the reactions in the mechanism. Comparison of the rate coefficients of this subset to literature values, where available, are generally reasonable and suggest that the kinetic model employed is adequate for describing reactions of small hydrocarbons in the anode channels of a SOFC. Thus such models should provide a useful tool to estimate the importance of gas-phase chemistry for various proposed SOFC operating conditions.

Acknowledgement. The authors would like to thank ITN Energy Systems, Inc. for the use of their facilities, where the experimental work was conducted under DARPA Contract Number MDA972-01-C-0068. The authors appreciate Katie O'Gara's contributions to the experiment and data compilation. We also would like to thank Hans-Heinrich Carstensen and Chitral Naik for providing some of the elementary reaction rates used in the current model. Chitral Naik also perfomred some of the modeling calculations.

References

(1) Zhu, H. and R.J. Kee, *A general mathematical model for analyzing the performance of fuel-cell membrane-electrode assemblies.* Journal of Power Sources, 2003. **117**(1-2): p. 61-74.

(2) Walters, K.M., et al., *Homogeneous Kinetics and Equilibrium Predictions of Coking Propensity in the Anode Channels of Direct Oxidation Solid-oxide Fuel Cells Using Dry Natural Gas.* Journal. of Power Sources, 2003. **123**(2): p. 182-189.

(3) Mims, C.A., et al., Radical chemistry in methane oxidative coupling: Tracing of ethylene secondary reactions with computer models and isotopes. J. Phys. Chem., 1994. 98(50): p. 13357-13372.

COMPUTATIONAL STUDIES OF BORON/NITROGEN AND ALUMINUM/NITROGEN COMPOUNDS FOR CHEMICAL HYDROGEN STORAGE

Maciej Gutowsk[1,2] and Tom Autrey[1]

[1] Chemical Sciences Division, Pacific Northwest National Laboratory, Richland, WA 99352, USA,
[2] Department of Chemistry, University of Gdansk, 80-952 Gdansk, Poland

Introduction

The DOE Office of Energy Efficiency and Renewable Energy have recently proposed a Grand Challenge for on-board Hydrogen Storage in response to the Presidents 2003 State of the Union Address.[1] To meet the target of the long-term DOE volumetric (0.09 kg H_2/kg) and energy density (3.0 kWh/kg) targets further development and understanding of hydrogen storage materials will require substantial new research effort.

Much work thus far has focused three systems to store hydrogen for potential on-board applications, metal hydride storage involving the reversible uptake and release of H_2 from $Na^+AlH_4^-$,[2] chemical hydrogen storage involving the irreversible hydrolysis of $Na^+BH_4^-$ → H_2 + borate[3] and storage on carbon materials involving physi- and chemi-sorption of hydrogen on single walled carbon nanotubes.[4] None of these current systems are likely to meet the long-term DOE goals system making a strong argument for the discovery of new storage possibilities. In this paper we discuss our computational approaches to screen for potential new hydrogen storage materials. Our hope is to find a material that is a solid, high weight percent hydrogen, and reversibly releases (or uptakes) hydrogen under moderate conditions. The thermodynamics of the ideal material would be thermoneutral for hydrogen release.

We start with an analysis of the current most studied hydrogen storage material, the complex hydride $NaAlH_4$. Since this material only stores hydrogen on the anionic site only, AlH_4^-, a dramatic improvement in capacity is envisioned if hydrogen is stored on both the cationic and anionic sites. Another improvement is feasible with the substitution of B (FW=10.8) for Al (FW=27). NH_4^+, BH_4^-, and AlH_4^- are known building blocks of ionic solids, which are isoelectronic with Na^+, F^-, and Cl^-, respectively. Ionic solids built of NH_4^+ and XH_4^- (X=B, Al) are expected to be insulating and dense (to meet the density requirements) and both Boron and Nitrogen are light elements (to meet the volumetric requirements). Furthermore, several of the NH_xBH_x series of compounds are reported to be both *water and air stable*[5] as opposed to many of the complex hydrides currently under investigation.

Given these favorable specifics we undertook a computational approach to investigate the potential of amine boranes as potential solid hydrogen storage materials.[6] These materials are quite attractive from both volumetric and gravimetric considerations, for example NH_4BH_4 and NH_3BH_3, store 0.24 kg H_2/kg and 0.19 kg H_2/kg respectively! The storage capacity is well above any currently studied material. The optimum decomposition reaction is NH_4BH_4 → $BN + 4H_2$, outlined in a stepwise process below, eqs 1-4. Even if only two of the four steps proved feasible H_2 storage capacities greater than 0.12 kg H_2/kg could be realized.[7]

$$NH_4BH_4 \rightarrow NH_3BH_3 + H_2 \quad (1)$$
$$NH_3BH_3 \rightarrow NH_2BH_2 + H_2 \quad (2)$$
$$NH_2BH_2 \rightarrow NHBH + H_2 \quad (3)$$
$$NHBH \rightarrow NB + H_2 \quad (4)$$

Methods

Computational studies have been performed for (i) isolated NH_4^+, BH_4^-, and AlH_4^- species and (ii) solids NH_4BH_4, NH_3BH_3, NH_4AlH_4, BN, and AlN. For molecular clusters and complexes we have used highly correlated electronic structure methods (coupled cluster level of theory with single, double, and non-perturbative triple excitations, Green's function (propagator) methods, etc.) and augmented correlation-consistent basis sets, as implemented in the NWChem code[8]. For solids, we used density functional theory with gradient-corrected exchange functionals (PW91, as implemented in the VASP code[9]). Periodic boundary conditions were assumed for the solids and static optimizations have been completed. The sodium chloride, cesium chloride, zinc blende, and wurtzite structures of NH_4AH_4 (A=B, Al) were explored. The hexagonal planar, zinc blende, and wurzite structures have been optimized for BN and the wurzite and zinc blende for AlN.

Results and Discussion

Relative stability of solid phase materials. Our computational results allow several thermodynamic comparisons to be drawn between the NH_4BH_4 (**1**) and NH_4AlH_4 (**2**) as potential chemical hydrogen storage materials. The first noticeable characteristic difference is the in thermodynamic stability between the zinc blende and wurzite crystalline structures for the two species (Figure 1). In the case of NH_4BH_4 the zinc blende phase was found the more stable then the wurzite phase by 0.23 eV per BN unit. The density of the zinc blende structure is 0.554 g/cm^3. The opposite was found for the case of NH_4AlH_4 where the wurzite phase was found to be more stable than zinc blende by0.12 eV per AlN unit. The density of the wurzite structure is 0.663 g/cm^3. The most stable phase of BN is hexagonal graphite-like, rather than cubic (zinc blende) or hexagonal (wurtzite). This unique feature will be important for the hydrogen mobility in the reloading/releasing cycles. Knowledge of these phase compositions will be important for the hydrogen mobility in the reloading/releasing cycles.

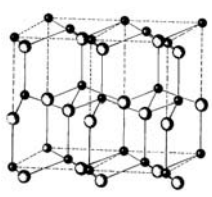

NH_4BH_4 (**1**) (zinc blende)

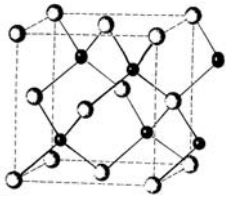

NH_4AlH_4 (**2**) (wurzite)

Figure 1. Thermodynamically stable phase of NH_4BH_4 (ammonium borohydride) is zinc blende. Thermodynamically stable phase of NH_4AlH_4 (ammonium aluminum hydride) is wurzite phase. Hydrogen atoms are not shown in structure for simplicity.

Relative energetics of decomposition pathways. Initial computational results on the solid materials show the reaction energetics are neither extremely exothermic nor too endothermic for loss of hydrogen for NH_4BH_4(solid). These results are promising because it strongly suggests that reversal uptake of hydrogen is feasible under moderate conditions. Furthermore, it is predicted by theory that hydrogen elimination, eq 5, is more favorable, than N-B bond scission, eq 6. Hydrogen elimination is exothermic by less than 0.3 eV/BN unit whereas B-N bond scission is predicted to be

endothermic by 1.1 eV. Similar results are predicted for hydrogen loss from NH_4AlH_4, eq 7, more favorable than N-Al bond scission, eq 8. However, in the case of NH_4AlH_4 hydrogen loss is far more exothermic, 1.07 ev per AlN unit compared to the endothermic Al-N bond scission of 0.7 eV. This is an interesting result that may have implications on regeneration of the hydrogen storage materials. If the reaction is too exothermic it likely require greater effort to regenerate the material. Alternatively, the system may still be reversible if the end product is NH_xAlH_x (x=1-3) rather than AlN.

$NH_4BH_4(s) \rightarrow BN(s) + 4H_2(g)$ (5)
$NH_4BH_4(s) \rightarrow NH_3(g) + \frac{1}{2} B_2H_6(g) + H_2(g)$ (6)
$NH_4AlH_4(s) \rightarrow AlN(s) + 4H_2(g)$ (7)
$NH_4AlH_4(s) \rightarrow NH_3(g) + AlH_3(g) + H_2(g)$ (8)

A more detailed investigation of the step-wise loss of hydrogen from NH_4BH_4 reveals some intriguing features in Scheme 1. The release of hydrogen from NH_4BH_4 proceeds through intermediate steps, forming linear polymers[10] and hydrogen gas with specific thermodynamic characteristics (ΔE in kcal/mol).

Scheme 1.

$NH_4BH_4(s) \rightarrow NH_3BH_3(s) + H_2(g)$ ΔE = -2.3
$NH_3BH_3(s) \rightarrow NH_2BH_2(poly) + H_2(g)$ ΔE = 8.8
$NH_2BH_2(poly) \rightarrow NHBH(poly) + H_2(g)$ ΔE = -3.2
$NHBH(poly) \rightarrow BN(s) + H_2(g)$ ΔE = -9.2

Alternatively, cyclic polymer structures, starting with perhydroborazine, **3**, as shown in Scheme 1, could be involved in the decomposition pathways of amine borane. Sneddon and coworkers[11] report that at moderate temperatures borazine, **4**, undergoes a dehydropolymerization to yield hydrogen and a borazine polymer. At higher temperatures the polymer undergoes further dehydrogenation to yield a polyborazylene (BN) polymer. This observations merit further study to investigate the feasibility of reversible hydrogen storage.

Scheme 2.

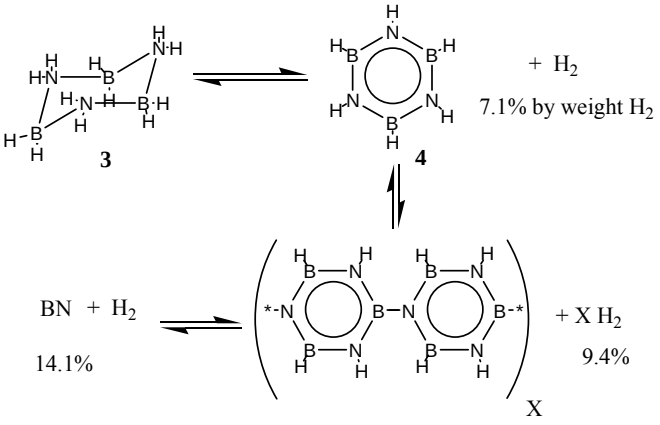

Conclusions

Computational methods offer an attractive approach to screen new potential chemical hydrogen storage materials. Two potential systems were examined in this study, hydrogen releases from NH_xBH_x (amine/ammonium borohydrides) and NH_xAlH_x (amine/ammonium alanates). Both materials could potentially meet the long term DOE requirements for volumetric and energy density requirements. Theoretical calculations predict that hydrogen loss is the thermodynamically favored pathway over B-N or Al-N bond scission. However, the loss of hydrogen from the NH_xBH_x series of compounds is predicted to be less exothermic than hydrogen loss from the NH_xAlH_x series of compounds. This could be an important observation to enhance the economic considerations for recycle.

Acknowledgement. The authors wish to acknowledge support from the Laboratory Directed Research and Development Program at the Pacific Northwest National Laboratory and the Nanoscience Initiative. Some calculations have been performed at the National Energy Research Scientific Computing Center (NERSC).

References

1 Hydrogen, Fuel Cells & Infrastructure Technologies Program, 2003 Merit Review and Peer Evaluation Meeting, May 19-22, **2003**, Berkeley, CA.
2 B. Bogdanovic and M. Schwickardi, *J. Alloys Comp.* **1997**, *253*, 1.
3 Y. Wu; R. M. Mohring, *Fuel Preprints* **2003**, *48*(2) 940.
4 A.C. Dillon; M. J. Heben. Appl. Physics A-Materials Science & Proc. **2001**, *72* (2), 133.
5 H.C. Brown, L. T. Murray, *Inorg. Chem.* **1984**, *23*, 2746.
6 The synthesis of NH4BH4 was first reported by S.G. Shore, R.W. Parry, *J. Am. Chem. Soc*. **1958**, *80*, 8.
7 The Freiberg group has been investigating hydrogen loss from amine borane (NH3BH3). See *Advances in Boron Chemistry*, Ed., W. Siebert, Royal Society of Chemistry **1997**, pp 514-517.
8 NWChem, A Computational Chemistry Package for Parallel Computers, Version 4.0.1, **2001**, R.H. Harrison et al.
9 G. Kresse and J. Hafner, Phys. Rev. B **47**, 558 (1993); G. Kresse and J. Furthmüller, Comp. Mat. Sci. **6**, 15 (1996).
10 It has recently been shown that catalytic loss of hydrogen from amine borane occurs by a bimolecular pathway. C. A. Jaska; K Temple; A. J. Lough; I. Manners. *J. Am. Chem. Soc*. **2003**, *125*, 9424.
11 P. J. Fazen; E. E. Remsen; J. S. Beck; P. J. Carroll; L. G. Sneddon. *Chem. Mater*. **1995**, *7*, 1942.

Tom.Autrey@pnl.gov
Maciej.Gutowski@pnl.gov

Developing and using mechanisms for the oxidation of organic compounds in the atmosphere

M. J. Pilling

School of Chemistry, University of Leeds, Leeds, LS2 9JT, United Kingdom

The master chemical mechanism (MCM) is an explicit chemical mechanism describing the tropospheric oxidation of 125 volatile organic compounds. It is mounted on the Leeds Chemistry website at:

http://www.chem.leeds.ac.uk/Atmospheric/MCM/mcmproj.html

The mechanism has been assembled using a protocol with comparatively few simplifications. The rate data and product yields are based on experiment, theory, estimation and analogy.

Following a brief outline of the website and the protocol, the following issues will be discussed:

- approaches to the determination of mechanism components using direct measurements of reaction rates and chamber experiments;
- uncertainty estimation;
- approaches to reduction and lumping;
- tests of the mechanism using outdoor chamber and field experiments, in clean and polluted environments

AB INITIO STUDY OF THE OXIDATION OF NCN BY O_2

R. S. Zhu, and M. C. Lin

Department of Chemistry
Emory University
Atlanta, GA 30322

I. Introduction

NCN is the major radical formed in the new prompt NO reaction, CH + N_2 → HNCN → NCN + H.[1] The oxidation of NCN radicals to NO is critical to our full understanding of the prompt NO formation mechanism.

In this series of studies, we have investigated the reactions of NCN with O, OH[2] and O_2 by ab initio MO calculations. We report here the result for the latter process NCN + O_2.

II. Computational Methods

The potential energy surface (PES) was calculated at the highest scheme of the G2M method.[3] The Gaussian 03 program[4] was used for the molecular orbital calculations.

The rate constants were computed with microcanonical variational RRKM (Variflex) code.[5]

III. Results and Discussion

A. Potential Energy Surface and Reaction Mechanism

The optimized geometries of the intermediates and transition states are shown in Figure 1. The potential energy diagram obtained at the G2M(CC1)//B3LYP/6-311G(d, p) level is presented in Fig. 2.

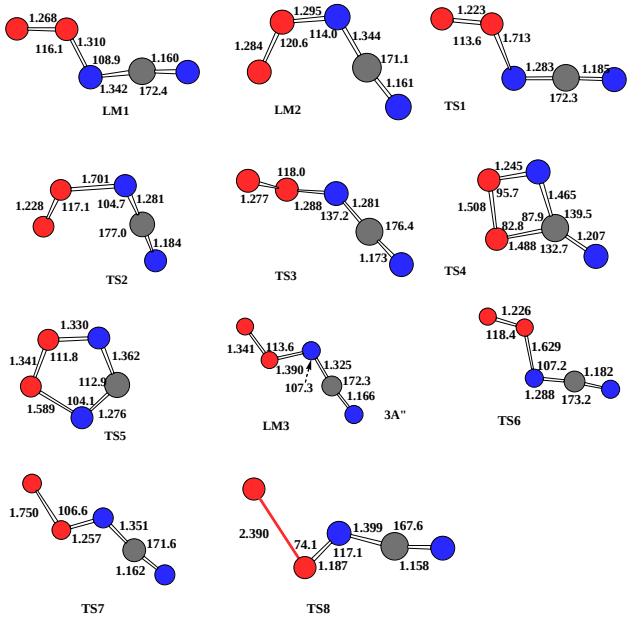

Figure 1. The optimized geometry of intermediates and transition states computed at the B3LYP/6-311G(d, p) level for the NCN + O_2 reaction.

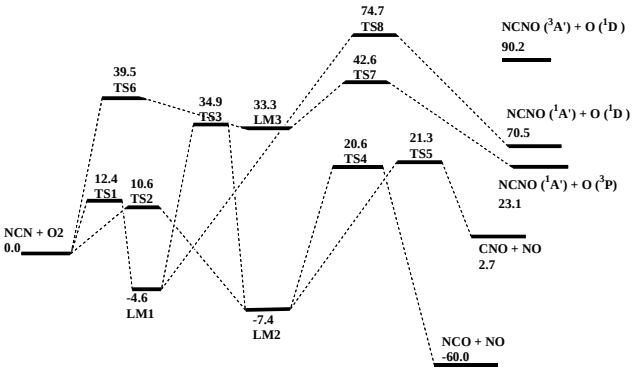

Figure 2. The schematic diagram of the potential energy surface for the NCN-O_2 system computed at the G2M(CC1) level.

The following possible channels are considered for this oxidation reaction:

NCN + O_2 → NCNOO† → NCO + NO (1)
→ CNO + NO (2)
→ NCNO + ^{1,3}O (3)

The lowest energy isomer is cis-trans-OONCN (LM2), it lies below the reactants by 7.4 kcal/mol at the G2M(CC1) level. It can dissociate to NCO + NO and CNO + NO via four- and five-member ring transition states with barriers of 28.0 and 28.7 kcal/mol. The entrance barrier for this channel is 10.6 kcal/mol. The other isomer, trans-trans-OONCN intermediate (LM1) lies below the reactants by 4.6 kcal/mol with a entrance barrier of 12.4 kcal/mol, which dissociates to NCNO + ^{1}O via a transition state with high barrier, 79.3 kcal/mol. In addition, the stability of the triplet intermediate is also considered, the results show that ^{3}A" trans-trans-OONCN (LM3) lies above the reactants by 33.3 kcal/mol, which means that the triplet path is not favorable for this reaction.

B. Rate constant calculations

The rate constants are calculated in the temperature range of 1000 - 3000 K, the results show that oxidation NCN by O_2 to produce NCO + NO and CNO + NO is rather slow because of the high entrance and exit barriers. The total rate can expressed as:
$k_t = 7.29 \times 10^{-15} T^{0.51} \exp(-12365/T)$ cm^3 molecule^{-1} s^{-1}.

IV. Conclusion

The mechanism for the oxidation of NCN by O_2 has been discussed and rate constants for the low-lying channels are calculated. The results show that oxidation NCN by O_2 to produce NCO + NO and CNO + NO is very slow because of the high entrance and exit barriers. This reaction can not compete effectively with the much faster oxidation processes, NCN + O and OH.[2]

Acknowledgement

This work is sponsored by the Office of Naval Research under contract no. N00014 – 02-1-0133, Dr. J. Goldwasser program manager. Acknowledgment is also made to the Cherry L. Emerson Center of Emory University for the use of its resources, which are in part supported by a National Science Foundation grant (CHE-0079627) and an IBM Shared University Research Award.

References

(1) Moskaleva, L. V.; Xia, W. S.; Lin, M. C.. Chem. Phys. Lett. **2000**, *331*(2,3,4), 269.

(2) Zhu, R. S.; Lin, M. C.; to be published.
(3) Mebel, A. M.; Morokuma, K.; Lin, M. C. *J. Chem. Phys.* **1995**, *103*,7414.
(4) M. J. Frisch, M. J. et al., *GAUSSIAN 03, REVISION B.0*1; Gaussian, Inc., Pittsburgh PA, **2003**.
(5) Klippenstein, S. J. ; Wagner, A. F.; Dunbar, R. C. ; Wardlaw, D. M. and Robertson, S. H. VARIFLEX: VERSION **1.00**, **1999**.

The Molecular Origins of NO Selectivity in the Thermal Reduction of NO_x by NH_3

Donghai Sun[†], William F. Schneider, James B. Adams[†], Debasis Sengupta[‡]*

[†]Department of Chemical and Materials Engineering, Arizona State University, Tempe, AZ-85287
*Ford Motor Company, Mail Drop 3083/SRL, Dearborn, Michigan 48121-2053
[‡]CFD Research Corporation, 215 Wynn Drive, Huntsville, AL 35805

Introduction

Thermal deNO_x process is an effective way for "lean" NO_x (x= 1, 2) control for stationary sources and attracting serious attention for selective catalytic reduction of NO_x by NH_3 from mobile-sources. The fundamental mechanism underlying the thermal deNO_x chemistry is the selective reduction of NO_x over a large excess of O_2. This mechanism involves generation of the amino (NH_2) radical through chain reactions that involve O atoms and OH radicals,[1, 2] and the NH_2 is reacting directly with NO to ultimately produce N_2. Competition between NO and O_2 for the "activated" NH_2 reductant is thus inherent to the overall chemistry. The reactions of NH_2 with NO and O_2 have been studied extensively both theoretically and experimentally: [3,4,5,6,7,8,9,10,11]

$NH_2 + NO \rightarrow$ Products (1)
$NH_2 + O_2 \rightarrow$ Products (2)

Fortunately, the rate of reaction (1) (10^{-12} cm^3 molecule^{-1} s^{-1} at 2000 K) is observed to be 10 orders of magnitude faster than that of reaction (2) (10^{-21} cm^3 molecule^{-1} s^{-1} at room temperature) although they proceed through topologically similar channels. The primary channels of reaction (1) are: [4,5,7,12]

$NH_2 + NO \rightarrow N_2 + H_2O$ (3)
$\rightarrow HN_2 + OH$ (4)

The reaction (2) analogs to channels (3) and (4) are:

$NH_2 + O_2 \rightarrow NO + H_2O$ (5)
$\rightarrow HNO + OH$ (6)

Although reactions (1) and (2) have been studied individually in great detail, little attention has been paid to understanding the origins of the very different kinetics of these superficially similar reactions. In this paper, the potential energy surfaces of these two reactions have been analyzed and the origin of the NO selectivity is attributed to the much greater stability of the initial H_2NNO adduct relative to H_2NOO radical with analysis of their electronic structures.

Computational Method

DFT calculations were performed with the Amsterdam Density Functional (ADF) package with the spin-polarized BLYP approximation. [13,14,15,16] A valence double-ζ plus polarization Slater-type basis was used on all atoms.

Results and Discussion

Figures 1 and 2 summarize the key potential energy surface for reactions (1) and (2) in which analogous steps of both reactions are considered together in parallel for comparison.

The mechanistic origins of the NO selectivity that underpin thermal deNO_x are readily apparent from Figure 1. NH_3 itself is unreactive towards NO and O_2; rather, NH_3 is activated for reaction by removal of an H atom to produces NH_2 radicals. NH_2 radical forms a relatively strongly bound (54 kcal mol^{-1} from BLYP) adduct with NO. Particularly favorable electronic interactions produce strong σ and π bonding in the molecular structure of H_2NNO. In contrast, NH_2 radical forms a relatively weakly bound adduct with O_2 (15 kcal mol^{-1} from BLYP): O_2 has one more electron and less accessible 2π acceptor levels than NO, and H_2NOO radical has neither the strong σ nor π bonds of H_2NNO. As seen in Figures 1 and 2, beyond the adduct formation step the potential energy surfaces for the two reactions are superficially quite similar. The paths to the thermodynamic products involve a sequence of H-transfer, isomerization, and decomposition steps, the most highly activated of which is the initial $H_2NXO \rightarrow HNXOH$ H-transfer (X=N, O). These steps compete with backwards decomposition to reactants, and the balance between forward and backward steps controls the overall reaction rate. For strongly bound H_2NNO, the forward reaction steps are all at lower energy than the entrance channel, and essentially all H_2NNO formed react forward to products in what is in effect a single elementary step. [17] In contrast, weakly bound H_2NOO radical is shifted upwards in energy such that the forward reaction channels involve energy barriers greater than the energy to decompose back to reactants, and only at high temperatures do any of the forward reaction channels occur at an appreciable rate. [18] Remarkably, then, the difference in initial adduct stability alone accounts for the much different rates of the $NH_2 + NO$ and $NH_2 + O_2$ reactions.

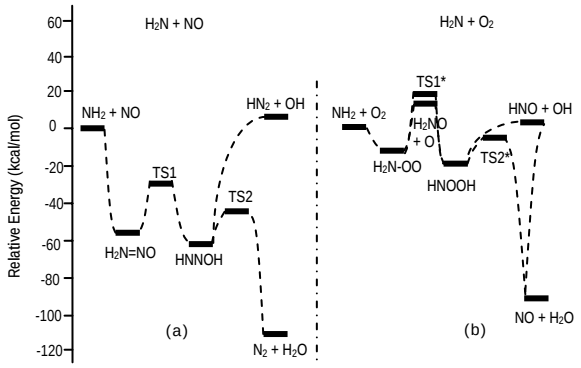

Figure 1. BLYP-calculated potential energy surfaces for reactions (a) $NH_2 + NO$ and (b) $NH_2 + O_2$. HNXOH (X = N, O) isomerization details hidden for clarity

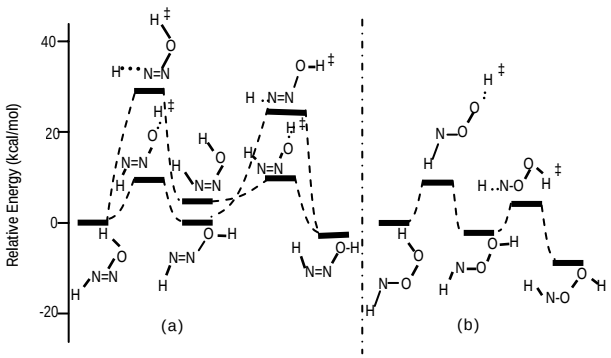

Figure 2. BLYP-calculated potential energy surfaces for isomerization of (a) HNNOH and (b) HNOOH.

It is interesting to consider the generality of this difference in reactivity between NO and O_2. Table 2 compares the R–NO and R–O_2 bond dissociation energies for a number of common alkyl and heteroatomic free radicals R for which data is available. NO is found to readily bind to all the radicals within this sample set: bond strengths range from around 40 to less than 60 kcal mol^{-1}, with the strongest bonds tending to be π donor radicals, such as NH_2 or OH radical. For practical purposes NO does not thermochemically discriminate within this set, and consistent with the behavior typical

Table 1. Comparison of 298 K R–NO and R–O_2 bond strengths (kcal mol^{-1}). All experimental values from ref. [19]

	R–NO	R–O_2	Δ
H	47	49	–2
CH_3	40	33	7
i-C_3H_7	37	37	0
CF_3	43	37[a]	6
HO	49	7[b]	42
CH_3O	42	–4[c]	46
F	57	13	44
Cl	38	6	33
NH_2	48[d]/54[e]	0[e]/15 [f]	~40-50

a. Calculated, ref. [20] b. Calculated, ref. [21] c. Calculated, ref. [22] d. Calculated, ref. e. Calculated, ref. f. Calculated, this work.

for free radical combination reactions, the corresponding R + NO high pressure limiting rate constants are large — typically within an order of magnitude of the gas-kinetic limit.[19] O_2 presents an interesting contrast. Within the H and alkyl radical group, the R–O_2 and R–NO bond strengths are comparable and the difference between the two is uniformly small. Consistent with this, the R + O_2 reaction rate constants are comparable to those for R + NO, and thus these R-radicals exhibit little inherent selectivity in reactions with NO over O_2; i.e. neither CH_3 radical nor H radical will selectively combine with or reduce NO in the presence of O_2.

The heteroatom (halogen, O, and N)-centered radicals behave much differently. Here the R–O_2 bond energies are very small—so small that accurate experimental determination is difficult, and the most reliable estimates tend to come from first-principles calculations. While there are uncertainties in some of these R–O_2 bond energies, what is not uncertain is that the bonds are on the order of 40 kcal mol^{-1} weaker the R–NO ones. Because these are association reactions, the relative bond energies dominate the relative reaction rate constants, and the corresponding R + O_2 reactions are similarly much slower than the R + NO ones.[23] (Precise reaction rate comparisons are complicated by the existence of multiple reaction channels, large sensitivities to pressure, temperature, and diluent, and the limited availability of data for the slow R + O_2 reactions.) Thus, these heteroatomic radicals are selective in their reactions with NO over O_2, not because of some inherent preference for NO but rather because of inherent unreactivity towards O_2. While we have only considered in detail the NH_2 radical case here, it is likely that the slow reactions of the other heteroatomic radicals with O_2 have similar explanations in terms of π repulsions and poor σ bonding. Any of these heteroatomic radicals will selectively combine with NO in the presence of O_2; NH_2 radical is particularly useful because reaction with NO ultimately leads to reduction to N_2.

Conclusions

Any useful system for catalytically reducing NO_x in lean exhaust must have as its basis very high selectivity for reactions of reductant with NO_x over O_2, both to counterbalance the great thermodynamic driving force for oxidation reactions and to overcome the large disparities in concentration between small amounts of NO_x and large amounts of background O_2. Within a limited range of conditions, this selectivity is achieved without catalysts in the thermal deNO_x process. NH_2 radicals generated in situ from NH_3 are many orders of magnitude more reactive towards NO than O_2. NH_2 radicals form a strong bond with NO to produce H_2NNO, which provides an entrance into rearrangement channels ultimately yielding the desired products N_2 and H_2O. What is unusual in this system, though, is not the fast rate of the NH_2 + NO reaction—in fact, this reaction proceeds at rates comparable to other radical + NO reactions. Rather, the key feature that underpins thermal deNO_x is the very slow reaction of NH_2 radical with O_2. The H_2NOO adduct is weakly bound, and fragmentation back to reactants competes very effectively with channels ultimately leading to NO and H_2O. This weak binding and slow reaction is characteristic of O_2 reactions with heteroatomic radicals, such as F, OH or NH_2, but not of reactions with H or carbon-centered radicals. Its origins lie in π repulsions and weak σ bonding between O_2 and electron-rich radicals.

These observations provide a different perspective on the selective catalytic reduction of NO_x with NH_3 or hydrocarbons. Effective catalysts clearly must be able to bind and activate reductants and to maintain or enhance selectivity in reductant reactivity between NO and O_2. While mechanistic emphasis tends to be placed on understanding the reactivity of NO_x, the absence of reactivity with O_2 is at least as important to understand.

Acknowledgement

The authors gratefully acknowledge helpful conversations with Ole John Nielsen, Steve Harris, Tim Wallington, Chris Wolverton and Paul Schuck, as well as support from the Department of Energy under grant DE-F603-99ER14985 and from the National Center for Supercomputing Applications for computer resources on their SGI Origin cluster at project RTM (8141).

References

1 Miller, J. A.; Bowman C. T. *Progress in Energy and Combustion Science*, **1989**, *15,* 287.

2 Lyon, R. K. *Diesel Engine Emissions Reduction (DEER) Workshop*, **2001**.

3 Wolf , M.; Yang, D. L.; Durant J. L. *J. Phys. Chem. A* **1997**, 101, 6243.

4 Vandooren , J.; Bian, J.; Tiggelen, P. J. *Combustion & Flame,* **1994,** 98, 402.

5 Diau, E. W.-G; Smith, S. C. *J. Chem. Phys.*, **1997,** 106, 9263.

6 Sumathi , R.; Peyerimhoff, S. D. *J. Chem. Phys.*, **1998**, 108, 5510.

7 Marcy, P. T.; Heard , E. D.; Leone, R. S. *J. Phys. Chem. A,* **2002**, 106, 8249.

8 Park, J.; Lin, M. C. *J. Phys. Chem. A*, **1997**, 101, 5.

9 Miller, J. A.; Glarborg, P. *Int J. Chem. Kinet.*, **1999**, 31, 757.

10 Diau, E. W.; Yu, T.; Wagner, M. A. G.; Lin, M. C. *J. Phys. Chem.*, **1994**, 98, 4034.

11 Yamasaki , K.; Watanabe, A.; Tanaka, A.; Sato, M.; Tokue, I. *J. Phys. Chem.*, **2002**, 106, 6563.

12 Votsmeier, M.; Song, S.; Hanson, R. K.; Bowman, C. T. *J. Phys. Chem. A*, **1999**, 103, 1566.

13 Baerends, E. J.; Ellis, D. E.; Ros, P. *Chem. Phys.*, **1973**, 41, 1.

14 Becke, A. D. *Phys. Rev. A*, **1998**, 38, 3098.

15 Lee, C.; Yang, W.; Parr, R. G. Phys. Rev. B, 1988, 37, 785.

16 Miehlich, B.; Savin, A.; Stoll, H.; Preuss, H. *Chem. Phys. Lett.*, **1989**, 157, 200.

17 Miller, J. A.; Klippenstein, S. J. *J. Phys. Chem. A*, **2000**, 104, 2061.

18 Bozzelli, J. W.; Dean, A. M. *J. Phys. Chem.*, **1989**, 93, 1058.

19 NIST Chemical Kinetics Database, Hhttp://kinetics.nist.govH.

20 Schneider, W. F.; Wallington, T. J. **J. Phys. Chem.**, **1993**, 97, 12783.

21 Denis, P. A.; Kieninger, M. O.; Ventura, N.; Cachau, R. E.; Diercksen, G. H. F. *Chem. Phys. Lett.*, **2002**, 365, 440.

22 Jungkamp, P. W.; Seinfeld, J. H. *Chem. Phys. Lett.*, **1996**, 257, 15.

23 Ruscic, B.; Berkowitz, J. *J. Chem. Phys.*, **1991**, 95, 4378.

Computer Aided Design of Complex Chemical Mechanism for Combustion Applications

F. Mauss

Division of Combustion Physics, Lund University, P.O. Box 118
SE-22100 LUND, Sweden

Introduction

Combustion, in technical applications, occurs under turbulent flow conditions. In modeling combustion devices with numerical tools it is necessary to consider the interaction of chemistry and flow. Chemistry-flow interaction models are demanding in both, computational time and memory. Thus, they limit the number of chemical species that can be explicitly taken into account. Technical fuels are mixtures of aliphatic and aromatic hydrocarbons that introduce chemical mechanism with hundreds of species and thousands of reactions. These numbers make it difficult to compile, analyze or optimize such mechanism; they make it impossible to use these mechanisms together with computational fluid dynamical (CFD) programs. In addition to computational tools for mechanism generation, analysis and optimization, a variety of reduction methods are needed to lump parallel reaction paths, to detect unnecessary reactions and species, and to simplify the model equations for species reacting on time scales that are much shorter than the relevant physical time scales. In this paper an overview over available methods and their interaction is given.

Mechanism development for combustion applications

The compilation of detailed kinetic reaction mechanisms is a difficult and time consuming task. A set of elementary reactions is stated for each fuel. The data for the kinetic rate constants are taken from experiments or, if experiments are not available, from quantum mechanical calculations. Together with the rate constants the uncertainty of the kinetic data has to be stated. If the set of chemical reactions is complete, the mechanism has to be validated against experiments for global parameter such as ignition delay times, flame velocities of freely propagating premixed flames, and extinction limits of counterflow diffusion flames.

The first estimation of the mechanism will, caused by the uncertainties in the elementary reactions, result in a poor agreement between simulation and experiments, and improvements are necessary. The next step in compiling the reaction mechanism is to perform a detailed sensitivity analysis of the global parameter against all chemical rate coefficients. As a result of the analysis one gets a set of reactions that is most important for the currant experiment. Hence the kinetic rate constants of these reactions need to be as accurate as possible. An iterative process of adjusting these rate coefficients and recalculating the experiments for the mechanism validation is utilized until the first set of optimized rate coefficients is reached.

In a second step the mechanism will be refined by controlling local parameter instead of the global ones. These are usually the time- or space resolved profiles for temperature, fuel, oxidizer, and for some intermediate and final products. Again an iteration procedure, as explained above, is employed that finally leads to a more improved reaction mechanism. Further improvement can be reached by controlling more sensitive local parameter like pollutants such as NO_x and soot. For each step, in refining the reaction mechanism special emphasis must be taken to guarantee that the prediction of the targets defined for the prior optimization step is not worsened.

In the past such mechanisms have been constructed manually for hydrocarbon fuels up to butane. These mechanisms contain about 600 reactions and 80 species (see for example reference [1]). But for most of the mechanisms, found in the literature, the more complicated low-temperature kinetics for butane is missing. This is partly caused by, that in most technical application the low temperature oxidation of butane is not sensitive.

For higher hydrocarbon fuels this neglect is not possible, since for some technical relevant processes—for example the occurrence of the engine knock phenomenon in spark ignition engines—low temperature reaction pathways are essential. However the detailed inclusion of low temperature reaction for fuels like *n*-heptane involves more than 500 species and 4000 reactions [2]. It is almost impossible to compile such a mechanism by hand, and early reaction mechanisms were based on simplified models for the low-temperature oxidation of aliphatic fuels. These mechanisms have been validated for global parameter such as ignition delay times and flame velocities, only.

A more detailed description of the low-temperature oxidation is weakly motivated, since the high number of reactions and species involve many practical problems—the demanded effort in computational time and memory, the high number of reactions with unknown rate coefficients. It became visible that an automation of the steps, performed to develop a chemical reaction mechanism is needed to accelerate the progress in the field.

Automation of the mechanism development

The first automation in the process was the development of tools to analyze the chemical processes during combustion processes, i.e. the reaction flow analysis and the sensitivity analysis (see for example the overview article [3]). For the former the reaction fluxes from species to species are calculated in a post process to the combustion calculation, and a map can be drawn that visualizes the flow of atoms. For the latter the frequency factor in the Arrhenius approximation for the reaction velocity is used as a parameter in the system of differential equations. The sensitivity of unknowns on the reaction rate coefficient can be calculated from the sensitivity of the residual of the respective differential equation and the jacobian matrix of the underlying system of equations.

The next automation was the automatic generation of reaction mechanisms. The definition of chemical reactions for certain molecules was replaced by the definition of reactions of certain groups appearing in the molecules [4, 5]. Programs were written that scan through the fuel molecules and the intermediate species to find the specific molecule groups and to apply the corresponding reactions. At the first glance, this approach appears to be simple but the approach is leading to explosions in the number of species and the number of reactions, if no limitation is set. The first generated reaction mechanisms appeared a decade ago, and the number of applications, where a generated reaction mechanism is used is still low.

Finally the optimization of the reaction rate coefficients was automated. In a first step sensitive reactions for the targets—for example, unknowns at certain data points—to be optimized are selected from the matrix of sensitivity coefficients and from the uncertainties in the rate coefficients. Response surfaces for the difference between the experimental values for the targets and the numerically calculated values are produced, and the optimum set of rate coefficients is found by searching the set of rate coefficients with the minimum difference for all targets [6, 7].

Mechanism Reduction

The gap between the number of species allowable for CFD-applications and the number of species introduced by detailed reaction mechanisms shows that the knowledge transfer from fundamental research in combustion kinetics to engineering applications relies on the availability of mechanism reduction

methods. The major reduction methods in use today can be divided into four groups. 1) removement of unnecessary reaction, 2) lumping methods, 3) simplification of the system of differential equation, through time scale analysis, and 4) tabulation methods.

The removal of unnecessary species and reactions is the oldest strategy in reducing chemical mechanism. It is intuitive to demand that an unnecessary species or an unnecessary reaction has a low chemical flux [8] and a low sensitivity on unknowns that the modeler wants to predict with high accuracy [9, 10]. However, the calculated sensitivity coefficients are only of first order accuracy and they may fail to predict, what happens if a species or a reaction is removed from a reaction mechanism. In addition the calculation of sensitivity coefficients is demanding in CPU-time. It is therefore often proposed to detect candidates for removal by reaction flow analysis, only. All strategies demand that the detailed reaction mechanism is first analyzed by a simple reactor model, for the chemistry flow interaction. Further it is demanded that the reduced reaction mechanism is validated against the detailed mechanism. The range of validity of the reduced mechanism is limited by the parameter range for the validation calculations, and by the physical importance of the employed reactor model.

A shortcoming of the necessity analysis is that it is not able to reduce the number of species or reactions in reaction systems, where the chemical flux occurs in many parallel and equally strong paths. This is the situation found for automatic generated reaction mechanisms for low temperature kinetics of aliphatic hydrocarbon fuels. In this situation the chemical lumping can lead to simplified reaction mechanisms [4, 5].

Instead of solving differential equations for the individual species one differential equation for the sum of the lumped species is solved. From this equation, the rate coefficients for the new (or general) species can be calculated. However, it is often necessary to estimate the ratio of concentrations of the lumped species [11]. This is possible if they have similar thermodynamic properties–they have almost equal concentrations.

The quasi steady state assumption (QSSA) is often applied in chemical systems. In combustion system it demands that the chemical processes are much faster than the relevant physical processes. [12] With computational singular perturbation (CSP) the set of equations governing the chemistry is described by a set of base vectors. The resulting eigenvalue problem allows the separation of fast and slow modes. Species found in the fast modes only are in steady state [13–15].

Another way to detect steady state species is to compare the chemical time of species consumption with the physical times of change in species concentration, convection and diffusion [16]. This species lifetime does not take coupled lifetimes into account. It assumes that the Jacobian matrix is diagonal [17].

Species concentrations can be solved from a set of algebraic equations if the QSSA is applied. This decreases the number of species that need to be transported in a CFD application, and thereby the demand on CPU-time and memory. In estimating how much a numerical error in species profile influences the accuracy of a target of a model calculation the sensitivity analysis, as described above can be applied [16]. In this application, sensitivity analysis gains a higher accuracy, since the error in the steady state species profile should be low; the influence of non-linearity in the sensitivity coefficients can be neglected. More steady state species can be detected, by combining the lifetime analysis with sensitivity analysis.

By using CSP fast and slow modes can be separated. A chemical system will move on the fast modes to a lower dimensional manifold, if it is started at any point in the number of species-dimensional chemical hyperspace. The development on the fast modes can be often described as a projection of the starting point on the low-dimensional manifold. A strong reduction in computational time is gained, if the intrinsic low-dimensional manifold (ILDM) is tabulated. This tabulation is done in a pre-process [18].

Conclusion

A variety of algorithms have been developed during the recent years that help the developer to generate, optimize and reduce reaction mechanisms for combustion applications. These developments build on each other and allow a fast knowledge transfer from chemical kinetic development to engineering applications. It got visible that a combination of these tools will allow computer aided design of chemical mechanism for technical applications in the near future.

References

[1] Warnatz, J, Maas, U. And Dibble, R.W., (1996), Combustion, Springer Verlag.

[2] Curran, H.J., Gaffuri, P., Pitz, W.J., and Westbrook, C.K., Combust. Flame, **114**:149–177 (1998).

[3] Tomlin, A.S. and Turnyi, T. and Pilling, M.J. (1997), "Mathematical tools for construction, investigation and reduction of combustion mechanisms", in : M.J. Pilling (Ed.), "Low-Temperature Combustion and Autoignition", Comprehensive Chemical Kinetics, Vol. 35, Elsevier.

[4] Ranzi, E., Faravello, T., Gaffuri, P., and Sogaro, A., Combust. Flame, **102**:179–192 (1995).

[5] Fournet, R., Warth, V., Glaude, P.A., Côme, G.M., Battin-LeClerc, F., and Scacchi, G. Int. J. Chem. Kin., **32**(1):36–51 (2000).

[6] Frenklach, M., Hai, W., and Rabinowitz M.J., Prog. Energy Combustion. Sci., **18**:47–73 (1992).

[7] Wang, H., Proc. Comb. Inst., **28**: (2000)

[8] Wang, H., and Frenklach, M., Combust. Flame **87**:365–370, (1991)

[9] Chen, J.Y., "Development of Reduced Mechanism for Numerical Modelling of Turbulent Combustion", Workshop on "Numerical Aspects of Reduction in Chemical Kinetics", CERMIPS-ENPS Cite Desortes – Campus sur Marne, France, 1997

[10] Soyhan, H.S., Mauss, F., and Sorusbay, C., Combust. Sci. Tech., **174**(11&12):73–91 (2002)

[11] Ahmed, S. S., Moréac, G., Zeuch, T., and Mauss, F., "Efficient lumping technique for the automatic generation of n-Heptane and iso-Octane oxidation mechanism", Prep. Pap.-Am. Chem. Soc., Div. Fuel. Chem. 2004

[12] Peters, N., and Rogg, B. (Eds.), "Reduced Kinetic Mechanism for Applications in Combustion Systems", Lecture Notes in Physics m15, Springer Verlag, 1993

[13] Lam, S.H., and Goussis, D.A., Prodc. Combust. Inst. **22**:931–941

[14] Lam, S.H., and Goussis, D.A., in "Reduced Mechanism and Asymptotic Approximations for Methane-Air Flames" (Smooke, M. Ed.), Lecture Notes in Physics 384, pp. 227–242, Springer Verlag, 1991

[15] Goussis, D.A., J. Comp.Physics, **128**:261–273, (1996)

[16] Lovås, T., Nilsson, D., and Mauss, F., Proc. Comb. Inst. **28**:1809–1815 (2000)

[17] Lovås, T., Amnèus, P., Mauss, F. and Mastorakos, E., Prodc. Comb. Inst. **29**:1387–1393 (2002)

[18] Maas, U. (1998), Efficient Calculation of Intrinsic Low Dimensional Manifolds for Simplification of Chemical Kinetics, Comput. Visual Sci. Vol. 1, pp. 69-81.

New Methods for Predictive Chemical Kinetics

William H. Green, Binita Bhattacharjee, Oluwoleo Oluwole, Jing Song, R. Sumathi, Catherina D. Wijaya, Hsi-Wu Wong, Paul E. Yelvington, & Joanna Yu

MIT Department of Chemical Engineering, Cambridge, MA 02319

Introduction

In most reactive fuel chemistry problems, there are far too many species and reactions for there to be any hope of experimentally determining the thermochemistry of each species and the rate constants of each reaction. Historically, modelers have modeled these systems empirically, constructing a small kinetic model with a few effective parameters which could be regressed from experiment. However, these small kinetic models usually do not capture the real chemistry/physics of the system, and so these models are typically only useful for interpolation, not for extrapolation or predictive design of new systems.

Recently, quantum chemistry has advanced so much that it can provide reliable values of missing rate and thermochemical parameters, at considerably less cost than determining the same values experimentally. However, these calculations are still rather difficult and unreliable, each requiring considerable care and attention. So it is not practical to compute every rate constant and thermochemical parameter that might conceivably be important in a fuel chemistry system.

Even if accurate values of all the rate constants and thermochemical parameters were available, it is still very challenging to construct and solve the appropriate kinetic models. Solving the models is particularly difficult in systems which are spatially inhomogeneous, where the chemistry is significantly coupled to transport.

Many researchers [1] have attempted to move forward in this way:
1) use the computer to construct an approximate kinetic model using approximate rate parameters
2) use this approximate model to identify the most important reactions and species
3) refine the rate parameters for the most important reactions using experiment or quantum chemistry
4) construct smaller kinetic models faithful to the original
5) use the small models in the coupled chemistry-transport simulations.

However, although this concept has been pursued by several research groups in both industry and academia, progress has been rather slow, since each step in the process involves several difficult issues, both from the point of view of chemistry, and from the point of view of computer science/numerics. This preprint reports significant progress we have made on all fronts, based on a radically different software design of the mechanism generation software, a new approach to estimating the reaction rates, and recent advances in numerical algorithms.

Results

A new software paradigm for automated mechanism generation has been developed, which cleanly separates the computer science and chemistry aspects of automated mechanism generation. The key idea is that all of the chemical detail is represented by functional group and reaction template structures and associated parameters. The computer then compares these functional group structures with each molecule in the system, to determine which molecules can react in which ways. The rate and thermochemical parameters are also based on these functional groups. The new approach has the major advantage that chemists can extend and update functional group definitions and reaction rate or thermochemistry estimates without ever touching the source code. This is very important, since our understanding of chemistry is far from complete, and it will be many years before accurate estimates will be available for all the types of reactions important in fuel chemistry. The computer science and numerical aspects of the problem are handled by a robust black box code, while the assumptions made about the chemistry are clearly visible, unambiguous, and easy to document.

Known reaction rates and thermochemistry are stored in an extensible library, and unknown reaction rates and thermochemistry are estimated based on functional group additivity. Classic Benson-type group additivity has been extended to include transition states (to predict rates).[2] This requires the use of larger functional group templates than the simple atom-centered Benson groups. This more flexible group concept is also found to be very useful for estimating the thermochemistry of polycyclic aromatics – using bond-centered groups rather than traditional atom-centered groups doubles the accuracy of the estimation procedure. Several hundred new group values have been determined using quantum chemical methods, some reported elsewhere[3,4,5] and carefully organized into tree structures to avoid ambiguity and to speed computation times. We plan to make these tree structures and the associated parameters publicly accessible over the internet, so that chemists anywhere on the globe can easily improve the estimates.

The new Java software package that implements this new concept, RMG, includes several state-of-the-art features, including on-the-fly computation of k(T,P) using the efficient and accurate algorithm developed by D.M. Matheu et al..[6,7] The software architecture of RMG is considerably different than previous reaction mechanism generation programs, being completely object-oriented, and documented structured using UML.

The large kinetic models generated by RMG can be automatically and optimally reduced to any desired size using the algorithm of Bhattacharjee et al..[8] Valid ranges of the both the large and the reduced models are automatically estimated using a new rigorous method. The reduced models are very useful in reacting flow simulation and in other compute-intensive applications. Several numerical issues arise when using large kinetic models, particularly when coupling them into reacting flow simulations. In particular, it has been found very helpful to take advantage of the inherent sparsity of the Jacobians of large kinetic models [9], and to use operator-splitting methods which converge to the correct solution (rather than popular methods which have $O((\Delta t)^2)$ errors at convergence, since these errors can be very large if the chemistry is stiff).[10] Very recently, new global optimization algorithms have been developed which can guarantee error tolerances over a continuous range of reaction conditions [11], and these allow one to rigorously control the errors introduced by using reduced models rather than the full model.

In some situations, one does not want to simulate a specific known system, but rather to determine an upper bound on what is possible in any process of a particular type. We have run several examples of these upper bound calculations for catalytic oxidations, where the energetics of the surface intermediates are unknown.[12] This problem, the model reduction and range analysis problem, and a variety of safety/operability problems are mathematically related:

they all can be written as types of semi-infinite programs (i.e. optimization problems with an infinite number of constraints). Recent algorithmic advances using interval analysis [11] will allow significant advances in solving all these problems.

Conclusions

The new extensible modular design of mechanism generation software promises to greatly accelerate progress towards predictive chemical kinetics for problems in fuels chemistry. The computer-constructed kinetic models based on a library of small molecule reactions and group-additivity-based estimates of rate and thermochemistry of larger molecules are already quite accurate [7], and the accuracy can be refined by use of sensitivity analysis to identify which rate constants and thermochemical parameters merit further study. The extensible and unambiguous format should encourage community-wide efforts to improve the accuracy of the rate estimates, and to broaden the range of chemistry which can be modeled.

Advances in numerics and computer science are needed to parallel improved understanding of the chemistry. Recent improvements in optimization algorithms and in methods for handling large systems of stiff differential-algebraic equations are keeping pace with our ability to construct large accurate kinetic simulations. Although reacting flow simulations are still very challenging, effective algorithms are becoming available. In most cases the accuracy of the simulations are limited more by our ignorance of the chemistry than by the approximations introduced in order to solve the differential equations.

As the simulations become more complex, a variety of additional software tools are needed to help humans check the accuracy of the models and to correctly interpret the model predictions. Our 20+ year old paradigm of kinetics assumes that a single human can construct, solve, and interpret an entire simulation, doing most of the steps by hand. As the simulations become more detailed, we need to move to a new paradigm that encourages teamwork, and where all of the "well-understood" aspects of the problem are automated, to allow the scientists and engineers to focus on the aspects and issues that are really unresolved.

Acknowledgements

The authors gratefully acknowledge financial support from the National Science Foundation, BP Chemical, and the Department of Energy.

References

[1] Tomlin, A.S; Turanyi, T.; Pilling, M,J.; in *Low Temperature Combustion and Auto-Ignition*, Pilling, M.J. ed., Elsevier (Amsterdam) **1997**, 293-437
[2] Sumathi, R.; Green, W.H. *Theor. Chem. Accts.* **2002**, *108*, 187.
[3] Sumathi,R.; Green, W.H. *J. Phys. Chem. A* **2002**, *106*, 7937.
[4] Sumathi, R.; Green, W.H. *J. Phys. Chem. A* **2002**, *106*, 11141.
[5] Sumathi, R.; Green, W.H. *Phys. Chem. Chem. Phys.* **2003**, *5*, 3402.
[6] Matheu, D.M.; Green, W.H.; Grenda, J.M. *Int. J. Chem. Kinet.* **2003,** *35*, 95.
[7] Matheu, D.M.; Dean, A.M.; Grenda, J.M.; Green, W.H. *J. Phys. Chem. A* **2003**, *107*, 8552.
[8] Bhattacharjee, B.; Barton, P.I.; Green, W.H. *Combust. Flame* **2003. (in press).**
[9] Schwer, D.A.; Tolsma, J.A.; Green, W.H.; Barton, P.I. *Combust Flame* **2002**, *128*, 270.
[10] Schwer, D.A.; Lu, P.; Green, W.H.; Semiao, V. *Combust. Theor. Modelling* **2003**, *7*, 383.
[11] Bhattacharjee, B.; Green, W.H.; Barton, P.I. *Computational Optimization and Applications* **2004** (in press).
[12] Su, Y.S.; Ying, J.Y.; Green, W.H. *J. Catalysis* **2003,** *218*, 321.

PRESSURE-DEPENDENT AUTOMATED MECHANISM GENERATION: SYSTEMATIC MODELS FOR DIFFICULT SYSTEMS

David M. Matheu[a], Anthony M. Dean[b], Jeffrey M. Grenda[c]

[a]National Institute of Standards and Technology
Physical and Chemical Properties Division
100 Bureau Dr. Stop 8380
Gaithersburg, MD 20899-8380

[b]Department of Chemical Engineering
Colorado School of Mines
451 Alderson Hall
Golden, CO 80401

[c]ExxonMobil Research and Engineering Company
1545 Rt. 22 East
Annandale, NJ, 08801

Introduction

Advancement in the design of such important gas-phase processes as hydrocarbon cracking, combustion, and partial oxidation hinges, in part, on the development of correct, detailed chemical kinetic models. But the complexity of the required chemical mechanisms can make them extremely difficult to construct by hand. Modelers turn to software algorithms that build these large mechanisms automatically (e.g. [1], [2]), but the current tools are too limited to treat many difficult systems. We present a new, elementary-step-based mechanism generation algorithm, called "XMG-PDep," which overcomes these limitations with a comprehensive approach to pressure-dependent reactions, and a rational, flux-based criteria for truncating mechanism growth. Applications to the previously intractable methane and high-conversion ethane pyrolysis systems yield predictions which agree well with experimental data, without any parameter adjustment. Important new pathways, not previously considered, but discovered entirely by the new approach, can explain unusual behavior in these systems, and suggest the power of this software tool.

Computational Method: The XMG-PDep Algorithm

XMG-PDep is based upon XMG [3], which developed from NetGen [4]. It employs flux-based termination of the otherwise combinatorial in species and reactions. To do this, the code periodically constructs and integrates the set of differential equations that represent the evolution of the reacting system in time (assuming a well-mixed batch reactor model). It evaluates a characteristic mechanism flux Rchar(t), which is similar to a root-mean-square average of chemical fluxes in the mechanism [5]. XMG-PDep then compares this flux with those to candidate species that have been discovered, but not yet included, in the mechanism. Those species whose fluxes exceed the cutoff flux (equal to a user-specified fraction of Rchar(t)) are included in the mechanism; the rest are not.

XMG-PDep can systematically discover and include arbitrary pressure-dependent reactions, using the algorithm of ref [6]. To allow the most flexibility, XMG-PDep considers any elementary step of the form $A + B \rightarrow C$, $B \rightarrow C$ or $B \rightarrow C + D$ to initiate a partial pressure-dependent network. For each partial network, XMG-PDep uses the QRRK/MSC code CHEMDIS [7] to estimate the k(T,P) values of every net pressure-dependent reaction. It also examines the maximum flux to all non-included portions of the partial pressure-dependent network. If this flux is greater than the cutoff flux, the partial network is "grown" by one isomer, with all its high-pressure-limit elementary steps, and the k(T,P) calculation is repeated. Growth of each partial pressure-dependent network is halted when the flux to non-included portions is less than the cutoff flux. In this way pressure-dependent reactions can be included systematically and rationally. A full description of the integrated algorithm for generating mechanisms is presented in ref. [8].

Finally, XMG-PDep includes a number of other features designed to make it accurate and useful. It employs literature-based libraries of rate constants and thermochemical parameters whenever possible. Its rate rules are subdivided as much as is reasonable to provide the best estimates for high-pressure-limit rates when these are not available from the library. Thermochemical data (when not available from the data library) are taken from a group contribution method [9] and used to ensure thermodynamic reversibility. The code will produce a CHEMKIN mechanism, and a number of analyses of the mechanism (such as the net radical rate of production for each reaction), when finished with generation.

Application to Methane and High-Conversion Ethane Pyrolysis

Methane pyrolysis has been extensively studied for many decades, both for its potential to convert methane to more valuable hydrocarbons, and its importance within larger combustion and pyrolysis mechanisms. But the strange, autocatalytic behavior of methane pyrolysis at extremely low methane conversion has defied mechanistic explanation for at least three decades. The most recent attempt, of Dean in 1990 [10], appeared successful until new thermochemical data for the cyclopentadienyl radical rendered its explanation inadequate.

Applying our tool with the rate rules and thermochemical data described in ref. [8] gives a mechanism which captures the low-conversion autocatalysis, without resort to parameter fitting or adjustment, as shown in Figure 1. The generator suggests that the autocatalytic behavior arises from a number of separate sources, none of which had been considered previously for these conditions. First, cyclopentadienyl radical, produced by the pressure-dependent addition of propargyl radical to acetylene, abstracts a hydrogen from methane to form cyclopentadiene. The cyclopentadiene in turn will dissociate easily to another H atom and cyclopentadienyl radical, causing chain-branching, or a net production of radicals. Second, the reverse disproportionation of methane and allene to form methyl radical and allyl radical plays an important chain-branching role, especially at early times. Finally, as an aggregated group, the set of all reverse disproportionations accounts for about 50% of the chain-branching.

Figure 2 shows a more comprehensive view of the pathways leading to autocatalysis. Many of these pathways are pressure-dependent and could not have been discovered by a tool without this capability. Further validation against other product data, and support for the mechanistic analysis, can be found in ref. [11].

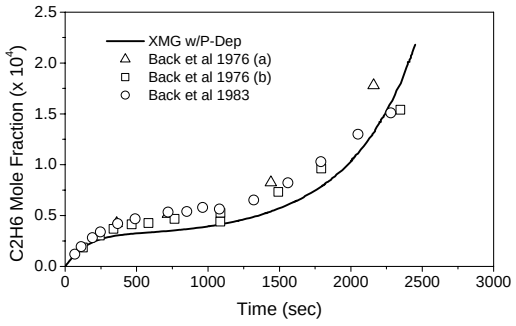

Figure 1. XMG-PDep predicted ethane concentration with time, during static batch pyrolysis of neat methane at 1038 K and 0.58 atm.

The prediction clearly captures the autocatalytic upturn in concentration as reflected in three experimental datasets [12-14].

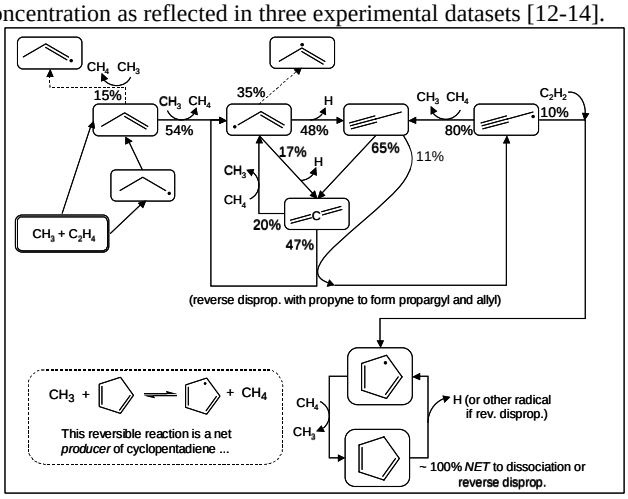

Figure 2. Partial depiction of pathways leading to autocatalysis in low-conversion methane pyrolysis. A number of these pathways are reverse disproportionations; as a whole, the set of all reverse disproportionations provides about 50% of the net radical production. A number of other important pathways (such as the addition of propargyl to acetylene, and the isomerization of allyl radical) are pressure-dependent.

High-Conversion Ethane Pyrolysis. Glasier and Pacey [15] used a laboratory flow reactor to study neat ethane pyrolysis at very high conversion (>98%, 900-1200K, 0.4 atm), in an effort to correlate the concentrations of proposed "soot precursors" with the formation of pyrolytic (deposited) carbon. No existing detailed kinetic mechanism exists for these conditions; the high conversion and large number of pathways make this system extremely difficult to consider by-hand. That fact, coupled with the detailed data available for minor products, makes this experimental work a good but challenging example case for our algorithm. Our generated model's agreement with the data is quite good (as seen in Figures 3 and 4), considering that once again no parameters were adjusted to fit the data, and all steps in the mechanism are "from scratch".

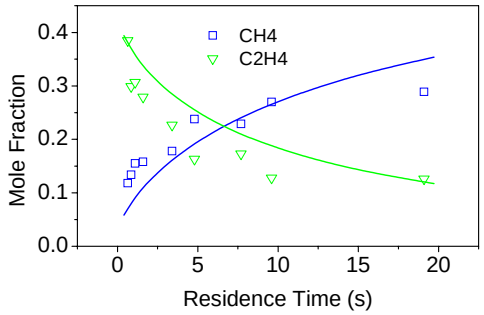

Figure 3. CH_4 and C_2H_4 concentrations with residence time in the Glasier and Pacey flow reactor. Symbols are experimental data points; lines are auto-generated model predictions.

Pathway analysis of the very large mechanism generated for this system suggests that the fates of the minor products, and some major ones, are governed in part by a large and complex set of interconnected reactions. Conventional mechanisms do not capture some of these pathways. Although the Glasier and Pacey system was chosen as a difficult example which would test the limits of strictly elementary-based, gas-phase mechanism generation, the resultant model for these unusual conditions may also prove useful as a base for the understanding of aromatics and soot formation.

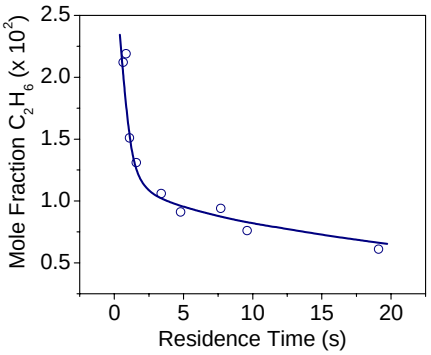

Figure 4. Experimental and predicted ethane concentration with residence time.

Discrepancies in the predictions of H_2 and benzene (not shown here) imply that XMG-PDep is missing whole reaction families for generation, though other explanations (such as globally incorrect rate rules, thermochemistry, or heterogeneous reactions) cannot be ruled out. The lack of good, publicly-available tools for understanding large (>1000 reaction) mechanisms severely hampers the analysis.

Conclusions. The XMG-PDep algorithm for building reaction mechanisms "from scratch", including pressure-dependence, shows promise in helping kineticists understand highly complex systems that could not otherwise be studied easily. The tool suggests new pathways that explain behavior in both of the "demonstration" systems; further work will involve systems of more industrial importance.

References

1. Wauters, S.; Marin, G. B. *Chem. Eng. J.* **2001**, *82*, 267-279.
2. DeWitt, M. J.; Dooling, D. J.; Broadbelt, L. J. *Ind. Eng. Chem. Res.* **2000**, *39*, 2228-2237.
3. Grenda, J. M. ; Androulakis, I. P.; Dean, A. M.; Green, W. H. Jr. *Ind. Eng. Chem. Res.* **2003**, *42*, 1000-1010.
4. Susnow, R. G.; Dean, A. M.; Green, W. H.; Peczak, P.; Broadbelt, L. J. *J. Phys. Chem. A* **1997**, *101*, 3731-40.
5. Song, J.; Stephanopoulos, G.; Green, W. H. *Chem. Eng. Sci.* **2002**, *57*, 4475-4491.
6. Matheu, D. M.; Lada, T. A.; Green, W. H.; Grenda, J. M.; Dean, A. M. *Comp. Phys. Comm.* **2001**, *138*, 237-249.
7. Chang, A. Y.; Bozzelli, J. W.; Dean, A. M. *Z. Phys. Chem.* **2000**, *214*, 1533-1568.
8. Matheu, D. M. *Integrated Pressure-Dependence in Automated Mechanism Generation: A New Tool for Building Gas-Phase Kinetic Models*, Ph.D. Thesis, Massachusetts Institute of Technology, **2002**.
9. Grenda, J. M. and Bozzelli, J. W., "Automated Elementary Reaction Mechanism Generation Incorporating Thermochemistry, Fall-off, and Chemical Activation Reactions of OH with Olefins, A6," *5th Int. Conf. Chem. Kin.*, Gaithersburg, MD, **2001**.
10. Dean, A. M. *J. Phys. Chem.* **1990**, *94*, 1432-39.
11. Matheu, D. M., Dean, A. M., Grenda, J. M., and Green, W. H. Jr. *J. Phys. Chem. A* **2003**, 107, 8552-8567.
12. Chen, C. J.; Back, M. H.; Back, R. A. *Can. J. Chem.* **1976**, *54*, 3175-3184.
13. Chen, C. J.; Back, M. H.; Back, R. A. *Can. J. Chem.* **1975**, *53*, 3580.
14. Chen, C. J.; Back, M. H.; Back, R. A. *Can. J. Chem.* **1977**, *55*, 1624-1628.
15. Glasier, G. F.; Pacey, P. D. *Carbon* **2001**, *39*, 15-23.

SIMULATION OF LIGHT PETROLEUM FRACTIONS

Tareq A. Albahri

Chemical Engineering Dept. - Kuwait University
P.O.Box 5969 - Safat 13060, Kuwait
albahri@kuc01.kuniv.edu.kw

Introduction

Petroleum refiners have not traditionally considered their products on a molecular basis but rather they have modeled and marketed their products as volatility fractions (e.g. gasoline, kerosene, and fuel oil). Current simulation procedures resort to pseudo-component approaches which suffer from many limitations. This work focuses on the development of a molecularly explicit characterization model (MECM) that will allow the simulation of the molecular composition of petroleum fractions using a pre-selected set of pure components. Such molecular-level characterization of petroleum fractions will allow us to simulate the physical separation processes and the chemical reaction processes, as well as allow for catalysts such as zeolites to be designed and optimized for processing complex, multicomponent mixtures such as petroleum.

Technical Development

The concept of the proposed model is that the global properties of a petroleum fraction such as the boiling point, specific gravity, vapor pressure, etc. must be equal to those calculated from the pure components contained in that petroleum fraction. When both bulk and pure component properties are available, the composition of the petroleum fraction may be predicted using optimization algorithms as simplified in Figure 1.

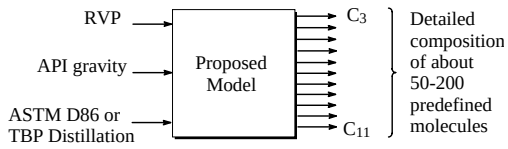

Figure 1. Simplified schematic representation of the proposed model.

Since petroleum fractions contain thousands of molecules the concentration of which is hard or even impossible to measure, it is imperative to simulate such mixtures using a limited set of pure components to avoid prohibitively extensive computation time during kinetic modeling or rigorous phase equilibrium calculations.

The minimum input properties for the model are the true boiling point (TBP), the API gravity, and the Reid vapor pressure (RVP). The internally calculated properties are the molecular weight, the true vapor pressure at 100°F, the specific gravity, the cubic average boiling point (CABP), the mean average boiling point (MeABP), the volumetric average boiling point (VABP), the weight average boiling point (WABP), the molar average boiling point (MABP), the Watson characterization factor (K_w), the refractive index, the carbon to hydrogen ratio (C/H), the kinematic viscosity at 100 and 210°F, the surface tension, the aniline point, the true and pseudo critical temperatures and pressures, the critical compressibility factor, the acentric factor, the freezing point, the heat of vaporization at the normal boiling point, the net heat of combustion at 77°F, the isobaric liquid heat capacity at 60°F, the isobaric vapor heat capacity at 60°F, the liquid thermal conductivity at 77 ºF, and the paraffins, naphthenes, and aromatics content. These properties are calculated for the petroleum fraction using well established methods in the literature or were developed specifically for this project. For example, the molecular weight for the light petroleum fraction is calculated from the boiling point and the specific gravity using the following API recommended equation[1],

$$MW = 42.965\,(T_b^{1.26007}\,S^{4.98308})\,[\exp(2.097.10^{-4}\,T_b - 7.78712\,S + 2.08476.10^{-3}\,T_b\,S)] \quad (1)$$

Whereas the same is calculated from the pure component composition using the following simple mixing rule,

$$MW=\sum_{i=1}^{n}(MW)_i(x)_i \quad (2)$$

When the pure component properties are not available in databases they can be estimated using group contribution methods available in the literature or others developed specifically for this project.

The difference between the values obtained from equations 1 and 2 for the molecular weight in addition to other equations and mixing rules for the other properties are minimized in the objective function (second line of Equation 3) the purpose of which is to calculate the values of x_i which is the mole fraction of the pure components in the petroleum fraction.

The First line in the objective function represents the sum of errors in the boiling points of the pure components and the corresponding value on the true boiling point (TBP) curve as shown in Figure 2.

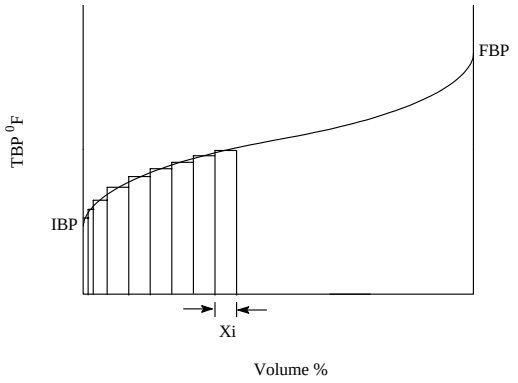

Figure 2. Simulation of a true boiling point (TBP) curve using real components.

The pure component concentrations are determined by minimizing the following objective function,

$$S = \sum_{j=1}^{n}\left((Tb_j - Tb'_j)\times W_o \times 100/Tb_j\right)^2 + \sum_{i=1}^{P}\left((Y_i - Y'_i)\times W_i \times 100/Y_i\right)^2 \quad (3)$$

where i is the index number of the physical property, j is the index number of the molecule, P is the total number of physical properties considered (except boiling point), and n is the total number of molecules. Y_i and Y'_i refer respectively to the actual and predicted property i. T_{bj} and T'_{bi} refer respectively to the boiling point of the pure component *j* and the corresponding value on TBP curve. W_i and W_o are weighting factors and S is the objective function to be minimized.

An optimization algorithm based on the least square method was used to minimize the objective function while calculating the concentration of the pure components. The nonlinear regression algorithm minimizes the sum of the difference between the fuels bulk properties and those estimated from pure components. Using the Microsoft Excel Solver tool and the Generalized Reduced Gradient (GRG2) nonlinear optimization code, convergence was achieved in less than one minute for all cases on a Pentium IV-1.7 GHz PC.

Discussion

The model was tested to simulate the separation process in an industrial naphtha splitter producing light and heavy naphtha from a Hydrocracked naphtha feed according to the validation procedure shown in Figure 3. In one run we used the ASTM D86 distillation data as the input assay for the feed naphtha. In another run we used the detailed hydrocarbon concentrations calculated using the proposed MECM model shown in figures 4 and 5. The MECM model results for the light and heavy naphtha products correlated better with the experimental ASTM D86 distillation data than those using the pseudo-component method incorporated in the HYSYS process simulator.

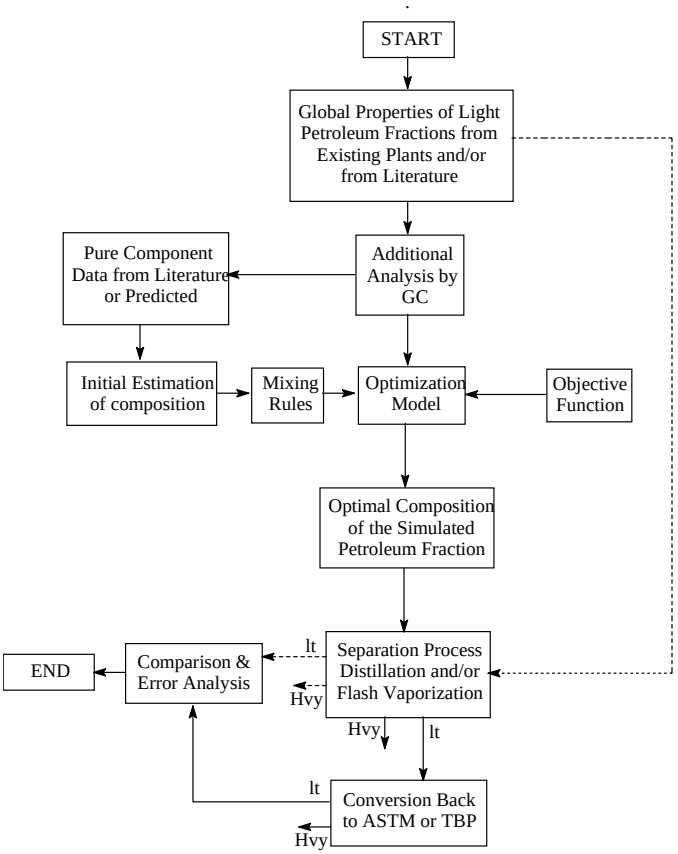

Figure 3. Flow Chart for the methodology used in the proposed model.

The MECM model proves to be a powerful tool for simulating the composition of petroleum fuels. The clear advantage of the method is that the list of pure components used may be tailored to include more or fewer components as needed by the user, to accommodate specific needs, which is an added advantage.

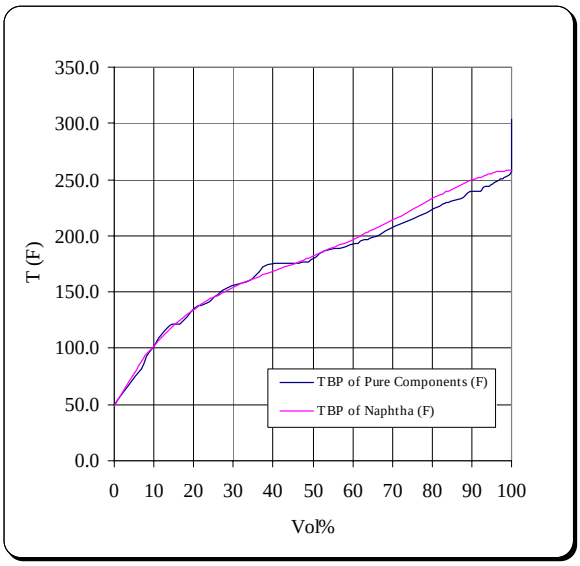

Figure 4. Comparison of Naphtha TBP and Simulated TBP from pure components.

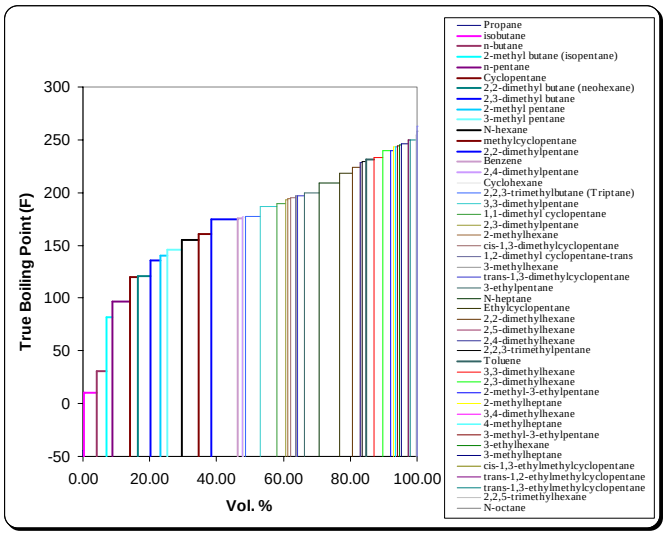

Figure 5. Calculated composition of representative model pure components

This work demonstrates that the complex nature of petroleum fuels may be modeled by a limited set of representative pure components using non-linear-regression optimization models. Considering the difficulty and complexity of accounting for the thousands of compounds in petroleum fuels and the limitations of the pseudo component technique, the proposed method can be an effective alternative.

Acknowledgment

This work was supported by Kuwait University, Research Grant No. EC04/01.

References

[1] Wauquier, J. -P. "Petroleum Refining 1', Editions Technip, Paris, **1995**.

OPTIMIZATION AND CONSISTENCY OF A REACTION DATASET

M. Frenklach, R. Feeley, A. Packard

Department of Mechanical Engineering, University of California at Berkeley, Berkeley, CA 94720-1740

and P. Seiler

Department of Mechanical and Industrial Engineering, University of Illinois at Urbana-Champaign, Urbana, IL

Understanding a variety of natural phenomena and industrial processes relies on the knowledge of chemical reaction mechanisms and kinetics. Endeavor in such cases begins with identification of underlying reaction pathways and fundamental mechanisms. When sufficient data accumulate, the interest often shifts to practical applications, motivating the development of mechanistic models.

The "textbook" approach to the development of mechanistic reaction models consists in conjecturing the reaction mechanism, expressing it in a suitable mathematical form, and comparing the predictions of the constructed model to available experimental observations. Typically, such tests result in a mixed outcome, some showing a reasonably close agreement and some not. The apparent inconsistency between the model and experiment obtained in the latter case is argued then to imply either that the model is inadequate or that the experiment (or rather its interpretation) is incorrect.

In some areas, such as heterogeneous catalysis and biochemical systems, the fundamental reaction mechanisms are largely unknown and establishing them form the challenge of the current research. Yet, in other fields, such as atmospheric chemistry and combustion of small hydrocarbons like methane, there are broad consensus over the reaction pathways underlying the mechanisms and the inadequacy of the kinetic models essentially rests in their parameter values. In the following we assume the latter situation.

If the kinetic parameters of such a "known" mechanism were known exactly, then a direct comparison of model prediction with a given experiment, within its uncertainties, would decisively indicate whether that experiment is consistent or inconsistent with the model. In reality, however, the model parameters themselves have uncertainties, and they have to be included in the analysis.

In principle, the parameter identification of chemical kinetic models can be posed as classical statistical inference: given a mathematical model and a set of experimental observations for the model responses, determine the best-fit parameter values, usually those that produce the smallest deviations of the model predictions from the measurements. The validity of the model and the identification of outliers is then determined using analysis of variance. The difficulty of applying standard statistical methods lies in the fact that chemical kinetics models are stated in the form of differential equations that do not possess a closed-form solution. Further complications arise from the highly "ill-structured" character of the objective function, with long and narrow valleys, resulting in ill-conditioned optimization and lack of unique solution.

The optimization problem for general, non-linear dynamic models has been addressed with a series of numerical methods: "direct" gradient search, gradient search based on sensitivities, solution mapping, genetic algorithms, and Monte Carlo techniques. In some cases, it was coupled with statistical inference and estimation of confidence regions. Recent developments also include formulation of the problem in the form of error propagation: given a set of uncertainty ranges of model parameters, estimate the intervals of variations for model predictions.

All of the above methods essentially view the problem as a two-step process: estimation of model parameters from fitting a selected set of experimental data followed by exercise of the obtained model, either as validation against an additional set of experiments or making predictions outside the experimentally accusable conditions.

Recently, we have pursued a different approach, which we call *data collaboration*.[1] In this approach we focus not on parametrization of the parameter uncertainty region, which the above methods engage in and rely upon, but rather on transferring the uncertainties of the "raw" (experimental) data into the model *directly*.[2] Doing so allows harvesting substantially more of the information content of the data, and to obtain more realistic bounds of model predictions. Our approach is anchored in the concept of a *dataset* that unites all the pertinent experimental data and the mechanistic knowledge for a given system, and the numerical analysis is based on combination of Solution Mapping and new developments of the Robust Control Theory. This numerical methodology avoids unnecessary over-constraining of model parameters, which plagues many other techniques due to inherent correlations among parameters, while exploring more closely the true *feasible set* of the parameter space in a computationally efficient manner.

The present work expands further on these ideas. New mathematical developments allow us to address the mutual consistency of experimental observations, within the framework of a dataset.

Acknowledgement. The work was supported by National Science Foundation, Information Technology Research Program, Grant No. CTS-0113985.

References

(1) Frenklach, M.; Packard, A.; Seiler; P.; Feeley, R. *Int. J. Chem. Kinet.* **2004**, in press.

(2) Frenklach, M.; Packard, A.; Seiler; P. In *Proceedings of the American Control Conference*, IEEE Catalog Number 02CH37301C, 2002, pp. 4135-4140.

REACTIVITY EXTRAPOLATION FROM SMALL TO LARGE MOLECULAR SYSTEMS VIA ISODESMIC REACTIONS FOR TRANSITION STATES (RESLIR)

Vadim D. Knyazev

Research Center for Chemical Kinetics, Department of Chemistry
The Catholic University of America, Washington, DC 20064
and
National Institute of Standards and Technology
Physical and Chemical Properties Division, Gaithersburg, MD 20899

Introduction

Numerous applications of chemistry benefit from computational methods of exploring reactivity. Quantum chemistry based techniques of evaluating reaction energy barriers, however, encounter problems when large molecular systems are considered. A number of high-level quantum chemical methods are capable of providing accuracy in evaluating reaction barriers on the order of 1 – 3 kcal mol^{-1}, which is sufficient for many (although not all) practical applications. Unfortunately, these methods are rarely used for the computational treatment of practical systems as they are generally applicable only to relatively small molecules. The computational resources required to use these methods scale as N^7 (where N is the number of atoms in the molecular system considered), making their use impossible in most cases of practical interest. The N^7 scaling also means that, even with the fast pace of progress in the development of computer hardware, one cannot expect a major improvement of these size limitations within the observable future.

Here, a method of evaluating barriers of chemical reactions involving large molecules is presented. The method is based on the extrapolation of reactivity from small molecular systems (for which high-level quantum chemical calculations can be performed) to large ones via low level (and thus low computational cost) calculations. The notation RESLIR (abbreviation of "Reactivity Extrapolation from Small to Large molecular systems via the formalism of Isodesmic Reactions for transition states") is proposed for ease of reference. The RESLIR method is a further development of the technique of isodesmic reactions for transition states (IRTS),[1,2] which has been demonstrated to yield very high accuracy in predicting reactivity in two classes of atom abstraction reactions.

Method Description

Background (IRTS[1,2]) Isodesmic reactions,[3] i.e., (usually) fictitious reactions which conserve the types of chemical bonds and their numbers, are often used in computational thermochemistry (e.g., refs 4-9). Enthalpies of these reactions are usually obtained in quantum chemical calculations and it is expected that computational errors that are specific to a particular bond type will, to a large extent, cancel on both sides of the chemical equation. The IRTS method[1,2] applies the same formalism to transition states. For example, for any two reactions of the same class expressed via chemical equations

$$\text{Reactants}(1) \rightarrow (\text{TS}(1)^{\ddagger}) \rightarrow \text{Products}(1) \quad (1)$$

$$\text{Reactants}(2) \rightarrow (\text{TS}(2)^{\ddagger}) \rightarrow \text{Products}(2) \quad (2)$$

one can write a formal isodesmic reaction

$$\text{Reactants}(1) + \text{TS}(2)^{\ddagger} = \text{Reactants}(2) + \text{TS}(1)^{\ddagger} + \Delta\text{H}(\text{ISO}) \quad (3)$$

provided that the class of reactions is defined by the similarity of the chemical transformations taking place and the structures of the transition states ($\text{TS}(i)^{\ddagger}$ where i in the reaction number).

In the IRTS technique, first, the energy barrier E(Ref) for one of the reactions within the reaction class (a "reference" reaction) is evaluated on the basis of reliable experimental data on the temperature dependence of the reaction rate constant, k(T). Then, for all other reactions within the class, formal isodesmic reaction schemes of the type

$$\text{Reactants}(i) + \text{TS}(\text{Ref})^{\ddagger} = \text{Reactants}(\text{Ref}) + \text{TS}(i)^{\ddagger} + \Delta\text{H}(\text{ISO}(i)) \quad (4)$$

are written and their 0 K enthalpies, $\Delta\text{H}(\text{ISO}(i))$, are obtained in quantum chemical calculations. Here, Reactants(Ref) and $\text{TS}(\text{Ref})^{\ddagger}$ are the reactants and the transition state for the "reference" reaction and i is the reaction number. Finally, energy barriers for all cognate reactions are calculated using the values of E(Ref) and $\Delta\text{H}(\text{ISO}(i))$:

$$\text{E}(i) = \text{E}(\text{Ref}) + \Delta\text{H}(\text{ISO}(i)) \quad (\text{I})$$

The values of $\Delta\text{H}(\text{ISO}(i))$ are expected to be accurate due to cancellation of errors on both sides of the chemical equation (4); this accuracy is expected to propagate into the values of E(i). Note that for any two reactions within the class (reactions 1 and 2), the 0 K enthalpy of the isodesmic reaction (3) equals the difference in the energy barriers of these reactions. Thus, the primary postulation of the IRTS technique is equivalent to the assumption that, although a particular quantum chemical method may not yield accurate absolute values of energy barriers, differences between the energy barriers of individual reactions can be calculated with a high degree of accuracy for a series of reactions of the same type.

The RESLIR method The RESLIR method is based on the use of the IRTS technique to extrapolate reactivity from small to large molecular systems within the same class of reactions. Unlike the previous applications[1,2] of the IRTS technique, it does not rely on the existence of extensive experimental information on the kinetics of at least one reaction within the class. Instead, high-level predictive calculations are performed for the reference reaction, which is chosen in such a way as to include only small molecules.

The algorithm of the RESLIR method is as follows.

1. A class of reactions is defined by the similarity of the chemical transformations occurring and the structures of the transition states. This class includes reactions involving both small and large molecules.
2. Within this class, a "reference" reaction involving only molecules of small sizes is chosen.
3. Two quantum chemical methods of different levels are selected: a low-level (LL) method and a high-level (HL) method.
4. High-level quantum chemical calculations are performed for the "reference" reaction to evaluate its energy barrier.
5. For other reactions of interest within the same class, including reactions involving large molecules, isodesmic reaction schemes of the type given by equation 4 are designed. 0 K enthalpies of these reactions, $\Delta\text{H}(\text{ISO}(i))$, are computed at the low level of theory.
6. Finally, energy barriers of the reactions of interest are calculated using the relationship of equation I.

The notation RESLIR(HL|LL) is proposed to indicate the HL and the LL methods used within the RESLIR algorithm.

Evaluation of Method Performance

Diels-Alder Reactions The RESLIR method was applied to calculation of energy barriers for a series of eleven Diels-Alder reactions involving molecules of various sizes, ranging from C_6H_{10} to $C_{12}H_{16}O_3$ for reaction products and transition states. The simplest of these reactions, that of cycloaddition of ethylene to butadiene, was

used as the "reference" reaction. A large body of experimental information on the temperature dependences of the rate constants of these reactions in the gas phase exists on the literature (e.g., see ref 10 and references cited therein.). Moreover, it is known that the kinetics of Diels-Alder reactions in non-polar solvents is not influenced by solvent effects; the same values of the rate constants have been obtained for some of these reactions in the gas and in the liquid phases. Thus, it is possible to use both the liquid phase[11] and the gas phase[10] kinetic information to compare theory and experiment.

In this work, the "experimental" values of the reaction energy barriers were derived from the experimental data on the reaction rate constant dependences using transition state theory models based on the molecular structures and frequencies obtained in calculations using the same (low-level) quantum chemical method. The calculated energy barriers were obtained using the RESLIR technique with the QCISD(T)/aug-cc-pvtz(extrapolated)//QCISD/cc-pvdz method as the high-level quantum chemical method. Here the QCISD(T)/aug-cc-pvtz(extrapolated) energies were obtained in a basis set extrapolation scheme via the following formula:

$$\text{QCISD(T)/aug-cc-pvtz(extrapolated)} = \text{QCISD(T)/aug-cc-pvdz} + (\text{MP2/aug-cc-pvtz} - \text{MP2/aug-cc-pvdz}) \quad \text{(II)}$$

For the low-level quantum chemical methods, the HF/6-311G(d)-level geometry optimization and energy calculation was used and, in addition, two different single-point-energy methods were used with the HF/6-311G(d)-level structures: BH&HLYP/cc-pvtz and MP2/6-311G(d,p).

For all three HL|LL combinations used, the application of the RESLIR algorithm resulted in significant improvement of the agreement between calculation and experiment compared with the results obtained at the LL methods alone. Figure 1 demonstrates the results obtained with LL= HF/6-311G(d). Here, the calculated values of the energy barriers are plotted as a function of those derived from the experimental data. The open symbols represent the barriers obtained at the LL level of quantum chemistry without the use of the RESLIR method. At this level, the barrier values are completely unrealistic. The filled symbols display the barriers obtained with the RESLIR method. As can be seen from the plot, application of the RESLIR method results in dramatic improvement of the agreement.

The average absolute deviations between calculations and experiment are 2.6, 2.5, and 3.1 kcal mol^{-1} for LL = HF/6-311G(d), LL = BH&HLYP/cc-pvtz//HF/6-311G(d), and LL = MP2/6-311G(d,p)//HF/6-311G(d), respectively. The maximum deviations are 7.2, 6.8, and 6.1 kcal mol^{-1}, respectively.

It should be noted that ideal agreement between the calculated barriers and those derived from the experimental rate data is not expected because of the finite accuracy of the determination of the "experimental" barrier values. The latter were derived from transition state theory fits to the experimental k(T) dependences. Since calculated preexponential factors, generally, do not provide perfect agreement with experiment, uncertainties in the preexponential factors propagate into the uncertainties in the derived values of the energy barrier. The "error limits" of the filled data points on the plot indicate the range of the expected uncertainties in the "experimental" energy barriers caused by the imperfect description of the preexponential factors. These "error limits" should be taken as pertaining not to individual data points but rather to the whole group of reactions, approximately indicating the range of uncertainty associated with the determination of the "experimental" reaction barrier values.

Other reactions Evaluation of the performance of the RESLIR method in other reactions, such as addition of radicals to double bonds, are currently underway.

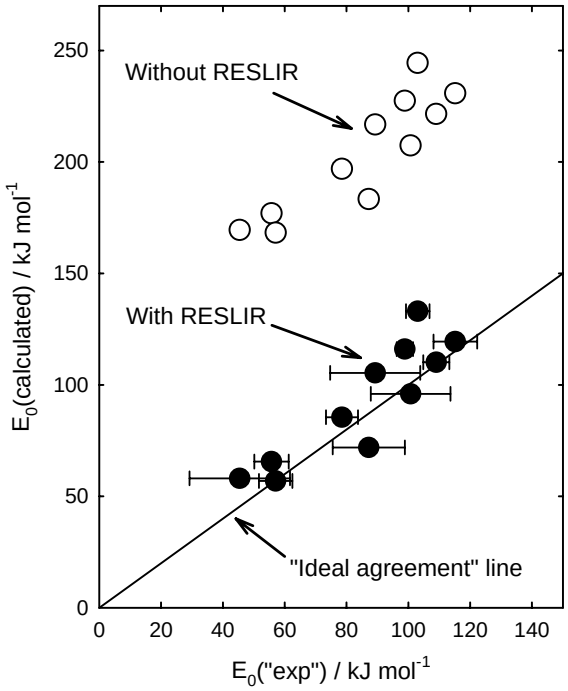

Figure 1. Calculated vs "experimental" values of the reaction energy barriers obtained for a series of Dials-Alder reactions with and without the RESLIR method. Open symbols, barriers obtained at the HF/6-311G(d) level. Filled symbols, barriers calculated using the RESLIR(QCISD(T)/aug-cc-pvtz(ex)//QCISD/cc-pvdz|HF/6-311G(d)) extrapolation method. Error bars for the "experimental" barrier values should be understood as indicating the range of uncertainty resulting from imperfect computational description of the preexponential factors for the group of reactions as a whole, as described in the text.

Acknowledgement. This research was supported, in part, by Division of Chemical Sciences, Office of Basic Energy Sciences, Office of Energy Research, U.S. Department of Energy under Grant No. DE/FG02-94ER14463

References

1. Knyazev, V. D. *J. Phys. Chem. A* **2002**, *106*, 11603.
2. Knyazev, V. D. *J. Phys. Chem. A.* **2003**, *107*, in press.
3. Hehre, W. J.; Ditchfield, R.; Radom. L.; Pople, J. A. *J. Am. Chem. Soc.* **1970**, 4796.
4. Schulman, J. M.; Peck, R. C.; Disch, R. L. *J. Am. Chem. Soc.* **1989**, *111*, 5675.
5. Raghavachari, K.; Stefanov, B. B.; Curtiss, L. A. *Molec. Phys.* **1997**, *91*, 555.
6. Raghavachari, K.; Stefanov, B. B.; Curtiss, L. A. *J. Chem. Phys.* **1997**, *106*, 6764.
7. Petersson, G. A.; Malick, D. K.; Wilson, W. G.; Ochterski, J. W.; Montgomery, J. A. Jr.; Frisch, M. J. *J. Chem. Phys.* **1998**, *109*, 10570.
8. Nicolaides, A.; Radom. L. *Molec. Phys.* **1996**, *88*, 759.
9. Chen, C. C.; Lay, T. H.; Bozzelli, J. W. *J. Phys. Chem. A* **2003**, *107*, 6451.
10. Sauer, J.; Sustmann, R. *Angew. Chem. Int. Ed. Engl.* **1980**, *19*, 779.
11. Craig, D.; Shipman, J. J.; Fowler, R. B. *J. Am. Chem. Soc.* **1961**, *83*, 2885.

Methodology for the modeling of chemical reactions on accurate potential energy surfaces

Michael R. Salazar

Department of Chemistry
Union University
1050 Union University Dr.
Jackson, TN 38343
msalazar@uu.edu

Introduction

The development of methods for the accurate description of how a chemical system changes in time is a very important field, but one that seems to have developed more slowly than methods for describing the stationary state properties of systems. This is very unfortunate since being able to accurately describe, from first principles (*ab initio*), collisional processes and the states of any products formed qualifies as a necessary step for a complete understanding of the chemical sciences.

One of the primary difficulties in being able to calculate the dynamics of a chemical system involves the accurate representation of the potential energy surface (PES) for the system.[1] The PES may be rather simple for some systems or extremely complex for other systems. In general the PES for chemical reactions will be complex and involve multiple electronic states and the couplings between these states. When performing dynamical simulations, one must have the ability to generate the potential and the gradient of the potential for the molecular system of interest at each nuclear configuration encountered during the course of the simulation. There exist an abundance of software packages for the evaluation of these *ab initio* stationary-state electronic energies and gradients. These software packages typically have many levels of theory that may be chosen to calculate these energies and gradients and the level chosen will ultimately depend on the computational cost that one is willing to absorb. Computational scaling factors ranging from linear scaling, *O(N)*, for the lowest level of theory to $O(N^7)$ for higher levels of theory must be spent for *each* energy evaluation, where N is the number of electrons in the system. This so-called method of direct dynamics, i.e., performing an *ab initio* energy and gradient evaluation at each time step has a considerable computational barrier for each simulation being performed. Furthermore, this computational barrier is markedly exacerbated when one must perform 10^3-10^5 simulations in order to obtain meaningful statistics of outcomes.

An alternative methodology for performing molecular dynamics simulations of a chemical system is to absorb the cost of calculating the global PES *a priori* by calculating energy points on a grid and using this grid of data as the basis for an analytic representation of the PES. This approach in no way diminishes the computational scaling factors for each *ab initio* energy evaluation (*O(N)* to *O(N7)*); instead, once enough of a grid of energies is calculated such that the multidimensional reaction pathway is manifest, then the *ab initio* energy evaluations may cease. Then, already having the *a priori* calculation of the PES, one may perform the dynamical calculations upon this grid of data using analytic representations of the data that have scaling factors that vary according to the number of grid points, K. The following properties of the analytic representations should be expected:[2]

1.) The method ought reproduce the *ab initio* PES data from which it is formulate, i.e., the method should be an interpolant.

2.) The method ought to be completely general and easily portable to the study of very different chemical systems and, thus, very different PESs.

3.) The method ought to be computationally inexpensive. The computational cost ought to reside in the *a priori* calculation of the PES of which the method is independent. If this criteria is satisfied, then this allows for fast dynamical calculations and the possibility of meaningful statistics of outcomes.

4.) The method should not assume any regularity to the grid of *ab initio* data, i.e., features of the PES that are thought to be of extra importance to the reaction should be allowed to have higher densities of *ab initio* data.

5.) The method should require only the *a priori* calculation of the PES and not higher order derivatives. This can be particularly important since it is often the case for higher levels of *ab initio* theory that the programming of higher order derivatives are more slowly developed and their computational costs often exceed that of the evaluation of the energy.

6.) The method should generate an analytic representation of the PES that is smooth and continuous. The conservation of energy and momentum for molecular dynamics simulations will be very sensitive to this requirement.

Methodology

The multiquadric interpolant has been used as an accurate and fast global representation of multidimensional *ab initio* PESs.[2-7] This interpolant may be written as:

$$E(P) = \sum_{i=1}^{K} c_i \sqrt{d_{i,P}^2 + \Delta} \,. \qquad (1.)$$

where $d_{i,P}^2$ is the distance from point i to the point P, (point P being where the energy is being evaluated) and Δ is an *ad hoc* parameter. The interpolant analytically reproduces the underlying grid of energies used in it's formulation. As can be seen from Eq. (1) going to higher dimensionality does not significantly alter the difficulty of employing the interpolant and the interpolant will work for both uniform grids and grids of scattered data. The primary computational cost in the formulation of the interpolant involves solving a K × K system of linear equations. The cost of this evaluation is only required once for a given PES. Once one has solved for the coefficients, c_i, the interpolant may be used to evaluate the energy and higher order derivatives anywhere inside the underlying grid. The computational cost of a single energy or gradient evaluation is *O(K)* with a very small prefactor. The primary difficulty with the utilization of this interpolant involves the *a priori* solution for the *ad hoc* parameter, Δ. As shown below, the interpolation of the energy is very stable with changes in Δ, but the accuracy of higher order derivatives may be significantly improved with optimization of this parameter. Methods have been developed[2,3] for the *a priori* solution of Δ, but they all involve solving the K × K system of linear equations multiple times.

Results

The multiquadric interpolant has recently been applied to the study of the spin-aligned Bose-Einstein condensate Li_3 system,[2,7] where an accurate and smooth representation of the *ab initio* PES is of critical importance. The global *ab initio* PES consisted of 1122 energy points calculated at the full configuration interaction (FCI) level of theory for the valence electrons and the grid of data was highly non-uniform. This is a very sparse global PES for a system of three degrees of freedom. The accuracy of the multiquadric interpolant was examined by formulating the interpolant using 1072 of the 1122 *ab initio* energies. The remaining 50 data points were used for the purposes of performing numerical tests on the accuracy of the interpolant. Table 1 shows the average, maximum, and minimum errors of the interpolated energies at these randomly

selected 50 points. The input coordinates of the PES had accuracy in the hundred-thousandth place (E-5), while the *ab initio* energies contained accuracy in the millionth place (E-6).

Table 1. Table of the average, maximum, and minimum errors in the interpolated energies at the 50 randomly scattered data points of the Li_3 PES.

Test	Avg. error (a.u.)	Max. error (a.u.)	Min. error (a.u.)
50 points	1.1E-5	1.52E-4	<E-6

As can be seen in Table 1 the interpolant has an average error of 1.1×10^{-5} Hartrees. This average error was found to be insensitive to changes in Δ. The maximum errors were found to reside at data points that were near the edge of the underlying grid of *ab initio* data where there were large gradients due to the close interactions of a Li_2 diatomic.

In addition to examining the accuracy of the energies of the multiquadric interpolant for the Li_3 PES, the accuracy of the interpolated gradients of the energy was also examined. Accuracy and smoothness of these gradients is critical for any molecular dynamics simulations since a classical Hamiltonian is often used for the propagation of the nuclei. Since these gradients were not calculated at the *ab initio* level of theory, the *ab initio* PES was fit to an analytic potential[7] and this analytic potential was used to generate a grid of data at the 1072 points where the *ab initio* energies are known. A new multiquadric interpolant was formulated using these 1072 energy points generated from the analytic potential and the gradients of this newly formulated interpolant were compared against the analytic gradients of the analytic potential. Displayed in Figure 1 is the root mean square error of the interpolated gradients along the symmetry coordinates S_1, S_2, and S_3 as a function of Δ for these 50 data points.

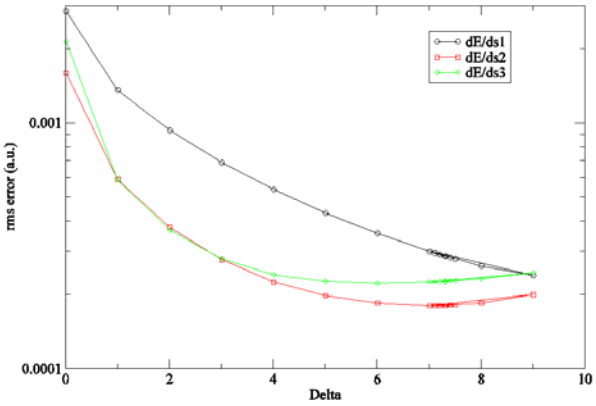

Figure 1. The root mean square error of the interpolated gradients of the energy with respect to the symmetry coordinates S_1, S_2, and S_3 as a function of the ad hoc parameter Δ.

Examining Figure 1 shows that the errors in the gradients are improved by an order of magnitude by the optimization of Δ. Figure 1 also shows that the optimized value of Δ for each of the coordinates resides at very similar values. At the optimized value of Δ, the root mean square error in the gradients at the 50 randomly selected data points ~2.0×10^{-4} Hartree/bohr along each coordinate.

Conclusions and Future

The multiquadric interpolant has been shown to be an accurate and robust method for obtaining an analytic representation of *ab initio* PESs and has further been shown to meet all of the desired properties outlined in the Introduction. The primary difficulty in the employment of the interpolant involves the *a priori* solution of the *ad hoc* parameter Δ for a given PES. Although methods have been developed for this purpose, this remains an area of active research.

Work is now being performed to utilize the multiquadric interpolant for the purposes of being able to model much larger reactive chemical systems. The goal of this work is to accurately model molecular dynamics simulations of large systems employing much higher levels of *ab initio* theory than methods of direct dynamics. As noted earlier, methods of direct dynamics, while having the benefit of using the *ab initio* PES, nevertheless often have the liability of very poor statistical outcomes. As a result, it is tempting to use levels of *ab initio* theory that may be inappropriate for systems that involve multiple electronic surfaces, which results in surface features (barriers, potential wells, etc.) that are highly over- or underestimated. Instead of applying direct dynamics, work is being performed that utilizes the *O(K)* scaling of the multiquadric interpolant to time dependent groups of the total potential for large systems.

Acknowledgement. I would like to thank Walter J. Stevens and James P. Burke for making their Li_3 PES available. I would also like to thank Union University for research support. Acknowledgement is made to the Donors of the American Chemical Society Petroleum Research Fund for partial support of this research. This research was also supported by an award from Research Corporation.

References

(1) Schatz, G. In *Reaction and Molecular Dynamics*; Lecture Notes in Chemistry; Lagana, A. and Riganelli A., Eds.; Springer, Berlin, 2000; pp. 15-32.
(2) Salazar, M. R. *Chem. Phys. Lett*. **2002**, *359*, 460.
(3) Salazar, M. R. and Bell R. *J. Comp. Chem*. **1998**, *19*, 1431.
(4) Salazar, M. R. and Simons J. *J. Chem. Phys*. **1996**, *105*, 10919.
(5) Salazar, M. R. and Simons J. *J. Chem. Phys*. **1999**, *110*, 229.
(6) Bell R. and Simons J. *J. Phys. Chem. A*. **1999**, *103*, 539.
(7) Colavecchia, F.D.; Burke, J.P. Jr; Stevens, W.J.; Salazar, M.R.; Parker, G. A.; Pack, R.T *J. Chem. Phys*. **2003**, *118*, 5484.

THE HIGH TEMPERATURE DECOMPOSITION OF HEXYL RADICALS

Wing Tsang

National Institute of Standards and Technololgy
Gaithersburg, MD 20899

Abstract: This paper is concerned with the breakdown of hexyl radicals to smaller fragments . It is meant as a first step in extending earlier kinetic databases for alkane fuels that have been validated for properties associated with the their combustion to cover soot/PAH formation problems. Sometime ago we experimentally determined the branching ratios for the decomposition of n-hexyl radicals during the pyrolysis of n-hexyl iodide. At that time we did not have the capability for treating the energy transfer effects in the multichannel fragmentation of hexyl radicals We are now able to do so and therefore have applied it to derive from the experimental measurements the high pressure rate constants consistent with bond scission and isomerization processes. From this information we project results over all relevant temperatures and pressures Some of the problems encountered in deriving the rate constants are discussed. Possibilities for reducing the number of new species and reactions for properly describing the overall processes are described.

Introduction: Kinetic databases for the simulation of combustion have usually been validated by reproducing processes such as ignition delay or flame speeds under stoichiometric or lean conditions (1). Validations of this type rarely cover the more general situations involving soot/PAH formation processes. This presentation represents an attempt to build into the database rate constants for the breakdown of hexyl radicals. This is the process that is competitive with hexyl radical oxidation through O_2 attack. The ultimate products are unsaturated compounds and radicals that can now be used as inputs to existing soot/PAH models (2). The inclusion of the pyrolytic reactions will thus generalize the database so that it can cover all combustion situations. Linear alkanes are important components of any hydrocarbon fuel (3). A kinetic database of a linear alkane fuel with n carbon atoms means that it will be necessary to consider all normal alkyl radicals with n-2 carbon atoms. Thus the present work will have an impact all normal alkane fuels with more than 6 carbon atoms.

Scope of work: There are three normal hexyl radicals. The overall decomposition process is complicated by the possibility of isomerization. The reactions involve 4 beta C-C bond cleavage reactions and 4 isomerization processes. Our aim is to derive rate expressions as a function of temperature and pressure for all these processes.

(1) 1-hexyl = ethylene + n-butyl
(2) 2-hexyl = propene + n-propyl
(3) 3-hexyl = 1-butene + ethyl
(4) 3-hexyl = 1-pentene + methyl
(5) 1-hexyl = 2hexyl
(6) 2- hexyl = 1 hexyl
(7) 1-hexyl = 3- hexyl
(8) 3-hexyl = 1-hexyl

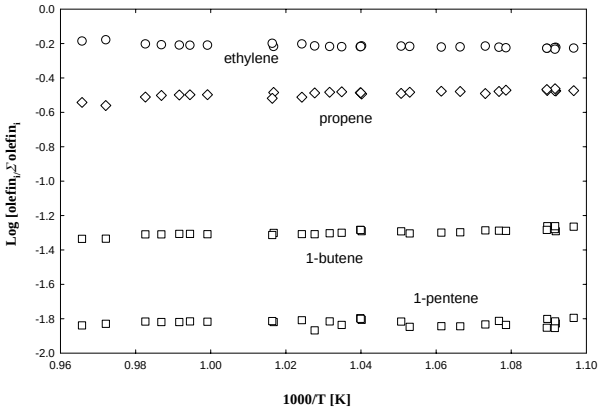

Figure 1: ***Product distribution from the decomposition of n-hexyl radical generated from n-hexyl iodide pyrolysis in single pulse shock tube experiments.***

Past work: Earlier kinetic databases have derived rate constants on the basis of results from similar reactions and thermokinetic assumptions(4). A serious problem is the neglect of energy transfer effects. Thus the effect of pressure is neglected, Several years ago we determined the branching ratio for olefin production from the decomposition of n-hexyl radical generated in single pulse shock tube experiments from the pyrolysis of n-hexyl iodide. Results are summarized in Figure 1 (5) From these data it is possible to assign the hexyl radical precursor for each olefinic product. For example 1-pentene and 1-buetene can only arise from 3-hexyl, 1-propene is derived from 2-hexene and products from 1-hexyl can only arise from the difference between the ethylene and propene yields.

Procedure: Energy transfer effects are of importance for this set of reactions as a consequence of the low reaction thresholds for the processes(6) . An additional complication is that unlike the situation for the single step decomposition reaction usually treated in standard texts it will be necessary to consider explicitly the multichannel nature of the process. Thus all eight reactions must be treated simultaneously, An additional complication is the comparatively large size of the molecule leading to the peak of the distribution function being above the reaction threshold. We have developed a general procedure to treat such situations (7,8). It involves the determination of the time and pressure dependent molecular distribution function from the solution of master equation. Convoluting these results with the RRKM specific rate constants for each channel leads to eight sets of time dependent rate constants. The purpose of this presentation is to demonstrate the procedures necessary to extract rate constants as a function of temperature and pressure and to organize the values in the most efficient manner.

Results: The treatment of the data involves first fitting experimental measurements and determining the high pressure rate expressions and then using the latter to project results over all pressure and temperature ranges. The high pressure rate expressions consistent with this procedure are summarized in Table 1. Even at temperatures as low as 600 K some pressure dependence on the rate constants can be observed. Increasing temperatures or lowering the pressure leads an accentuation of the pressure dependence. The general situation can be seen in Figure 2. This contains a plot

Reactions	Rate Expressions Rate constants at 950
k1: C6H13-1 => C2H4 + nC4H9	$1.5x10^{13}exp(-13988/T)$ 6.8
k2: C6H13-2 => C3H6 + nC3H7	$2.7x10^{13}exp(-14085/T)$ 7.0
k3: C6H13-3 => 1-C4H8 + C2H5	$2.7x10^{13}exp(-14070/T)$ 7.0
k4: C6H13-3 => 1-C5H10 + CH3	$2.7x10^{13}exp(-15080/T)$ 6.55
k5: C6H13-2 => C6H13-1	$8.9x10^{11}exp(-10923/T)$ 6.96
k6: C6H13-3 => C6H13-1	$4.0x10^{12}exp(-13788/T)$ 6.30
k7: C6H13-1 => C6H13-2	$6.7x10^{11}exp(-9297//T)$ 7.58
k8: C6H13-1 => C6H13-3	$3.0x10^{12}exp(-12494/T)$ 6.77

Table 1*: High pressure rate expressions consistent with the experimental data summarized in Figure 1*

of the temporal history of the four rate constants associated with beta C-C bond fission and the concentration of the three radicals.
Attention is called to the differences from what can be expected for a single channel process. For example the presence of the isomerization channels is responsible for the structure in the rate constants for the decomposition of the 1-hexyl radical. All the other hexyl radicals are formed from isomerization. Therefore their initial rate constants for beta bond scission is higher than the high pressure limiting values. Ultimately of course all the rate constants relax to constant values. It can be seen that these steady state values are only slightly smaller than those at the high pressure limit. However a great deal of interesting chemistry occurs before this is achieved. This can be seen from the plots of the concentrations of the hexyl radicals as a function of time. It is clear that much of the conversion has occurred before steady state distributions have been achieved. This then raises the issue of how to represent the rate constants when they are not constant. We have found it possible, in the cases where rate constants do not vary greatly to reproduce the calculated concentrations in terms of average rate constants

Discussion: When the temperature is increased, without changing the pressure, rate constants will of course increase. However this means that the ultimately all of the molecule will have reacted before the time where reactions can be described in terms of a constant rate constant. Under these conditions it becomes increasingly difficult to fit the data in terms of average rate constants. However rate constants under these conditions are extremely large and they becomes so large that they conversions to the fragments will no longer be disturbed by the oxidation reaction involving radical attack by oxygen molecule. Under such conditions all that is needed is the branching ratios for conversion.

It is of interest to consider the boundary for this process. The reaction of alkyl radicals with oxygen is in the range of $4x10^{12}$ $cm^3mol^{-1}s^{-1}$ (9) .At 1 bar of air this leads to a lifetime of approximately $T/10^{10}$ s^{-1}. It appears that above 1000 K oxidation will no longer be competitive. Under such conditions all that need be considered will then be the branching ratios for the formation of the olefins. It is then possible to ignore the presence of the alkyl radicals and express results in terms

Radical + alkane =olefin(s) + small alkyl radical + Radical-H

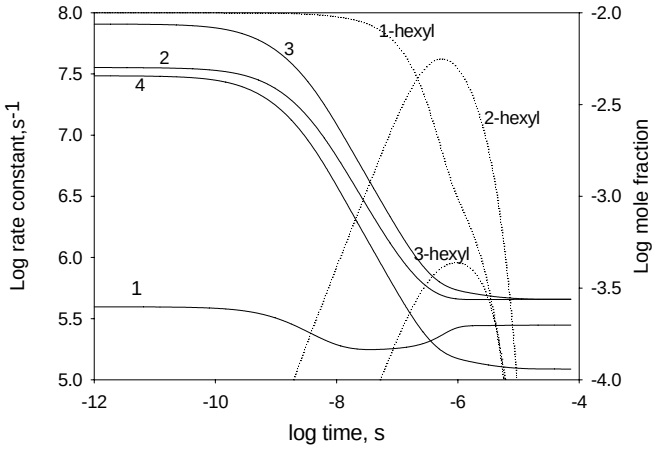

Figure 2: ***Rate constants (solid line) and radical concentrations (dotted line) as a function of time at 800 K and 1 bar. The numbers refer to the reactions listed earlier***

Thus under high temperature conditions introducing the pyrolytic reactions necessary to describe the formation of the precursors to PAH/soot does not require the introduction of many more species.

There remains the problem of treating species and reactions in the intermediate temperature region where pyrolytic and oxidation processes are competitive. There are no obvious intuitive ways of carrying this out. More rigorous procedures will probably be necessary. The general situation is made more confusing by the slowness of the isomerization products to achieve the steady state values. We have mentioned the possibility of using an average rate constant to capture most of the features of the temporal behavior of these compounds. It is possible that these problems are accentuated by the treatment of these unimolecular processes in the traditional manner; as a closed system. For these reactions with the thresholds below the peak of the Boltzmann distribution the more appropriate treatment is that of an open system as in chemical activation.

References

(1) Curran, H.J., Gaffuri, P., Pitz, W.J., Westbrook, C.K. (1998) *Combust.Flame, 114.* (1-2):149-177
(2) Richter H, Howard J.B., Prog. Energ. Combust.: 4 565, 2000
(3) Edwards, T., Harrison, W. E. III, and Maurice, L. Q., "Properties and Usage of Air Force Fuel: JP-8", AIAA 2001-0498, 39th AIAA Aerospace Sciences Meeting and Exhibit, Jamuary , 2001 Reno. NV
(4) Benson, S. W. "Thermochemical Kinetics" John Wiley, New York, 1974
(5) Tsang, W., "Pathways for the Decomposition of 1-Hexyl Radicals"; Chemical and Physical Procesess in Combustion", 1996 Fall Technical Meeting, Eastern States Section of the Combustion Institute, Hilton Head, SC., pg 515
(6) Gilbert, R. S. and Smith S. C.,"Theory of Unimolecular and Recombination Reactions", Blackwell Scientific, London, 1990
(7) Tsang, W., "A Pre-processor for the Generation of Chemical Kinetics Data for Simulations" AAIA-2001-0359, 39th AIAA Aerospace Sciences Meeting and Exhibit, Jamuary 8-11, 2001 Reno.
(8) Tsang, W., Bedanov, V. and Zachariah, M. R., J. Phys. Chem., 1996, 100, 401
(9). Baulch, D. L., Cobos, C. J., Cox, R. A., Frank, P., Hayman, G., Just, T., Kerr, J. A., Murrells, T., Pilling, M. J., Troe, J., Walker, R. W. amd Warnatz, J.,J. Phys. Chem. Ref. Data, 24, 1609, 1995

Multi-Channel Chemically Activated Reactions: Comparison of Troe's Weak Collision Model and Exact Solution of Collisional Energy Transfer by Monte Carlo Method

Ameya V. Joshi[1], *Scott, G. Davis*[2], *and Hai Wang*[1]

[1]Department of Mechanical Engineering, University of Delaware, Newark, DE 19716
[2]Exponent, Inc., 21 Strathmore Road, Natick, MA 01760

Knowledge of the collisional energy transfer for a large number of multi-channel unimolecular and chemically activated reactions is often required to successfully model chemically reacting systems. Much progress has been made in our understanding of the collisional energy transfer process[1-5]. Early studies have questioned the "strong collision" hypothesis, which allowed for large energy transfer during collisions. It is known that inefficient collision energy transfer causes the population distribution of molecules above the threshold energy to deviate from the Boltzmann distribution. This results in a pressure fall-off of the thermal rate constant that is different from that predicted using the strong collision approach. For this reason, the strong collision model has in general been abandoned and collisions are effectively treated as "weak collisions".

Kineticists have employed Troe's modified strong collision model[6] to account for weak collisions. In this treatment, a collision efficiency factor β_c is introduced. This factor relates the weak collision rate constant with the strong collision rate constant through $k^{wc} = \beta_c\, k^{sc}$. Although Troe's treatment was intended for use only with single-channel unimolecular reaction, it has been nevertheless used for multi-channel reactions. In recent years, it was recognized that while Troe's collision efficiency factor is simple to calculate, for multi-channel unimolecular reactions the treatment represents a gross simplification of the collision process and the accuracies of the resulting thermal rate constants are highly questionable. Direct solution of master equation[7,8] of collisional energy transfer is a logical approach for multi-channel unimolecular and chemically activated reactions. Nevertheless it is far from trivial to analyze a reaction network of arbitrary complexity and to solve the collision energy transfer coupled with the isomerization of vibrationally excited adducts for such a reaction network.

Here, we approach the solution of master equation of collisional energy transfer and the estimation of thermal rate constants using a Monte Carlo method[9] based on Gillespie's exact stochastic method[10-12]. Our computational capability resolves reaction networks of arbitrary complexity. In this work, we compare the rates computed using the Monte Carlo approach and Troe's modified strong collision method. Rates have been computed for the chemically activated reaction of OH + CO $\rightarrow$ products[13], C_2H_2 + CH_3 $\rightarrow$ products[14] and C_6H_6 + O $\rightarrow$ products. Results show that the rate constants are systematically overpredicted for the stabilization channels by Troe's weak collision model, and as expected, the extent to which the rates are overpredicted increases as the stabilization rates deviate further from their high-pressure limits. On the other hand, the modified strong collision model is sufficiently accurate for rate estimation under many practical conditions.

Acknowledgement. The work was supported by the National Science Foundation (CTS-9874768).

References

(1) Tardy, D. C.; Rabinovitch, B. S. *Chem.Rev.* **1977**, *77*, 369.
(2) Quack, M.; Troe, J. *Gas Kinetics and Energy Transfer*; The Chemical Society: London, **1977**, Vol.2.
(3) Flynn, G.W. *Acc. Chem. Res.* **1981**, *14*, 334.
(4) Krajnovich, D.J.; Parmenter, C.S.; Catlett, D.L.,Jr. *Chem. Rev.* **1987**, *87*, 237.
(5) Oref, I.; Tardy D.C. *Chem. Rev.* **1990**, *90*, 1407.
(6) Troe, J. *J. Chem. Phys.* **1977**, *66*, 4745.
(7) Holbrook, K.A.; Pilling, M.J.; Robertson, S.H. *Unimolecular Reactions*; 2nd Ed.; Wiley: Chichester, **1996**.
(8) Gilbert, R.G.; Smith, S.C. *Theory of Unimolecular Reactions and Recombination Reactions*; Blackwell Scientific: Oxford, **1990**.
(9) Barker, J.R. *Int. J. Chem. Kinet.* **2000**, *33*, 232.
(10) Gillespie, D.T. *J. Comp. Phys.* **1976**, *22*, 403.
(11) Gillespie, D.T. *J. Comp. Phys.* **1978**, *28*, 395.
(12) Gillespie, D.T. *J. Comp. Phys.* **1977**, *81*, 2340.
(13) Larson, C.W.; Stewart, P.H.; Golden, D.M. *Int. J. Chem. Kinet.* **1988**, *20*, 27.
(14) Davis, S.G.; Law, C.K.; Wang H. *J. Phys. Chem. A.* **1999**, 103, 5889.

A study on the initial product channels of cyclohexane pyrolysis behind reflected shock waves

M. Braun-Unkhoff, C. Naumann, P. Frank

German Aerospace Center, Institute of Combustion Technology
Stuttgart, Germany

Introduction

The chemical kinetics of combustion processes of fuels has been the subject of many investigations over the past years. In the last decade, the chemistry of naphthenes – which belong to the main components of practical fuels such as gasoline, diesel, and kerosene – has attracted much attention as their contribution to the formation of aromates can be significant. For example, due to the complexity of kerosene composition – kerosene Jet A1 is a complex mixture of long-chained alkanes as dominant components, of mono- and poly-aromatics and of cycloalkanes or naphthenes (mono- and polycyclic) –, usually a model fuel is designed for simulating its oxidation. In this context, cyclohexane is discussed as a representative for naphthenic species, see e.g. ElBakali et al. /1/. Therefore, a detailed reaction mechanism is needed to describe oxidation of cyclohexane and its way to aromatic species in order to model the formation of aromatics in the oxidation of practical fuels.

Presently, investigations on the thermal decomposition of cyclohexane do not show a consistent picture regarding the initiation steps. From a single-pulse shock tube study (Tsang, 1978 /2/) it was deduced that the main initial process involves isomerisation to 1-hexene, followed by subsequent decomposition of the primary products. The same dominant end products have been also found in VLPP experiments (Brown et al., 1986 /3/). From a flow reactor study at relatively low temperatures, Gulati and Walker (1989) /4/ assumed that benzene was formed in a reaction sequence starting from cyclohexane → cyclohexene → 1,3-cyclohexadiene → benzene. Recently, from high pressure JSR experiments on cyclohexane oxidation (Voisin et al., 1998, /5/) at different mixture conditions, it was concluded that the main initiation step on cyclohexane decomposition occurs via C-C bond fission and results in ethene as the main product. In the same study, a much slower rate coefficient was attributed to the H-elimination reaction step. Furthermore, this scheme was used as part of a big reaction scheme for calculating species profiles measured in a flow reactor study (ElBakali et al., 2000, /1/) for temperatures between 900 K and 1200 K at pressures up to 10 atm over a wide range of equivalence ratio (0.5 to 2). It was found that 1-hexene which is produced via cyclohexane isomerization was formed at 1 atm, but not at 10 atm. A submechanism of 1-butene which was formed in higher concentration at 1atm than at higher pressures was included in the reaction scheme to improve the prediction of 1-hexene. As the main product, ethene was found stemming from a direct C-C fission of cyclohexane. The molecular decomposition channel was found to be mainly responsible for the decay of cyclohexane besides H-atom abstraction via OH– and H-radicals. The model was also able to model laminar burning velocities of atmospheric cyclohexane / air flames at T_0 = 298 K /6/. Therefore, the aim of the present work is to give more insight into the initial decomposition steps during the pyrolysis of cyclohexane, especially to find out whether H atoms, which are most important with respect to ignition, may be formed directly in the thermal decomposition.

Experimental

The experiments were performed behind reflected shock waves under highly diluted conditions applying a very sensitive detection method. Atomic resonance absorption spectroscopy at a wavelength λ = 121.6 nm was applied to monitor time dependent H-atom concentrations. Very small initial concentrations of cyclohexane were used, ranging from 1 to 11 ppm diluted in highly purified argon. Cyclohexane exhibited a relatively strong propensity for wall adsorption. Therefore, in most experiments, its initial concentration was examined by the use of gas chromatography analysis of samples taken from the shock tube immediately before the experiment. The uncertainty was found to be about ± 20% due as an internal standard technique has been applied. Thus it was possible to study the reaction system under very isolated conditions, with only minor influence of subsequent reactions. The experiments cover a temperature range of 1180 to 1900 K at pressures between 1.5 and 2 bar. All experiments of the present study were conducted in a stainless steel shock tube of 7.5 cm internal diameter which was heated to 363 K. Measurements were performed 5 mm away from the end flange. An oxygen spectral filter combined with a L_α-interference-filter (10 nm FWHM) was used. Calculated absorption profiles reported are based on calibration experiments, using the reaction of O-atoms – stemming from the decomposition of N_2O – with H_2 to produce H-atoms.

Results and Discussion

From previous investigations, one might expect that the dominant decomposition reaction occurs via C-C bond fission leading to ethene as the main product:

c-C_6H_{12} → open chain-C_6H_{12} (e.g. 1-hexene) → 3 C_2H_4 (R1a).

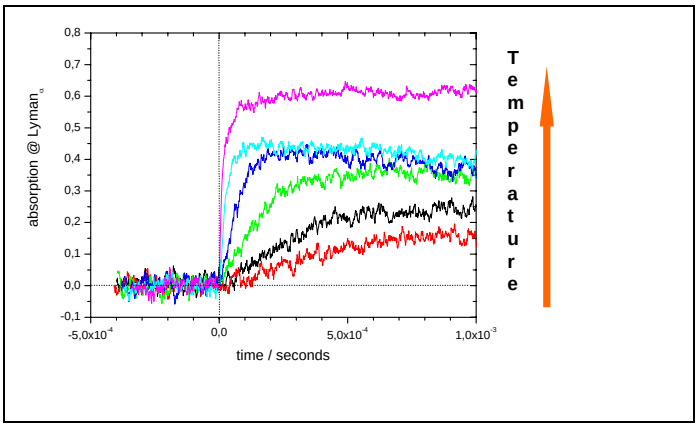

Figure 1: H-atom absorption measured behind reflected shock front. 1.05ppm cyclohexane diluted with argon for T_5 = 1335-1895K & p_5 = 1.77–1.93bar.

Therefore, hydrogen atoms can only be produced by subsequent reaction steps which should reveal a pronounced delay time under the highly diluted conditions of the present investigation. However, time resolved H-absorption profiles measured at the lowest initial cyclohexane concentrations of about 1 ppm (Figure 1) in the temperature range 1335 – 1895 K, clearly show that hydrogen atoms are produced immediately at the onset of the reaction. Therefore it was assumed that H-atoms are produced directly by an additional C-H bond fission according to reaction path R1b, which is followed by a fast H elimination reaction leading (R2) to cyclohexene:

c-C_6H_{12} → c-C_6H_{11} + H (R1b)
c-C_6H_{11} → c-C_6H_{10} + H (R2) .

As a base set for modeling the measured H-atom absorption profiles, the rate coefficient expressions of Voisin et al. (1998) have been used. For the conditions of very low initial concentration used in the present study, a reaction scheme was set up which essentially consisted of the initiation reactions R1a / R1b, R2 and bimolecular reactions like c-C_6H_{12} / c-C_6H_{11} + H → c-C_6H_{11} / c-C_6H_{10} + H_2 which are only of minor influence. Figure 2 shows for a typical experimental profile at about 1450 K the influence of the rate values and of the branching ratio of reactions R1a and R1b. With the original values for k_{1a} and k_{1b}, nearly no H-atoms are calculated (full line). Neglecting channel R1a, gives absorption profiles which are still too small (dashed line). Only if the value of k_{1b} is increased considerably by a factor of 7.5, the initial slope of the measured profile is met, but in the later stage, too much H-atoms are predicted (dotted line). With the latter value for k_{1b} and the original value for k_{1a}, the predicted profile is much too low, compared with the observed one (dashed-dotted curve).

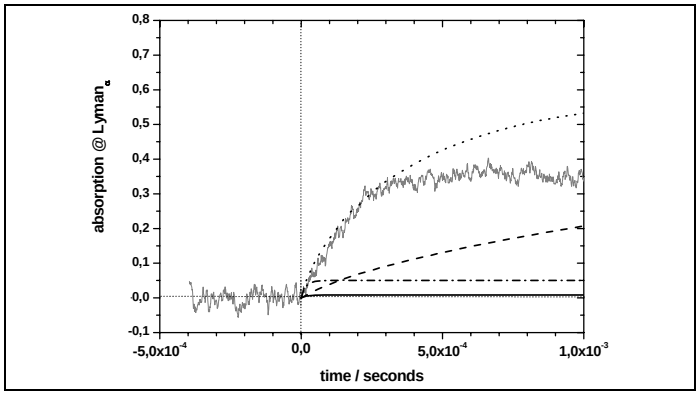

Figure 2. H-atom absorption profile measured behind reflected shock front. 1.05 ppm cyclohexane diluted in argon. T_5 = 1447 K; p_5 = 1.92 bar. Influence of molecular channel. Full line: k1a & k1b from /5/; dashed line: k1a*0, k1b from /5/; dotted line: k1a*0, k1b*7.5; dashed dotted line: k1a from /5/ & k1b*7.5.

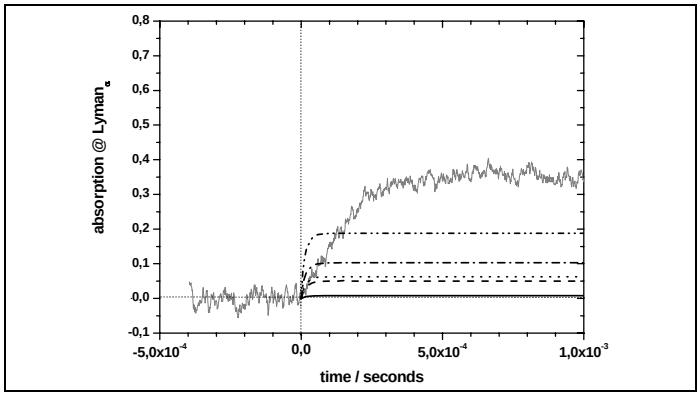

Figure 3. H-atom absorption profile measured behind reflected shock front. Same experimental condition as in Figure 2. Influence of H-atom producing channel. Full line: k1a & k1b from /5/; dashed line: k1a from 5/, but k1b*7.5; dotted line: k1a from /5/, but k1b*10; dashed dotted line: k1a from /5/, but k1b*20; dashed-dotted-dotted-line: k1a from /5/, but k1b*50.

The influence of the H-atom producing channel R1a is depicted in Figure 3. The molecular channel R1a was sticked to the value given by Voisin et al. whereas the rate coefficient of the H-atom producing channel was increased within factors of 7.5 and 50. It can clearly be seen from Figure 3 that the predicted absorption is much too high at the onset of the reaction time interval if R1b proceeds faster and faster. This leads to the conclusion that it is not possible to match the observed H-atom absorption without reducing the rate coefficient of the molecular channel.

Consequently, both values for the rate of the two initial decomposition steps of cyclohexane were modified, with respect to the data given in /5/. As can be seen in Figure 4, the measured absorption profile is reproduced over the entire observation time interval, if the rate coefficient of the molecular channel is reduced considerably by about a factor of 50 and if simultaneously, the H-atom producing channel R1b is increased by a factor of 7.5 (full line).

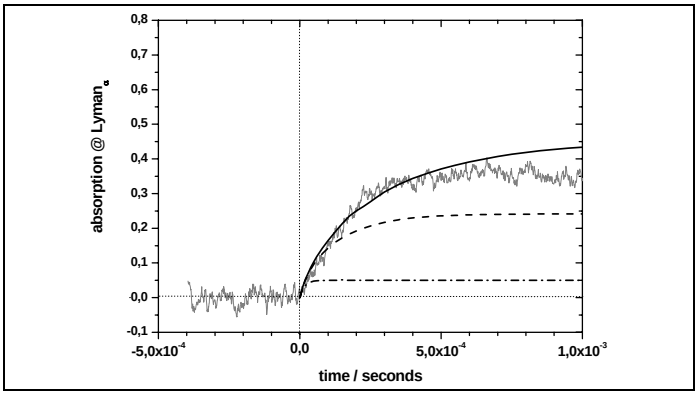

Figure 4. H-atom absorption profile measured behind reflected shock front. Same experimental condition as in Figure 2. Dash dotted line: k1a from /5/, k1b*7.5; dashed line: k1a*0.1, k1b*7.5; full line: k1a*0.02, k1b*7.5

Conclusions

The results of the present study lead to a branching ratio of about 0.5 for k_{1a} / (k_{1a} + k_{1b}). Hence, the molecular channel R1a is much slower than considered up to now, whereas the hydrogen elimination path R1b proceeds much faster, by about a factor of 5 - 10. Further measurements such as non-resonant absorption either of the educt itself and/or some of the product species are needed to determine the rate of the molecular channel R1a. Thus, a much better understanding of the initial reaction steps of the decomposition of cyclohexane would be enabled.

Acknowledgement. The authors are grateful to N. Ackermann for technical assistance. The financial support of the Deutsche Forschungsgemeinschaft DFG, SFB 606 *Instationäre Verbrennung, Transportphänomene, Chemische Reaktionen, Technische Systeme* is gratefully acknowledged.

References

(1) ElBakali, A., Braun-Unkhoff, M., Dagaut, P., Frank, P, Cathonnet, M., Proc. Comb. Inst. 28, 2000, pp. 1631-1638
(2) Tsang, W., 1978, Int.J.Chem.Kinet., **10**, pp. 1119
(3) Brown, T.C., King, K.D,. Nguyen,T.T., J.Phys.Chem. **90**, 1986, pp. 419
(4) Gulati, K.S. and Walker, R.W,. 1989, J.Chem.Soc.Faraday Trans. **2**, 85, pp. 17
(5) Voisin, D., Marchal. A., Reuillon, M., Boettner, J.-C. and Cathonnet, M., 1998, Combust. Sci .and Tech., **138**, pp. 137
(6) Davis, S.G. and Law, C.K., 1998, Combust. Sci. Tech. 140, pp. 427-449

Quantum Monte Carlo study of the thermochemistry of small hydrocarbons*

Alexander C. Kollias[1,2], Dominik Domin[1], Michael Frenklach[3], David Golden[4], and William A. Lester, Jr.[1,2]

[1]Kenneth S. Pitzer Center for Theoretical Chemistry, Department of Chemistry, University of California, Berkeley, CA 94720-1460; [2]Chemical Sciences Division, Lawrence Berkeley National Laboratory Berkeley, CA 94720-1460; [3]Department of Mechanical Engineering, University of California at Berkeley, Berkeley, CA 94720-1740, and Environmental Energy Technologies Division, Lawrence Berkeley National Laboratory Berkeley, CA 94720-1460; [4]Department of Mechanical Engineering, Stanford University, CA 94305

A theoretical study is reported on the thermochemical properties of 20 small hydrocarbons based on the diffusion Monte Carlo (DMC) variant of the quantum Monte Carlo method. The 20 hydrocarbons include both radicals and closed-shell molecular systems containing 1 to 4 carbons centers that appear in combustion reactions. Using DMC trial functions constructed from Hartree-Fock (HF) and multi-configurational self-consistent field (MCSCF) wave functions, we have computed the atomization energies, heats of formation and bond dissociation energies for these systems. The DMC thermochemical results are compared to experimental data as well as complete basis set extrapolations for Moller-Plesset second-order perturbation theory, coupled-cluster singles-doubles (CCSD) with perturbative triples (CCSD(T)), and B3LYP methods to gauge the accuracy of the DMC method.

The amount of non-dynamical correlation energy, or single-reference character in CCSD, was determined by examining the T1 diagnostic test of CCSD calculations.[1] This diagnostic test has been demonstrated to be a better quantifier of multi-reference character than the leading coefficient in a multi-configurational wave function. The results of the T1 diagnostic are correlated with DMC atomization energies in order to provide a measure of the quality of HF trial wave functions. The idea is to gauge the accuracy a priori of a DMC calculation that uses a HF trial function from the T1 diagnostic. In cases where DMC atomization energies from HF trial functions are poor, multi-determinant trial functions will be used to improve the results.

[1]T. J. Lee and P. R. Taylor, *Int. J. Quant. Chem. Symp.* **23**, 199 (1989).

*This work was supported by the Director, Office of Science, Office of Basic Energy Sciences, Chemical Sciences Division of the U.S. Department of Energy under Contract No. DE-AC03-76SF00098. The calculations were carried out at the National Energy Research Supercomputer Center (NERSC).

Thermodynamics of Jahn-Teller molecules

Timothy A. Barckholtz

Corporate Strategic Research
ExxonMobil Research and Engineering
1545 Route 22 East
Annandale, NJ 08801
tim.barckholtz@exxonmobil.com

Introduction

The vast majority of molecules and radicals important in combustion or atmospheric kinetics have relatively simple electronic and vibrational structures. Most stable molecules have singlet ground states with excited states that are close to 100 kcal/mol higher in energy. The vibrational structure of most molecules can be readily described using the simple harmonic oscillator model, possibly with some anharmonic corrections. The thermodynamics of these molecules can be easily handled using standard statistical treatments. While the chemistry of free radicals is quite different from that of molecules, their treatment under statistical thermodynamics is for the most part very similar to that of molecules.[1]

A class of molecules for which the above statements do not hold are those subject to the Jahn-Teller effect. These molecules have by necessity open-shell electronic structures with orbitally degenerate ground states. Two important combustion radicals, the methoxy radical, CH_3O,[2] and the cyclopentadienyl radical, C_5H_5,[3] have ^2E ground states that are subject to a Jahn-Teller distortion. While these two radicals have been investigated for over 50 years, the details of their vibrational structure have only been resolved in the last 5 years.

Quantum mechanics of Jahn-Teller states

The quantum mechanics of Jahn-Teller molecules has been examined in excruciating detail elsewhere.[2] For the purposes of this paper, only a few key points will be summarized.

(1) The quantum mechanis of a Jahn-Teller molecule are most efficiently described via a few small perturbations to the Hamiltonian appropriate for a ^2E state. The molecule is distorted from the higher symmetry geometry, but this distortion is dynamic, not static, for CH_3O and C_5H_5. To analyze the spectroscopic energy levels based on a Hamiltonian appropriate for the distorted geometry would require many more correction terms than the Hamiltonian derived from the higher symmetry geometry.

(2) For most molecules, the Hamiltonian for the vibrational energy levels is separable from the electronic and spin Hamiltonians. This is not the case for ^2E states. Thus, the partition function cannot in general be written as the product of the individual components ($q_{JT} \neq q_{spin}*q_{elec}*q_{vib}$).

In the absence of any Jahn-Teller coupling, q_{elec} is equal to the orbital degeneracy of the state; i.e., 2 for a ^2E state. If the spin-orbit coupling is small, like in C_5H_5, then q_{spin} can be separated out as $q_{spin}=2*S+1$ for all temperatures. The entire spin-vibrational-electronic Hamiltonian must be diagonalized in order to compute q_{JT}. Rotational and translational contributions can still be separated, to make $q_{tot} = q_{JT}*q_{rot}*q_{trans}$.

(3) For non-zero spin-orbit coupling, like in CH_3O, all vibrational energy levels are split into pairs. The splitting energies vary widely, with a general diminishment to zero as the total internal energy is increased. For the purposes of statistical thermodynamics, the spin-orbit splitting of the zero-point level can be used to compute q_s using the normal Boltzman equation.

(4) The vibrational energy levels are not evenly spaced, but instead have very irregular spacings for the first few thousand cm^{-1} of internal energy. However, they maintain intervals that are of the order of vibrational intervals (a few 100 cm^{-1}), rather than spacings of rotational energy levels (a few cm^{-1}). To compute the partition function of the Jahn-Teller vibrations requires a numerical calculation of the energy levels and a numerical calculation of the partition function based on those energy levels.

Conclusions

Several qualitative conclusions regarding the statistical thermodynamics of Jahn-Teller molecules can be made. A quantitative description will be given in the full paper to be published.

(1) The vibrational modes of a Jahn-Teller molecule are not harmonic, but the harmonic approximation may give a reasonably accurate partition function, especially at high temperatures.

(2) Treatment of the electron spin must be included in the thermodynamic calculation. For C_5H_5, the spin-orbit coupling is essentially zero, giving a full contribution of R ln 2 to the entropy at all temperatures. For CH_3O, it is small (60 cm^{-1}), making a difference only at low temperatures. For sulfur-centered radical such as CH_3S, the 250 cm^{-1} spin-orbit splitting makes a larger difference.

(3) The use of the phrase "pseudo-rotation" to describe the motion of a Jahn-Teller molecule is misleading. This phrase implies that the degrees of freedom that account for the Jahn-Teller distortion can be treated by some type of rotational function. In actuality, what is "pseudo-rotating" about the Jahn-Teller moat is not the nuclei, but the electronic wavefunction. Thus, the energy level spacings of the Jahn-Teller distortion are closer to that of a vibration rather than any type of rotation.

(4) The electronic degeneracy must be included in the entropy via an R ln 2 contribution. At low temperatures the contribution is not exactly R ln 2, and but must be computed from the full numerical diagonalization of the Hamiltonian. The commonly used *ab initio* find a singly degenerate state at a distorted geometry, and a singly degenerate excited state that usually is a maximum on the surface. If the excited state is omitted from the partition function, then the computed entropy will be low.

(5) *ab initio* calculations of the minimum can be used as a reasonable approximation to the full Jahn-Teller statistical thermodynamics, provided that the entropy due to the excited states is included. The errors of this approximation are largest at lower temperatures, and diminish significantly at combustion temperatures.

References

(1) Benson, S. W. *Thermochemical Kinetics*; Wiley: New York, NY, 1976.
(2) Barckholtz, T. A.; Miller, T. A. *Int. Rev. Phys. Chem.* **1998**, *17*, 435-524.
(3) Applegate, B. E.; Miller, T. A.; Barckholtz, T. A. *J. Chem. Phys.* **2001**, *114*, 4855-4868; Applegate, B. E.; Bezant, A. J.; Miller, T. A. *J. Chem. Phys.* **2001**, *114*, 4869-4882.
(4) Barckholtz, T. A.; Miller, T. A. *J. Phys. Chem. A* **1999**, *103*, 2321-2336.

Thermochemistry and Reaction Paths for Dimethyl Sulfide Radical with O2

Fei Jin and Joseph w Bozzelli

Chemistry, New Jersey Institute of Technology, Newark, NJ 07102

Abstract

The thermo property data on CH_3SCH_2OOH and two radicals $CH_3SCH_2OO\cdot$ and $C\cdot H_2SCH_2OOH$ are important to understand the stability, reaction paths and kinetics of reactions of sulfur hydrocarbons (sulfides) in atmospheric and combustion processes. Thermochemical properties for species and transition states in the methylthiomethyl ($CH_3SC\cdot H_2$) radical + O_2 reaction system are analyzed to evaluate reaction paths and kinetics. Isodesmic working reaction are employed to determine enthalpies of formation ($\Delta H_f^\circ{}_{298}$) using density functional (B3LYP/6-311G(d,p)) and complete basis set (CBS-QB3) computational methods. Entropy (S°_{298}) and heat capacities $C_p(T)$ ($300 \leq T/K \leq 1500$) are determined using geometric parameters and vibration frequencies obtained at B3LYP/6-311G(d,p) level of theory. $\Delta H_f^\circ{}_{298}$ values estimated at the CBS-QB3 level (unit in kcal/mol): $CH_3SC\cdot H_2$ (32.66±0.50), CH_3SCH_2OOH(–29.14±0.12), $CH_3SCH_2OO\cdot$ (5.17±0.36), $C\cdot H_2SCH_2OOH$ (11.48±1.44). Quantum Rice-Ramsperger-Kassel(QRRK) analysis is used to calculate energy- dependent rate constants, $k(E)$ and master equation analysis is used to account for collisional stabilization of adduct and isomer. The methylthiomethyl radical adds to O_2 to form a methylperoxy racial with a 37.82 kcal/mol well depth. The peroxy radical can undergo dissociation back to reactants, isomerize via hydrogen shift (TS1,E_a=17.06kcal/mol) to form a hydroperoxide methyl radical $C\cdot H_2SCH_2OOH$, decompose via hydrogen transfer (TS2, E_a=37.79kcal/mol) to form $CH_3SC(=O)H$ plus OH radical , or the peroxy radical can also attack the sulfur atom via TS3(E_a=32.92kcal/mol) to form $CH_3S(=O)$ + CH_2O. The $C\cdot H_2SCH_2OOH$ isomer can decompose via TS4 (E_a=24.09kcal/mol) to CH_2O+CH_2S+OH, or through a four-member ring transition state (TS5, E_a =30.77kcal/mol) to form 1,3-Oxathietane + OH.

Introduction

Dimethyl sulfide (DMS) has been recognized as the main natural source of sulfur in the atmosphere[1], which emitted into the atmosphere over the global oceans has a range of effects upon atmospheric composition (mediated through various oxidation products) that may be significant with regard to issues as important as climate regulation. The roles played by DMS oxidation products within these contexts are diverse and complex, and in many instances are not well understood.

At present, the main step of the DMS oxidation in the atmosphere is the reaction with OH radical during daylight and the reactions with NO_3 radical and Cl radical, which will lead to the formation of the $CH_3SC\cdot H_2$ radical.

The $CH_3SCH_2OO\cdot$ peroxy radical is an important intermediate in the atmospheric degradation of dimethyl sulfide. The $CH_3SCH_2OO\cdot$ peroxy radical is produced through the addition of O_2 to the CH_3SCH_2 radical.

$$CH_3SC\cdot H_2 + O_2 \rightarrow CH_3SCH_2OO\cdot$$

It is believed that the reaction of the $CH_3SCH_2OO\cdot$ with the HO_2 radical will lead to the following products:

$$CH_3SCH_2OO\cdot + HO_2 \rightarrow CH_3SCH_2OOH + O_2$$

In this chapter, reaction pathways of the addition of O_2 atoms to $CH_3SC\cdot H_2$ radical are analyzed. CBS-QB3 and density functional methods are utilized estimate thermodynamic properties ($\Delta\Delta H_f^\circ{}_{298}$, S°_{298} and $C_p(T)$) for reactant $CH_3SC\cdot H_2$, intermediate radicals $CH_3SCH_2OO\cdot$, $C\cdot H_2SCH_2OOH$ and transition states:

TS1: $\overline{CH_3SCH_2OO\cdot}$ Intramolecular hydrogen shift to form a hydroperoxy radical.

TS2: $CH_3S\overline{CH_2OO\cdot}$ Intramolecular hydrogen shift to form $CH_3S\cdot CHOOH$ radical, and $CH_3S\cdot CHOOH$ rapidly dissociates $CH_3SC(=O)H$ + OH.

TS3: $CH_3\overline{SCH_2OO\cdot}$ The peroxy radical can also attack the sulfur atom form $CH_3S(=O)H + CH_2O$.

TS4: $C\cdot H_2S\text{-}CH_2O\text{-}OH$ β,γ-scission reaction to form a thioformaldehyde plus a formaldehyde and OH.

TS5: $\overline{CH_2SCH_2O}\text{-}OH$ 1,3-Oxathietane + OH.

Isodesmic working reactions are applied to evaluate enthalpies of formation. Contributions to entropy and heat capacities from internal rotation are estimated using direct integration over energy level of the intermolecular rotation potential energy curve, with B3LYP/6-311g(d,p) level calculations for rotation barrier. Activation energies for the transition states are determined and the kinetic analysis is detailed on the base of the thermodynamic properties.

Quantum Rice-Ramsoerger-Kassel (QRRK) analysis is used to calculate the energy dependent rate constant $k(E)$, and master equation analysis is applied to account for collisional stabilization in the $CH_3SCH_2\cdot + O_2$ adduct and isomers. The thermochemical and kinetic data at relevant pressures and temperatures should be useful to both atmospheric and combustion models

Calculation Methods

Density functional B3LYP/6-311g(d,p) is utilized to calculate structures and vibrational frequencies and potentials for internal rotors. CBS-QB3 methods are utilized to calculate enthalpy in working reaction analysis.

Entropy (S^o_{298}) and Heat Capacities($C_p(T)$, $300 \leq T/K \leq 1500$)

Entropies and heat capacities (T) were calculated using the rigid – rotor-harmonic – oscillator approximation based on scaled vibrational frequencies and moments of inertia of the optimized BLYP/6-311G(d,p) structures. Contribution to entropy and heat capacity from internal rotation are determined using Pitzer et al,'s treatment based on rotational barrier height and corresponding moments of inertia for the rotors.

High-Pressure Limit A Factors(A) and Rate Constant (k_∞)

For the reactions where thermochemical properties of transition states are calculated by density functional methods and CBS-QB3 methods. k_∞ values are fit by three parameters, A, n, and E_a over the temperature range from 200k to 2000k, expressed by:

$$\boldsymbol{k_\infty = A(T)^n \exp(-E_a/RT)}$$

Activation energies of reactions are calculated as follows:

$$\boldsymbol{E_a = [\Delta H_f^o{}_{298,TS} - \Delta H_f^o{}_{298,reactant}]}$$

Entropy differences between reactant and transition state are used to determine the pre-exponential factor A, via classical, cannonical TST for a unimolecular reaction, $A = (\kappa_b T/h_p)\exp(\Delta S^{\neq}/R)$ where h_p is the Planck constant and κ_b is Boltzman's constant.

Results and Discussion

Enthalpies of Formation ($\Delta H_f^o{}_{298}$)

The enthalpies of formation ($\Delta H_f^\circ{}_{298}$) are estimated using total energies and calculated ΔH_{rxn298} for the listed reactions. The total

energies are determined at the CBS-QB3 level; scaled ZPVE's and thermal corrections to 298.15K are listed in Table 1.2.

Thermochemical Kinetic Analysis of the Reaction $CH_3SC{\cdot}H_2 + O_2 \rightarrow (CH_3SCH_2OO{\cdot})^* \rightarrow$ Products

A potential energy diagram for the methylthiomethyl radical with O2 is illustrated in Figure 1.6; energies are calculated at the CBS-QB3 level. Addition of oxygen to the $CH_3SC{\cdot}H_2$ radical forms an energized adduct.

$$CH_3SC{\cdot}H_2 + O_2 \rightarrow CH_3SCH_2OO{\cdot}^* \rightarrow \text{Products}$$

Possible reactions for this activated adduct are described as follows:

Rxn1: $CH_3SCH_2OO{\cdot}^* \rightarrow$ rev rxn - to reactants $CH_3SC{\cdot}H_2 + O_2$

Rxn2: Stabilization ($CH_3SCH_2OO{\cdot}^* \rightarrow CH_3SCH_2OO{\cdot}$)

Rxn3: Hydrogen atom shift from the methyl group to form a hydroperoxide methyl radical:

$CH_3SCH_2OO{\cdot}^* \rightarrow C{\cdot}H_2SCH_2OOH$ isomer (TS1).

Rxn4: Hydrogen atom transfer from peroxy carbon (TS2)

$CH_3SCH_2OO{\cdot}^* \rightarrow CH3SC{\cdot}HOOH \rightarrow CH_3SC(=O)H + OH$

Note CH3SC·HOOH is unstable and immediately dissociates to $CH_3SC(=O)H$ plus OH radical (TS2)

Rxn5: The peroxy radical can also attack the sulfur atom to form a cyclic transition state structure (TS3, a 4-member ring) where the relatively strong S=O bond (near double bond) starts to form; and the weak (SO—OC) peroxide bond in the transition state starts to cleave (ring opening). The initial product from this reaction: a radical intermediate $CH_3S(=O)CH_2O{\cdot}$ will undergo beta scission (carbonyl formation) resulting in $CH_3S(=O) + CH_2O$

The methylthiomethyl radical ($\Delta H_f^o{}_{298}$ =32.66 kcal/mol) adds to O_2 to form $CH_3SCH_2OO{\cdot}$ peroxy radical. The activation energy of TS1 is 17.06 kcal/mol, and TS1 is below the reactants. The $\Delta H_f^o{}_{298}$ for the $CH_3SC{\cdot}HOOH$ radical in Reaction VI are estimated on the base of the result of $C{\cdot}H_2SCH_2OOH$ and their difference of total energy calculated under MP2/6-31G(d,p) level. The activated $CH_3SCH_2OO{\cdot}^*$ adduct crossed TS2, which then undergoes OH elimination to form $CH_3SC(=O)H$, with the barrier 37.79kcal/mol. Reaction V has a barrier of 32.92 kcal/mol.

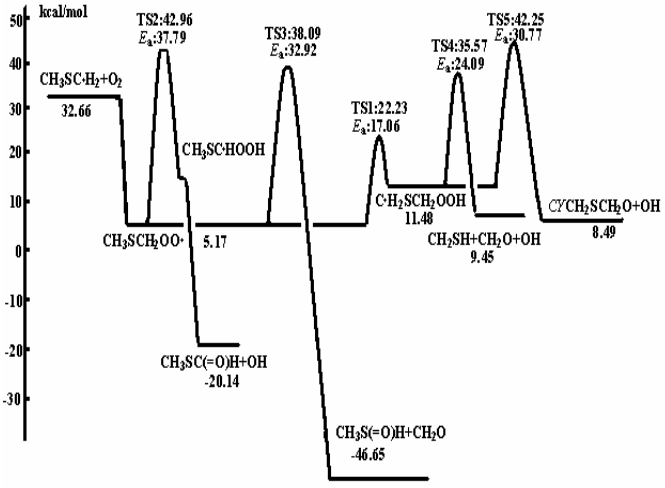

$CH_3SCH_2OO{\cdot} \rightarrow$ Products

The energized $C{\cdot}H_2SCH_2OOH$ can undergo four different reactions, which include reverse reaction back to $CH_3SCH_2OO{\cdot}$ radical, stabilization, CH_2S+CH2O+OH forming through TS4 and reaction through a four-member ring transition state (TS5) to form 1,3-Oxathietane + OH. The activation energy of TS4 and TS5 are respectively 24.09 and 30.77 kcal/mol, based on the CBS-QB3 level of theory.

High-Pressure Limit Rate Constants, - Input Parameters for QRRK Calculations

	Reaction	$A(s^{-1})$	n	E_a (kcal/mol)
k_1	$CH_3SC{\cdot}H_2 + O_2 \rightarrow CH_3SCH_2OO{\cdot}$	5.82E+12	0.00	0.00
k_{-1}	$CH_3SCH_2OO{\cdot} \rightarrow CH_3SC{\cdot}H_2 + O_2$	4.28E+14	0.00	26.90
k_2	$CH_3SCH_2OO{\cdot} \rightarrow C{\cdot}H_2SCH_2OOH$	1.2231E+07	1.20	17.06
k_{-2}	$C{\cdot}H_2SCH_2OOH \rightarrow CH_3SCH_2OO{\cdot}$	7.5535E+10	-0.26	10.75
k_3	$CH_3SCH_2OO{\cdot} \rightarrow CH_3SC(=O)H + OH$	8.3158E+09	0.92	37.79
k_4	$CH_3SCH_2OO{\cdot} \rightarrow CH_3S(=O)H + CH_2O$	1.7013E+10	0.53	32.92
k_5	$C{\cdot}H_2SCH_2OOH \rightarrow CH_2S+CH2O+OH$	6.4507E+13	-0.47	24.09
k_6	$C{\cdot}H_2SCH_2OOH \rightarrow CYCH_2SCH_2O+OH$	3.7282E+13	-0.70	30.77

Lennard-Jones paramenters : σ =5.54Å,ϵ/k=460 Geometric mean frequency (from CPFIT, :

$CH_3SCH_2OO{\cdot}$ (904.0cm^{-1} ×22.5), $C{\cdot}H_2SCH_2OOH$(736.9 cm^{-1} ×23.0)

k_{-1}, k_{-2} : microscopic reversibility

CH3SCH2. + O2 => Products

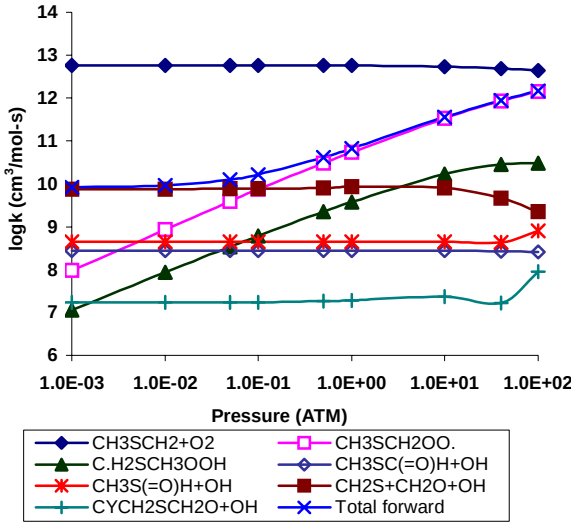

References

(1) Charlson R. J.; Lovelock, J.E.; Andreae. M. O.; Warren, S. G. *Nature* **1987**, *326*, 655.

(2) Hynes A. J.;Wine P. H.;Semmes D. H., J. Phys. Chem., **1986**, *90*, 4148.

(3) Butkovskaya N. I.;LeBras G., *J. Phys. Chem*., **1994**, *98*, 2582.

(4) Resende S. M. ; Almeida W. B. De, *J. Phys. Chem. A*, **1997**, *101*, 9738.

(5) Lovelock J. E., Maggs R. J.;Rasmussen R. A., *Nature*, **1972**, *237*, 452.

(6) Saltzman E. S.; Cooper W. J., in Biogenic Sulfur in the Environment, American Chemical Society, Washington, DC **1989**

(7) *Gaussian 98*, Revision A.9;Gaussian, Inc.: Pittsburgh, PA, **1998**.

(8) Pitzer, K. S.; Gwinn, W. *J. Chem. Phys*. **1942**, *10*, 428

(9) Sheng, C.; Bozzelli, J. W.; Dean, A. M.; Chang, A. Y. *J. Phys.Chem. A* **2002**, *106*, 7276.

Modeling the Reaction of $C_2H_5+O_2$

Chitralkumar V. Naik, Hans-Heinrich Carstensen, and Anthony M. Dean

Chemical Engineering Department
Colorado School of Mines
Golden, CO 80401

Introduction

Modeling of low temperature ethane oxidation requires an accurate description of the reaction of $C_2H_5+O_2$, since its reaction channels either accelerate the oxidation process via chain branching, or inhibit it by forming stable less-reactive products. Before the discovery of the new concerted elimination channel[1], which is the direct formation of $C_2H_4+HO_2$ from ethylperoxy, the isomerization of ethylperoxy ($CH_3CH_2OO\bullet$) to hydroperoxyethyl ($C\bullet H_2CH_2OOH$) was considered the lowest energy channel. According to the Walker and Morley[2] scheme, subsequent reactions of hydroperoxyethyl lead to chain branching, thus promoting ignition. The new lower-lying concerted elimination path is significantly faster than the isomerization, reducing the importance of the isomerization channel and its subsequent chain-branching reactions.

Data are available on different aspects of the $C_2H_5+O_2$ system, for example, on the overall rate constant[3,4] of the reaction and on the production of ethylene[5,6], HO_2[7], and ethylene oxide[6]. Different groups have characterized this reaction theoretically. The latest theoretical studies by Miller et al.[8,9] and Sheng et al.[10], both of which incorporated the concerted elimination channel, can in general explain the observations. However, no reaction mechanism is available that can accurately predict all experimental data.

Our main objective is to develop an accurate mechanism for the $C_2H_5+O_2$ system. We started with a CBS-QB3 potential energy surface (PES) with bond additivity corrections (BAC). Tunneling corrections were included in the calculation of the high-pressure rate constants. These values are used in a chemical activation analysis to calculate pressure-dependent rate coefficients. We tested this mechanism against the wide range of experimental data and found good agreement.

Calculation Methods

The PES was calculated using the CBS-QB3 compound method as implemented in Gaussian 98W[11]. Vibrational frequencies were scaled by 0.99, and vibrational modes resembling internal rotations were replaced by a hindered rotor treatment. Standard statistical mechanics formulas were used to calculate the entropies, heat capacities and thermal contribution to the enthalpy. The electronic energies were converted to heats of formation via the atomization method. We applied bond additivity corrections, similar to the work of Petersson et al.[12] Canonical transition state theory was used to calculate high-pressure rate constants for all reaction channels with pronounced barriers. Contributions from tunneling were incorporated in high-pressure rate constants using Wigner's tunneling correction method[13]. There is no pronounced barrier found for the recombination of C_2H_5 with O_2. In this case, high-pressure rate constants were taken from Miller et al.[9]

The chemically activated reaction of $C_2H_5+O_2$ was then analyzed with the Fortran code CHEMDIS[14]. It uses QRRK theory to calculate energy dependent rate constants k(E). The collisional deactivation is described using the modified strong collision (MSC) approach. Frequency information, to calculate density of states, is provided in form of three representative frequencies with non-integer degeneracies calculated from the heat capacities. The collision parameters required for the MSC model are similar to those used by Sheng et al.[10] In addition to the MSC approach, for a few cases we used solutions of the steady state master equation as described by Sheng et al.[10] The CHEMKIN 3.6.2 package[15] is used for the numerical integration.

Results and Discussion

The major features of the PES calculated at the CBS-QB3 level of theory compare well to those reported by Sheng et al.[10] and Miller et al.[8,9] For example, we find ethylperoxy to be –34.0 kcal/mol relative to the reactants at 0K, compared to –33.9 kcal/mol given by Miller et al. The corresponding value of –34.5 kcal/mol at 298K is reasonably close to –35.3 kcal/mol reported by Sheng et al. All three studies find the barrier of the concerted elimination to be clearly below the reactants: ~2.8 kcal/mol at 0K and ~4.5 kcal/mol at 298K. The differences are somewhat larger for the isomerization reaction. Miller et al. report this barrier to be 3.2 kcal/mol above the reactants at 0K while our calculations yield 1.9 kcal/mol. Our value at 298K is within 0.2 kcal/mol of that reported by Sheng et al. On the other hand, the agreement is not so good when compared to the calculations of the Schaefer group[1].

The high-pressure rate constants calculated in this work are generally higher than those from Sheng et al.[10] The largest difference is found for the isomerization reaction where our value is ~14 times higher at 500K. Many factors may contribute to this deviation. Tunneling accounts for the increase in the rate constant by a factor of 2.7 at this temperature. Another reason may lie in differences in entropy values of the reactants and transition states. The resulting set of pressure-dependent rate coefficients together with additional reactions of peroxy radicals, chlorine and other secondary reactions, will be published elsewhere.

We compared our predictions to the pressure dependence of the overall rate constants of the $C_2H_5+O_2$ reaction observed by Kaiser et al.[3] at 298K. We found our model to underpredict the data in the falloff region by about a factor of two. Moreover, a modified mechanism using rate coefficients for the $C_2H_5+O_2$ system from Klippenstein et al.[16], which were obtained from solutions of the time dependent master equation, showed the same problem. We concluded that the energy transfer process for this system might not be correctly described by generic collision parameters, and that they might underpredict the collision efficiency of He. Thus, we increased the collision cross section by a factor of 2.4 to improve the fit to the falloff curve, and then used this value for all calculations.

Though we cannot present detailed comparisons due to space limitations, we find that our model captures the temperature and pressure dependence of the overall rate constants measured by Slagle et al.[4] Similarly, the predicted pressure dependence of the ethylene yield agrees well with measurements of Kaiser[5].

In recent experiments, Kaiser[6] measured the complex temperature dependence of the ethylene production relative to ethyl chloride. These measurements are compared to the prediction using the current model in Figure 1. We accurately predict the sharp increase in ethylene at 440K that is attributed to the thermal activation of the stabilized $CH_3CH_2OO\bullet$. Also shown are our predictions using the rate coefficients reported by Sheng et al. Their mechanism captures the overall temperature dependence but uniformly underpredicts the ethylene yield.

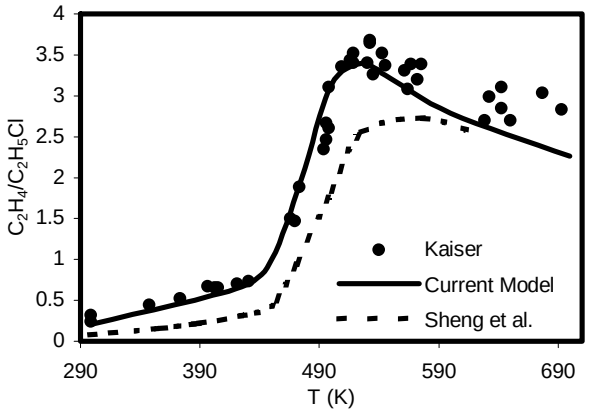

Figure 1. Comparison of the predicted temperature dependence of ethylene production to that reported by Kaiser[6] at a total density of $6.8*10^{18}$ molecules/cm^3. Values shown are the ratio of ethylene to ethyl chloride.

Ethylene oxide (C_2H_4O) is a minor product formed from $C•H_2CH_2OOH$. Kaiser's[6] experimental data provide a test case to validate the relative barriers for isomerization and further reactions of the isomer. Kaiser measured the ethylene oxide production as a function of ethane conversion and of temperature. The comparison of the predicted and measured temperature dependence of the ethylene oxide yield is shown in Figure 2. Initially our model underpredicted ethylene oxide using the originally-calculated barriers. However, by decreasing the isomerization barrier by 1 kcal/mol, the predictions agree well with the measurements. This change did not affect predictions of overall rate constants as well as major products.

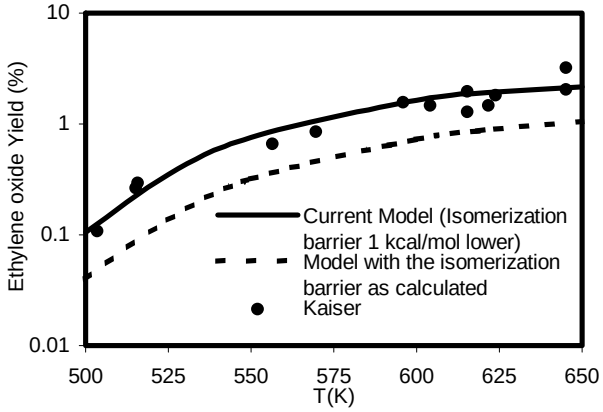

Figure 2. Comparison of the predicted temperature dependence of ethylene oxide yield to that reported by Kaiser[6] at a total density of $6.8*10^{18}$ molecules/cm^3.

Finally, we compared our model to the measurements of HO_2 production by Clifford et al.[7] Since HO_2 reacts quickly with other species, it is important to incorporate secondary reactions in the mechanism. The comparison of the predicted and measured HO_2 concentration profile relative to the initial atomic chlorine concentration at 623K is shown in Figure 3. Note that a fraction of the HO_2 is produced at very early time (due to reaction of the chemically-activated adduct). This is followed by a slower production rate (due to thermally-activated dissociation of ethylperoxy). The entire time profile is predicted accurately. Our prediction of the temperature dependence of the "total" HO_2 yield is also consistent with the measurements of Clifford et al.

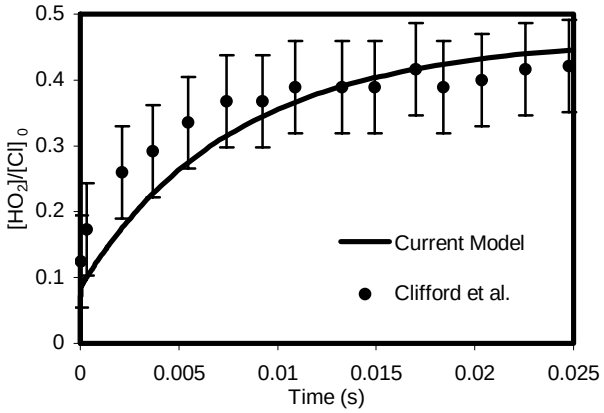

Figure 3. Comparison of the predicted HO_2 time profile relative to the initial chlorine atom concentration to that measured by Clifford et al.[7] at 623K and a total density of $9*10^{17}$ molecules/cm^3.

Conclusions

We have calculated the PES for the $C_2H_5+O_2$ system at CBS-QB3 level with BAC. Tunneling is included in high-pressure rate constants that were used in a QRRK/MSC analysis of the system. The resulting pressure-dependent reaction mechanism accurately predicts a wide range of experimental results including ethylene, HO_2 and ethylene oxide. We feel that this mechanism is suitable to be incorporated in a model of ethane oxidation at low temperatures.

References

(1) Rienstra-Kiracofe, J. C. et al. *J. Phys. Chem. A* 2001, *104*, 9823-9840.
(2) Walker, R. W.; Morley, C. In *Low Temperature Combustion and Autoignition*; Pilling, M. J., Ed.; Elsevier, 1997; Vol. 35, pp 1-124.
(3) Kaiser, E. W. et al. *Chem. Phys. Lett.* 1990, *168*, 309-313.
(4) Slagle, I. R. et al. *J. Phys. Chem.* 1984, *88*, 3648 - 3653.
(5) Kaiser, E. W. *J. Phys. Chem.* 1995, *99*, 707-711.
(6) Kaiser, E. W. *J. Phys. Chem. A* 2002, *106*, 1256-1265.
(7) Clifford, E. P. et al. *J. Phys. Chem. A* 2000, *104*, 11549-11560.
(8) Miller, J. A.; Klippenstein, S. J. *Int. J. Chem. Kinet.* 2001, *33*, 654-668.
(9) Miller, J. A. et al. *Proc. Comb. Symp.* 2000, *28*, 1479-1486.
(10) Sheng, C. Y. et al. *J. Phys. Chem. A* 2002, *106*, 7276 - 7293.
(11) Frisch, M. J. et al.; Revision A.9 ed.; Gaussian, Inc: Pittsburgh, PA, 1998.
(12) Petersson, G. A. et al. *J. Chem. Phys.* 1991, *94*, 6091 - 6101.
(13) Wigner, E. *Zeitschrift fuer physikalische Chemie* 1932, *B 19*, 203.
(14) Chang, A. Y. et al. *Zeitschrift fur Physikalische Chemie* 2000, *214*, 1533-1568.
(15) Kee, R. J. et al.; Release 3.6 ed.; Reaction Design, Inc.: San Diego, CA, 2000.
(16) DeSain, J. D. et al. *J. Phys. Chem. A* 2003, *107*, 4415-4427.

THERMOCHEMICAL AND KINETIC ANALYSIS OF THE ALLYL RADICAL WITH O_2 REACTION SYSTEM

Jongwoo Lee and Joseph W. Bozzelli

Department of Environmental Science and Chemistry,
New Jersey Institute of Technology, Newark, NJ 07102

Introduction

Olefins (Alkenes) are major initial products from pyrolysis, oxidation or photochemical reactions of alkanes and ethers. The double bond in alkenes provides both an unsaturated site for addition reactions and an allylic site for facile abstractions, where the corresponding activation energy is lowered due to electron delocalization on the radical formed. The stability and low reactivity of these alkenyl radicals have been connected to the antiknock effect of fuel additives such as ethyl tert-butyl ether (ETBE).[1] The relatively high octane ratings for olefin blending suggest that olefins play an important role in pre-ignition chemistry related to engine knock. It is valuable to understand the fundamental chemical reaction pathways and kinetics of olefin oxidation in moderate to low temperature combustion chemistry for model development.

Ruiz et al.,[2] Morgan et al.,[3] and Slagle et al.[4,5] have reported the R—O_2 bond energy (17.2, 18.2, 18.4 kcal/mol, respectively) for the allyl (CH_2CHCH_2•, • : radical site) radical. Walker and co-workers[6,7] had studied at a total pressure of 60 Torr between 400 and 520 °C, where the equilibrium in the R + O_2 ⇔ RO_2 addition reaction is shifted to left, the rate constants of the CH_2CHCH_2• + O_2 → products reaction are significantly lower than those observed in the case of alkyl radicals. Baldwin et al.[8] and Lodhi and Walker[6] reported similarly low rate constants for the substituted allyl radicals, $CH_3CH_2CHCHCH_2$• and $CH_3CHCHCH_2$• reactions with O_2. Knyazev and Slagle[5] also studied the kinetics of the reaction $CH_3CHCHCH_2$• + O_2 ⇔ $CH_3CHCHCH_2O_2$• using laser photolysis/photoionization mass spectrometry. Room temperature decay constants of the $CH_3CHCHCH_2$• radical were determined in time-resolved experiments as a function of bath gas density ([He] = (3-24) × 10^{16} molecule cm^{-3}) and the rate constant at 297 K is k = (6.42 ± 0.54) × 10^{-13} cm^3/ (molecule s). At high temperatures (600 – 700K), no reaction of $CH_3CHCHCH_2$• with O_2 could be observed and upper limits to the rate constants were determined (1 × 10^{-16} cm^3/ (molecule s) at 600 K and 2 × 10^{-16} cm^3/ (molecule s) at 700 K).

Chen et al.[9] studied allylic isobutenyl radical with O_2. They reported the forward and reverse rate constants for initiation reaction, $CH_2C(CH_3)_2H + O_2 ⇔ CH_2C(CH_3)_2• + HO_2$ to be 1.86 × 10^9 × $T^{1.301}$ × exp(-40939 cal/RT) cm^3/ (mol s) and 6.39 × 10^8 × $T^{0.944}$ × exp(-123.14 cal/RT) cm^3/ (mol s), respectively. They also proposed an important new reaction path, $CH_2C(CH_2•)COOH$ ⇔ $CH_2C(CH_2•)CO• + OH$ ⇔ $CH_2Y(\underline{CCOC}) + OH$, for methylene oxirane formation.

This study focuses on the reaction mechanism of the allyl radical association with O_2. Thermochemical properties are estimated for reactants, intermediates, products and transition states in the reaction paths using *ab initio* and density functional calculations. The thermochemical parameters are used to calculate high-pressure limit rate constants using canonical Transition State Theory (TST). Rate constants as a function of temperature and pressure are estimated using a multifrequency quantum RRK analysis for k(E) and master equation for falloff. The data at relevant pressures and temperatures should be useful to both atmospheric and combustion models.

Calculation methods

Enthalpies of formation ($\Delta H_f°_{298}$) for reactants, intermediate radicals, transition states and products are calculated using the CBS-Q//B3LYP/6-31G(d,p) composite method and density functionals. The initial structure of each compound or transition state is determined using ROHF or UHF/PM3 in MOPAC,[10] followed by optimization and vibrational frequency calculation at B3LYP/6-31G(d,p) level of theory using GAUSSIAN 98.[11] Transition state geometries are identified by the existence of only one imaginary frequency, structure information and the TST reaction coordinate vibration information. Zero-point vibrational energies (ZPVE) are scaled by 0.9806 as recommended by Scott and Radom.[12] Single point energy calculations are carried out at the B3LYP/6-31G(d,p), /6-311+G(d,p), or /6-311++G(d,p). The CBS-Q method of Petersson and co-workers for computing accurate energies[13,14] is chosen as the determining enthalpies used in our kinetic analysis.

The CBS-Q//B3LYP/6-31G(d,p) calculation sequence is illustrated in Scheme 1 [Corrections for unpaired electron and spin contamination in intermediate overlap (i.e., $0< {}^{\alpha\beta}S_{ij} <1$) between the α- and β-spin orbitals[15] are included].

Scheme 1. CBS-Q//B3LYP/6-31G(d,p) Calculation Sequence

	Level of Theory
Optimized Geometry	B3LYP/6-31G(d,p)
Single Point Calculation	QCISD(T)/6-31+G(d')
	MP4(SDQ)/CBSB4
	MP2/CBSB3 CBSExtrap = (Nmin=10,Pop)

Determination of enthalpy of formation. The method of isodesmic reactions is used to determine the enthalpy of formation ($\Delta H_f°_{298}$) for parent and radical species. It provides higher accuracy for estimates of $\Delta H_f°_{298}$ than heats of atomization does.[16-18]

CH_2=CHCH_2OOH + CH_3CH_3 ⇔ CH_2=$CHCH_3$ + C_2H_5OOH (IR1)

CH_2=CHCH_2OO• + C_2H_5OH ⇔ CH_2=$CHCH_2OH$ + C_2H_5OO• (IR2)

C•H=CHCH_2OOH + C_2H_4 ⇔ CH_2=$CHCH_2OOH$ + C_2H_3• (IR3)

CH_2=C•CH_2OOH + CH_2=$CHCH_3$ ⇔ CH_2=$CHCH_2OOH$ + CH_2=C•CH_3 (IR4)

Y$\underline{CCCOO}$ + $(CH_3)_3CH$ ⇔ CY$\underline{CCOOC}$ + $CH_3CH_2CH_3$ (IR5)

Y$\underline{CC•COO}$ + CY$\underline{CCOOC}$ ⇔ Y$\underline{CCCOO}$ + CY$\underline{C•COOC}$ (IR6)

HOCH_2Y$\underline{CCO}$ + CH_3CH_3 ⇔ Y$\underline{CCO}$ + $(CH_3)_2C(OH)H$ (IR7)

O•CH_2Y$\underline{CCO}$ + CH_3OH ⇔ $HOCH_2Y\underline{CCO}$ + CH_3O• (IR8)

Ab initio calculations for ZPVE and thermal correction energy are performed on all of four compounds in the reaction. The three reference compounds in the working reaction (IR1), excepting the target molecule, CH_2=$CHCH_2OOH$ in (IR1), have experimental or theoretical determined values of $\Delta H_f°_{298}$. The unknown $\Delta H_f°_{298}$ of CH_2=$CHCH_2OOH$ is obtained with the calculated $\Delta H°_{rxn(298)}$ and known $\Delta H_f°_{298}$ of the three reference compounds. The other parent and radical species are calculated in the same manner.

Determination of entropy and heat capacity. The contributions of external rotations, translations, and vibrations to entropies and heat capacities are calculated from scaled vibration frequencies and moments of inertia for the optimized B3LYP/6-31G(d,p) structures. The number of optical isomers and spin degeneracy of unpaired electrons are also incorporated. Contributions from hindered internal rotation for S and $Cp(T)$ are determined using direct integration over energy levels of the intramolecular rotational potential curves. A program, "ROTATOR[19]", is used for calculation

of the energy levels. This technique employs expansion of the hindrance potential in the Fourier series (Eq. I), calculation of the Hamiltonian matrix on the basis of wave functions of the free internal rotor, and subsequent calculation of energy levels by direct diagonalization of the Hamiltonian matrix.[20,21] The torsional potential calculated at discrete torsion angles is represented by a truncated Fourier series:

$$V(\Phi) = a_0 + \Sigma\, a_i \cos(i\Phi) + \Sigma\, b_i \sin(i\Phi) \quad i = 1, 2, 3, \ldots \quad \text{(Eq. I)}$$

Values of the coefficients (a_0, a_i and b_i) are calculated to provide the minimum and maximum of the torsional potentials with allowance of a shift of the theoretical extreme angular positions.[20,21]

High-pressure limit A factor (A) and rate constant (k_∞) determination. For the reactions where thermochemical properties of transition state are calculated by ab initio or density functional methods, k_∞'s are fit by three parameters A, n, and *Ea* over temperature range from 298 to 2000K, $k_\infty = A\,(T)^n \exp(-Ea/RT)$. Entropy differences between reactant and transition state are used to determine the pre-exponential factor, A, via canonical Transition State Theory (TST)

$$A = (k_b T/h_p)\exp(\Delta S^{\ddagger}/R),\ Ea = \Delta H^{\ddagger}$$

(h_p is the Planck constant and k_b is the Boltzmann constant.) Treatment of the internal rotors for *S* and *Cp*(*T*) is important here because these internal rotors are often lost in the cyclic transition state structures.

Kinetic analysis. Thermochemical properties for each species on the potential energy surface for the reaction system are evaluated. Forward or reverse rate constants (high-pressure limit) for each, elementary reaction step are determined from the calculations and use of literature data for enthalpies of stable molecules. Reverse rate constants are calculated from microscopic reversibility.

Multifrequency quantum Rice-Ramsperger-Kassel (QRRK) analysis is used to calculate *k*(E) with a master equation analysis[22] for fall-off in order to obtain rate constants as a function of temperature and pressure. This kinetic analysis is for the chemical activation and the dissociation reaction systems. The master equation analysis[22] uses an exponential-down model for the energy transfer function with $(\Delta E)^\circ_{down}$ = 1000 cal/mol,[23,24] for N_2 as the third body and a 500 cal energy grain is used.

The QRRK/master equation analysis is described by Chang et al.[22,25] Further validated by recent work of Sun et al. ((JP030667l) in press 2003). The QRRK code utilizes a reduced set of three vibration frequencies which accurately reproduce the molecules' heat capacity; the code includes contribution from one external rotation in calculation of the ratio of the density of states to the partition coefficient ρ(E)/Q. Comparisons of ratios of these ρ(E)/Q with direct count ρ(E)/Q's have been shown to result in good agreement.[26] Rate constant results from the quantum RRK-Master equation analysis are shown to accurately reproduce (model) experimental data on several complex systems. They also provide a reasonable method to estimate rate constants for numerical integration codes by which the effects of temperature and pressure can be evaluated in complex reaction systems.

Results and Discussion

Enthalpy of formation ($\Delta H_f^\circ{}_{298}$). The enthalpies of formation for CH_2=$CHCH_2OOH$ are –13.53 and –13.49 kcal/mol by B3LYP/6-31G(d,p) and CBSQ//B3LYP/6-31G(d,p), respectively. The enthalpy of formation for the parent hydroperoxide is important because it allows the evaluation of peroxy radicals.

The bond energies of CH_2=$CHCH_2OOH$, $C(OOH)H_2CHO$,[27] C_2H_5OOH,[22] and $CH_3C(=O)OOH$[28] are compared in **Table 1**. The R–OOH bond energy in CH_2=$CHCH_2OOH$ is 14 kcal/mol lower than that of C_2H_5OOH, because the radical site is resonantly stabilized. The RO–OH and ROO–H bonds in CH_2=$CHCH_2OOH$ are 45.4 and 86.6 kcal/mol, similar to those in C_2H_5OOH, 45.1 and 85.3 kcal/mol, respectively.

Table 1. Comparison of Bond Energies between Allyl Hydroperoxide and three C2 Hydroperoxide

(Units in kcal/mol)	**CH_2=$CHCH_2OOH$**	$C(OOH)H_2CHO$	C_2H_5OOH	$CH_3C(=O)OOH$
ROO—H	**86.61**	87.28	85.27	98.33
RO—OH	**45.39**	45.13	45.12	50.95
R—OOH	**57.05**	63.21	71.35	85.22
H--CH=$CHCH_2OOH$	**112.36**	n/a	n/a	n/a
CH_2=C(--H)CH_2OOH	**110.17**	n/a	n/a	n/a
$C(OOH)H_2C(=O)$--H,	n/a	88.65	n/a	n/a
H--CH_2CH_2OOH,	n/a	n/a	103.21	n/a
H--$CH_2C(=O)OOH$	n/a	n/a	n/a	103.95

Entropy ($S^o_{(298)}$) and heat capacity ($Cp(T)$, $300 \le T/K \le 1500$). Entropy and heat capacities are calculated based on vibration frequencies and moments of inertia of the optimized B3LYP/6-31G(d,p) structures. Symmetry, number of optical isomers and electronic spin are incorporated in estimation of $S^o_{(298)}$. Torsion frequencies are omitted in these calculations, instead, contributions from internal rotation for $S^o_{(298)}$ and $Cp(T)$'s are determined, using direct integration over energy levels of the intramolecular rotational potential curves[20,21].

Potential energy diagram for CH_2=$CHCH_2$• + O_2 reaction system. The energy diagram for the allyl (CH_2=$CHCH_2$•) + O_2 reaction is illustrated in two **Figures 1 and 2**. The reactions involving intramolecular hydrogen transfer and direct HO_2 elimination are illustrated in **Figure 1**. Reactions involving peroxy radical addition to each of the π bond carbons, ring formation, and subsequent reactions of the two cyclic peroxide alkyl radicals are illustrated in **Figure 2**. The 14 reaction paths, 6 reaction intermediates, and 14 transition states are illustrated. Enthalpies of formation are from CBSQ// B3LYP/6-31G(d,p) calculations and in units of kcal/mol. Transition state enthalpies are relative to the corresponding stabilized adduct.

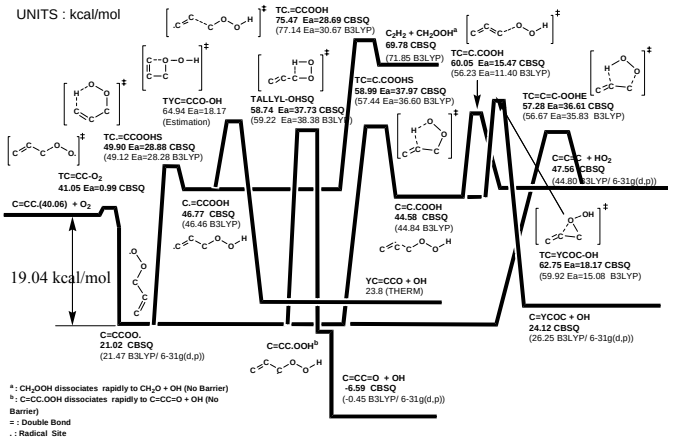

Figure 1. Potential energy I of II for allyl + O_2 (I) Isomerizations via H shifts.

The allyl radical adds to O_2 (*Ea* = 0.99) to form an energized peroxy adduct [CH_2=$CHCH_2OO$•]* with a shallow well (ca. 19

kcal/mol); which predominantly dissociates back to reactants under combustion conditions. The reaction channels of the [CH_2=$CHCH_2OO$•]* adduct include reverse reaction to reactants, stabilization to CH_2=$CHCH_2OO$• radical ($\Delta H_f°_{298}$ = 21.02), decomposition to products, CH_2=C=CH_2 + HO_2 via direct HO_2 elimination with a barrier (*Ea* = 36.61), isomerizations via hydrogen shifts to form C•H=$CHCH_2OOH$ or CH_2=C•CH_2OOH isomers ($\Delta H_f°_{298}$ = 46.77 or 44.58, respectively) with barriers (*Ea* = 28.88 or 37.97, respectively), or a hydrogen transfer (*Ea* = 37.73) from the ipso carbon to the peroxy radical to form the unstable intermediate {CH_2=CHC•HOOH}, which immediately dissociates to more stable products, 2-propenal plus OH.

The C•H=$CHCH_2OOH$ isomer can undergo β scission to products, (C_2H_2 + {C•H_2OOH} → C_2H_2 + CH_2O + OH) (*Ea* = 37.73), a ring closure to form the unstable intermediate {YCCCO} plus OH, (Y = cyclic) which rapidly dissociates to more stable products, 2-propenal plus OH, or isomerize via a hydrogen shift (*Ea* = 3.13) to form a CH_2=$CHCH_2OO$• isomer.

The CH_2=C•CH_2OOH isomer can undergo β scission to products, CH_2=C=CH_2 + HO_2 (*Ea* = 15.47), a ring closure to form methyene oxirane plus OH radical (*Ea* = 18.17), or isomerize via a hydrogen shift (*Ea* = 14.41) to form a CH_2=$CHCH_2OO$• isomer.

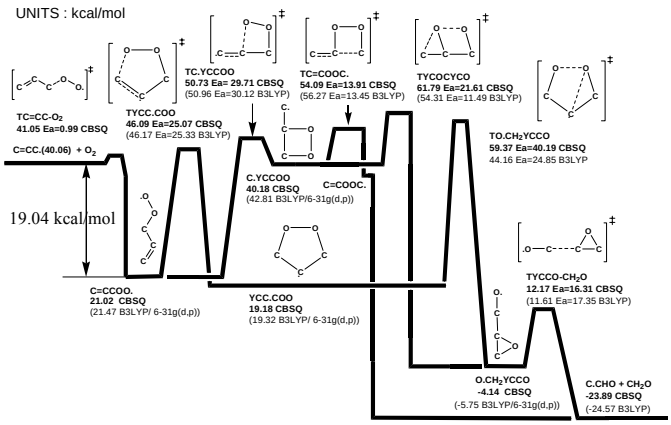

Figure 2. Potential energy II of II for allyl + O_2 (II) Cyclization pathways to form cyclic adducts and further reactions.

Intramolecular peroxy radical addition to sp^2 hybridized carbons - cyclization reaction paths. The [CH_2=$CHCH_2OO$•]* adduct can also cyclize to four- or five-member cyclic peroxide-alkyl radicals, C•H_2YCCOO and YCC•COO ($\Delta H_f°_{298}$ = 40.18 and 19.18, respectively). CH_2=$CHCH_2OO$• cyclization to four- or five-member cyclic peroxides require barriers, *Ea* = 29.71 and 25.07, respectively), which have slightly higher barriers than reverse reaction (*Ea* = 20.03).

The C•H_2YCCOO adduct can undergo β scission to products, C•H_2CHO + CH_2O (*Ea* = 13.91), form a cyclic epoxide-alkoxy radical, O•CH_2YCCO ($\Delta H_f°_{298}$ = -4.14) via TYCOCYCO (*Ea* = 21.61), or undergo ring open to form CH_2=$CHCH_2OO$• adduct (*Ea* = 10.55). The O•CH_2YCCO intermediate will undergo β scission to products, C•H_2CHO + CH_2O via TYCCO-CH_2O (*Ea* = 16.31).

The 5-member ring YCC•COO can also form the epoxide-alkoxy radical (above), O•CH_2YCCO via TO•CH_2YCCO (*Ea* = 40.19), undergo ring open to form CH_2=$CHCH_2OO$• adduct (*Ea* = 26.91). This cyclic YCC•COO adduct further reacts with O_2 to chain branching products: CH_2O + C(=O)HC(=O)H + OH.

Comparison of CH_2=CHC•H_2, C•H_2CHO, C_2H_5, and CH_3C•O with O_2. The CH_2=CHC•H_2 + O_2, C•H_2CHO + O_2,[27] C_2H_5 + O_2,[22] and CH_3C•O + O_2[28] reaction systems have significant differences. The CH_2=CHC•H_2 + O_2 reaction system of this study has a lower well depth of 19.04 kcal/mol compared to C•H_2CHO + O_2, C_2H_5 + O_2 and CH_3C•O + O_2, which have well depths of 27.5, 35.3 and 35.5 kcal/mol, respectively.

The H shift barriers in the CH_2=$CHCH_2OO$•, C(OO•)H_2CHO and CH_3C(=O)OO• peroxy radicals are lower than those of concerted HO_2 elimination, whereas in C_2H_5OO•, direct HO_2 elimination has a lower barrier than the H shift.

The well depth and barriers of H shift and HO_2 elimination in the CH_2=CHC•H_2, C•H_2CHO, C_2H_5•, and CH_3C•O with O_2 reaction systems are compared in **Table 2**.

Table 2. Comparison of CH_2=CHC.H_2, C.H_2CHO, C_2H_5, and CH_3C.(=O) with O_2

(Units in kcal/mol)		CH_2=CHC.H_2 + O_2	C.H_2CHO + O_2	C_2H_5 + O_2	CH_3C.(=O) + O_2
Well Depth		**19.04**	27.5	35.3	35.5
Barrier in	1) H Shift[a]	**28.88**	20.25	36.36	26.42
	2) HO_2 Elimination[a]	**36.61**	48.31	30.48	34.58

[a] H shift and HO_2 elimination for the CH_2=$CHCH_2OO$., C(OO.)H_2CHO, C_2H_5OO., and CH_3C(=O)OO.

Kinetic analysis for allyl + O_2. The QRRK calculations for *k*(E) and master equation analysis for fall-off are performed on this allyl (CH_2=$CHCH_2$•) + O_2 reaction system to estimate rate constants and to determine important reaction paths as a function of temperature and pressure. Rate constants at 1 atm pressure versus 1000/T are illustrated in **Figure 3**. Stabilization CH_2=$CHCH_2OO$• is important below 600 K, with reverse dissociation above 600 K. CH_2=$CHCH_2OO$• adduct, cyclic isomers, and H-shift isomers exhibit significant falloff at higher temperatures (above 800 K). Allene + HO_2 products via a HO_2 molecular elimination path, YCC•COO via cyclization, and H transfer from primary vinyl group to peroxy radical; then β-scission reaction leading to C_2H_2 + CH_2O + OH are major product channels at higher temperatures (above 600 K).

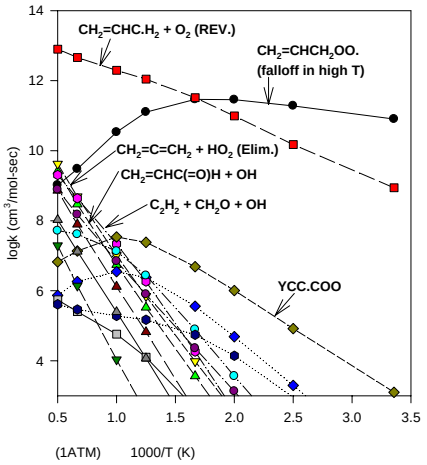

Figure 3. CH_2=$CHCH_2$ + O_2 -> products *k* vs. 1000/T at 1 atm.

Conclusions

Thermochemical properties for important species in the allyl radical (CH_2=$CHCH_2$•) + O_2 reaction system are calculated using density functional and *ab initio* methods. Enthalpies of formation ($\Delta H_f°_{298}$) are determined using isodesmic reactions at the CBSQ level. Entropies ($S°_{298}$) and heat capacities ($Cp(T)$) include internal rotor contributions.

The CH_2=CHC•H_2 + O_2 reaction system is found to have a relatively shallow well depth of 19.04 kcal/mol and all product formation pathways from the peroxy radical, involve barriers that are above the energy of the initial reactants. Major reaction paths at 1 atm pressure are stabilization of the peroxy adduct (CH_2=$CHCH_2$OO•) below 600 K, with reverse dissociation above 600 K. Important reaction products are allene + HO_2 products via a HO_2 molecular elimination, YCC•COO which dissociates or further reacts to chain branching products. C•H=$CHCH_2$OOH from hydrogen transfer, which undergoes β-scission reaction leading to C_2H_2 + CH_2O + OH is important product channel above 600 K.

Acknowledgements. We acknowledge the USEPA Northeast Regional Research Center and the USEPA Airborne Organics Research Center for funding. We would also like to thank to C. Sheng for the SMCPS program.

References

(1) Bach, R. D.; Ayala, P. Y.; Schlegel, H. B. *J. Am. Chem. Soc.* **1996**, *118*, 12758.
(2) Ruiz, R. P.; Bayes, K. D.; Macpherson, M. T.; Pilling, M. J. *J. Phys. Chem.* **1981**, *85*, 1622.
(3) Morgan, C. A.; Pilling, M. J.; Tulloch, J. M.; Ruiz, R. P.; Bayes, K. D. *J. Chem. Soc. Faraday Trans. 2* **1982**, *78*, 1323.
(4) Slagle, I. R.; Ratajczak, E.; Heaven, M. C.; Gutman, D.; Wagner, A. F. *J. Am. Chem. Soc.* **1985**, *107*, 1838.
(5) Knyazev, V. D.; Slagle, I. R. *J. Phys. Chem. A* **1998**, *102*, 8932.
(6) Lodhi, Z. H.; Walker, R.W. *J. Chem. Soc., Faraday Trans.* **1991**, *87*, 681.
(7) Stothard, N. D.; Walker, R. W. *J. Chem. Soc. Faraday Trans.* **1992**, *88*, 2621.
(8) Baldwin, R. R.; Bennett, J. P.; Walker, R. W. *J. Chem. Soc. Faraday Trans. 1* **1980**, *76*, 2396.
(9) Chen, C.; Bozzelli, J. W. *J. Phys. Chem. A* **2000**, *104*, 9715.
(10) Stewart, J .J. P. MOPAC 6.0, J. Frank Seiler Research Lab., US Air Force Academy: Colorado, **1990**.
(11) Frisch, M. J.; Trucks, G. W.; Schlegel, H. B.; Scuseria, G.; Robb,M. A.; Cheesman, J. R.; Zakrzewski, V. G.; Montgomery, J. A., Jr.; Stratmann, R. E.; Burant, J. C.; Dapprich, S.; Millam, J. M.; Danicls, A. D.; Kudin, K. N.; Strain, M. C.; Farkas, O.; Tomasi, J.; Baronc, V.; Cossi, M.; Cammi, R.; Mennucci, B.; Pomelli, C.; Adamo, C.; Clifford, S.; Ochterski, J.; Petersson, G. A.; Ayala, P. Y.; Cui, Q.; Morokuma, K.; Malick, D. K.; Rabuck, A. D.; Raghavachari, K.; Froesman, J. B.; Cioslowski, J.; Ortiz, J. V.; Baboul, A. G.; Stefanov, R. B.; Liu, G.; Liashenko, A.; Piskorz, P.; Komaromi, I.; Gomperts, R.; Matrin, R. L.; Fox, D. J.; Keith, T.; Al-Laham, M. A.; Peng, C. Y.; Nanayakkara, A.; Gonzalez, C.; Challacombe, M.; Gill, P. M. W.; Johnson, B.; Chen, W.; Wong, M. W.; Andres, J. L.; Head-Gordon, M.; Pople, J. A. *Gaussian 98*; Gaussian Inc.: Pittsburgh, PA, **1998**.
(12) Scott, A. P.; Radom, L. *J. Phys. Chem.* **1996**, *100*, 16502.
(13) Nyden, M. R.; Petersson, G. A. *J. Chem. Phys.* **1991**, *75*, 1843.
(14) Petersson, G. A. *J. Chem. Phys.* **1994**, *94*, 6081.
(15) Montgomery Jr., J. A.; Petersson, G. A. *J. Phys. Chem.* **1994**, 101, 5900.
(16) Hehre, W. J.; Radom, L.; Schleyer, P. R.; Pople, J. A. *Ab-Initio Molecular Orbital Theory*, John Wiley & Sons: New York, NY, 1986.
(17) Lay, T. H.; Bozzelli, J. W. *J. Phys. Chem. A* **1997**, *101*, 9505.
(18) Sun, H.; Bozzelli, J. W. *J. Phys. Chem. A* **2001**, *105*, 4504.
(19) Shokhirev, N. V. http://www.chem.arizona.edu/faculty/walk/nikolai/programs.html #programs July, 2002.
(20) Lay, T. H.; Krasnoperov, L. N.; Venanzi, C. A.; Bozzelli, J. W. *J. Phys. Chem.* **1996**, *100*, 8240.
(21) Yamada, T.; Lay, T. H.; Bozzelli, J. W. *J. Phys. Chem. A* **1999**, *103*, 5602.
(22) Sheng, C. Y.; Bozzelli, J. W.; Dean, A. M.; Chang, A. Y. *J. Phys. Chem. A* **2002**, *106*, 7276.
(23) Troe, J. *In Combustion Chemistry*, W.C. Gardiner Jr., Ed.; Springer-Verlag: New York, 1984.
(24) Knyazev, V. D.; Slagle, I. R. *J. Phys. Chem.* **1996**, *100*, 5318.
(25) Chang, A. Y.; Bozzelli, J. W.; Dean, A. M. *Int. J. Res. Phys. Chem. Chem. Phys. (Zeit. Phys. Chem)* **2000**, *214*, 1533.
(26) Bozzelli, J. W.; Chang, A. Y.; Dean, A. M. *Int. J. Chem. Kinet.* **1997**, *29*, 161.
(27) Lee, J.; Bozzelli, J. W. *J. Phys. Chem. A* **2003**, *107*, 3778.
(28) Lee, J.; Chen, C.; Bozzelli, J. W. *J. Phys. Chem. A* **2002**, *106*, 7155.

Computational Study of the Oxygen Initiated Decomposition of 2-Oxepinoxy Radical

John K. Merle and Christopher M. Hadad

Department of Chemistry, The Ohio State University, Columbus, Ohio 43210

Introduction

Benzene is the archetypal aromatic hydrocarbon. Benzene and its derivatives are common fuel constituents in addition to a suitable model from which its oxidative pathways can be used to infer similar oxidation processes for larger polycyclic aromatic compounds. Benzene oxidation has therefore been the subject of numerous studies. Experimental studies using mass spectrometric detection[1,2,3,4,5] at high and intermediate temperatures indicate that the most common products of benzene oxidation are CO_2, CO, C_2H_2 (acetylene), cyclopentadienyl radical, and various unsaturated C_2O_x and C_3O_x species. The commonly accepted mechanism based on intermediate to high temperature experiments for the initiation of benzene oxidation with molecular oxygen is the generation of phenyl radical via reaction (Eqn. 1)[1,4] followed by the addition of molecular oxygen and concomitant lose of oxygen atom (^{3}P) (Eqn. 2).[1,2,3]

$$C_6H_6 + O_2 \rightarrow C_6H_5 + HO_2 \qquad (1)$$

$$C_6H_5 + O_2 \rightarrow C_6H_5O + O(^3P) \qquad (2)$$

Yu and Lin,[6] however, performed kinetic studies to determine the rate of reaction of phenyl radical with O_2 using cavity-ring down (CRD) spectroscopy and detected phenyl peroxy radical up to 473 K. Norrish and Taylor[7] via identification of ortho and para dihydroxybenzenes, in experiments using a flow system to analyze the reaction of benzene with O_2 in a nitrogen diluent at 685 K, predicted the inclusion of phenyl peroxy radical as a probable intermediate.

Computational studies have also been undertaken in order to determine the most thermodynamically and kinetically viable mechanistic pathways involved in benzene oxidation.[8,9,10] Theoretical studies, based on B3LYP/6-311+G**//B3LYP/6-31G* free energies, by this group, predict that the phenylperoxy radical is the more thermodynamically favored intermediate, verses phenoxy radical at $T \leq \sim 450$ K, while at $T > 450$ K, entropy dominates thereby making phenoxy radical the prominent intermediate. This implies that under low temperature combustion and atmospheric conditions the phenyl peroxy radical is likely to play an important role in the decomposition of phenyl radical.

Carpenter utilized PM3/UHF semiempirical calculations to elucidate possible decomposition pathways for phenylperoxy radical to form cyclopentadienyl radical and CO_2. He considered a pathway in which phenylperoxy radical proceeds through formation of a spirodioxiranyl radical, with an enthalpic barrier of 26.1 kcal/mol, to form thermodynamically stable seven-membered ring radical, 2-oxepinoxy (**1**) shown in Figure 1. Barckholtz et.al. and Fadden et. al. have refined the same energy surface using density functional theory and high-level *ab initio* calculations to study this decomposition process as well as the formation of a dioxetanyl radical intermediate leading to the 2-oxepinoxy radical (**1**).[9,10] Decomposition through the spirodioxiranyl radical was shown to be the most viable reaction path leading to 2-oxepinoxy radical, with a free energy barrier of ~41.6 kcal/mol at 298 K, due to the inclusion of an additional high energy triradical intermediate (Figure 1). Despite the inclusion of the high energy triradical species, this pathway exhibited a lower barrier than that for the formation of phenoxy radical and oxygen atom at ~51.0 kcal/mol. These barriers are rough estimates, however, because of spin contamination in the wavefunctions of the key intermediates. At the B3LYP/6-311+G**//B3LYP/6-31G* level, 2-oxepinoxy radical was calculated to have a $\Delta G(298\ K)$ energy which is 79.9 kcal/mol lower than separated phenyl radical and $O_2(^3\Sigma_g)$ reactants. Consistent values were obtained with UMP4(SDQ)/6-31G** and UCCSD(T)/6-31G** energy calculations in the same study. Mebel and Lin[11] in a theoretical study of $C_6H_5O_2$ geometrical isomers estimated 2-oxepinoxy radical (**1**) to have a $\Delta H(0\ K)$ of -91.8 kcal/mol based on PUMP3/6-31G*//UHF/6-31G* energies. The stability of 2-oxepinoxy radical indicates that it should be relatively long-lived upon formation and therefore susceptible to further oxidation by reactive species contained in a typical radical pool.

In this study, we will utilize the B3LYP hybrid density functional theory functional to analyze the potential energy surface for the decomposition of 2-oxepinoxy radical after further peroxy radical formation via addition of O_2 ($^3\Sigma_g$). The energies of minima and activation barriers for decomposition following the initial formation of 1,2-dioxetanyl, 1,3-peroxy, 1,4-peroxy, scission of the O-O peroxy bond, and abstraction of an H-atom by the geminal peroxy moiety. The energies for these surfaces will be evaluated from T = 298-1250 K, the range in which phenylperoxy radical has been shown to be a viable combustion component.

Figure 1. Reaction scheme for the generation of 2-oxepinoxy radical

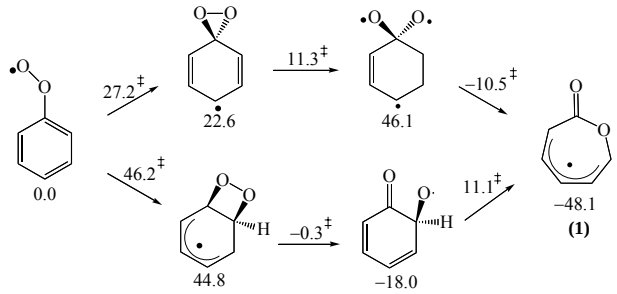

(1). Energies are B3LYP/6-311+G**//B3LYP/6-31G* $\Delta G(298\ K)$ relative to phenylperoxyl radical.

Oxygen Addition to 2-Oxepinoxy Radical

The addition of O_2 to 2-oxepinoxy radical (**1**) is most likely to occur at three different positions on the 2-oxepinoxy radical ring, forming three distinctive peroxyoxepinone radicals (**1a, 1b,** or **1c, Figure 2**), due to delocalization of the lone electron within the π network of the ring carbons. Addition can occur at the 2, 4 and 6 ring positions, numbered relative to the carbonyl carbon, as position 1, moving counterclockwise. Figure 2 shows the structure of 2-oxepinoxy radical (**1**) and the peroxy radical structures formed after the addition of molecular oxygen. Also shown in Figure 2 are the 298 K free energies ($\Delta G(298\ K)$) for each intermediate and transition state relative to reactants at infinite separation. Each free energy of activation barrier is relative to the reactant for that individual step.

2-Addition. Three unique transition state **(TS)** structures for the formation of 2-peroxyoxepinone radical **(1a)** were found. In each transition state, the oxygen molecule approaches perpendicular to the ring plane and differs in the relation of the O-O bond rotation about the forming C-O bond. All three TS wavefunctions have considerable spin contamination, giving $\langle S^2 \rangle$ values of ~ 1.0, rendering the transition state barriers to be suspect. Regardless, the 298 K free energy barrier ($\Delta G^{\ddagger}(298\ K)$) for the lowest energy TS structure, with the O-O oxygen bond setting above the C_1-C_2 ring bond, is 17.7 kcal/mol with $\langle S^2 \rangle$ value of 0.96, the least spin contaminated of the

three wavefunctions. The 298 K reaction is endoergic by 10.4 kcal/mol with a reverse ΔG‡(298 K) of only 7.3 kcal/mol.

4-Addition. Two TS structures were found for addition of oxygen to the 6 ring carbon to form 6-peroxy-oxepinone radical **(1b)**. In both transition structures, the oxygen molecule enters from above the ring plane. In the lower energy TS, the O-O bond adds anti to the C-H bond and over the inside of the ring while the higher energy structure has the O-O bond almost eclipsing the C-H bond. Spin contamination for both transition states was also significant, ($\langle S^2 \rangle \sim 1.0$). The ΔG‡(298 K) for the lowest energy transition structure was 17.0 kcal/mol. This barrier is also the lowest for molecular oxygen addition at the three carbon positions. A simple Hückel analysis for the 5-carbon ring π system for **1** indicates that most of the electron density should be localized on the 4 carbon. Examination of the C-C bond lengths on the ring are consistent with Hückel theory, with the two C-C bonds containing the 4 carbon at 1.40 and 1.42 Å, with bond lengths intermediate between typical C–C single and double bond character. The C-C bonds adjacent have lengths of 1.38 and 1.36 Å exhibiting more pure C–C double bond character. Formation of **1b**, however, is endoergic by 13.2 kcal/mol. It is the most unstable addition product likely due to disruption of resonance in the carbon ring π system caused by its formation. Recrossing back to reactants costs a mere 3.8 kcal/mol.

6-Addition. Three transition state structures for the formation of 6-peroxy-oxepinone radical **(1c)** were also found. Each TS structure has the oxygen molecule approaching from above the ring plane and differs only by a rotation of the O-O bond about the forming C-O bond. All three wavefunctions again have considerable spin contamination, $\langle S^2 \rangle$ values of ~ 1.0, making the TS energies suspect. The ΔG‡(298 K) for the lowest energy TS, with the O-O oxygen bond setting above the C-O ring bond, is 17.5 kcal/mol and an $\langle S^2 \rangle$ value of 1.1. The reaction is endoergic by 9.0 kcal/mol making it the most stable of the peroxyoxepinone radical species. Return to reactants has a ΔG‡(298 K) of 8.5 kcal/mol, the largest of the return barriers.

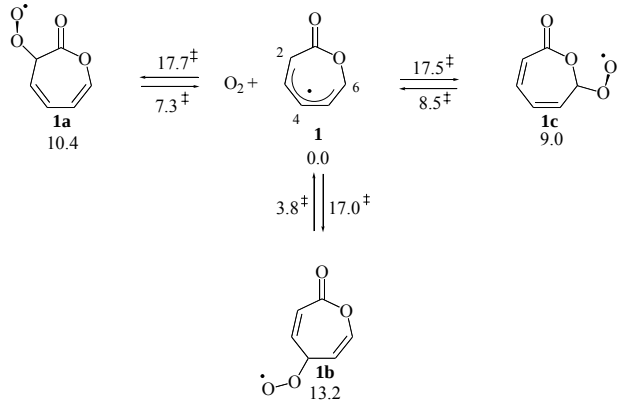

Figure 2. Reaction scheme for the addition of oxygen molecule (^3P) to 2-oxepinoxy radical (1). Energies are B3LYP/6-311+G**//B3LYP/6-31G* ΔG(298 K) relative to O_2 and 2-Oxepinoxy at infinite separation.

Conclusions

Subsequent unimolecular fragmentations emanating from **1a**, **1b**, and **1c** have also been calculated at the same level of theory. Several possible pathways for the decomposition of 2, 4, and 6-peroxyoxepinone radical have been examined at 298, 500, 750, 1000, and 1250 K. Pathways initiated via the formation of a dioxetane, 1,3-peroxy, 1,4 peroxy or hydrogen abstraction via geminal peroxyl radical are competitive with the pathways proposed by Fadden[12] for the unimolecular decomposition of 2-oxepinoxy radical (**1**). The kinetically most favored decomposition pathway at all temperatures involves formation of the 1,4-peroxy intermediate resulting in the formation of furan, CO_2 and formyl radical. Thermodynamically, the most favored pathway forms a 1,2-dioxetanyl intermediate and decomposes to form 1-oxo-pent-2,3-dienyl radical, CO_2 and CO. However, a large entropic penalty is incurred at higher temperatures, thereby making the O_2-addition pathways to the 2-oxepinoxy radical less competitive.

Acknowledgements. We would like to thank the Ohio Supercomputer Center for computing resourses JKM acknowledges support from a GAANN Fellowship.

References

(1) Venkat, C.; Brezinsky, K.; Glassman, I. *Symp. (Int.) Combust., 19th* **1982**, 143-152.
(2) Rotzoll, G. *Int. J. Chem. Kinet.* **1985**, *17*, 637-653.
(3) Frank, P.; Herzler, J.; Just T.; Wahl, C. *Symp. (Int.) Combust., 25th* **1994**, 833-840.
(4) Bermudez, G.; Pfefferle, L. *Combustion and Flame* **1995**, *100*, 41-51.
(5) Chai, Y.; Pfefferle, L. D. *Fuel* **1998**, *77*, 313-320.
(6) Yu, T.; Lin, M. C. *J. Am. Chem. Soc*. **1994**, *116*, 9571-9576.
(7) Norrish, R. G. W.; Taylor, G. W. *Proc. R. Soc*. **1965**, *A234*, 160-177.
(8) Carpenter, B. K. *J. Am. Chem. Soc.* **1993**, *113*, 9806-9807.
(9) Barckholtz, C.; Fadden, M. J.; Hadad, C. M. *J. Phys. Chem. A* **1999**, *103*, 8108-8117.
(10) Fadden, M. J.; Barckholtz, C.; Hadad, C. M. *J. Phys. Chem. A* **2000**, *104*, 3004-3011.
(11) Mebel, A. M.; Lin, M. C. *J. Am. Chem. Soc*. **1994**, *116*, 9577-9584.
(12) Fadden, M. J.; Hadad, C. M. *J. Phys. Chem. A* **2000**, *104*, 8121-8130.

HYDROGEN ATOM CATALYZED ISOMERIZATION OF AROMATIC COMPOUNDS

Mark N. Nimlos[1], Jonathan Filley[2], J. Thomas McKinnon[2]

National Bioenergy Center
National Renewable Energy Laboratory
Golden, Colorado 80401
Department of Chemical Engineering
Colorado School of Mines
Golden, Colorado 80401

Introduction

Isomerization of aromatic compounds plays an important role in the formation of flame-synthesized fullerenes, nanotubes, and in the growth of soot during combustion. During flame synthesis, unfavorable geometries often arise by the proposed zipper mechanism[1,2] in which biaryl molecules zip together losing molecular hydrogen. For instance, the acephenanthrylene molecule, **1**, can zip together to form **3**. At flame temperatures (> 2000 K) the positive entropy of these reactions makes them significant. However, the resulting molecule, **3**, contains adjacent 5-membered rings, which is energetically undesirable. In fullerenes, the 5-membered rings are isolated by 6-membered rings and it is unlikely that a zipper mechanism will lead directly to this type of configuration. An isomerization needs to occur.

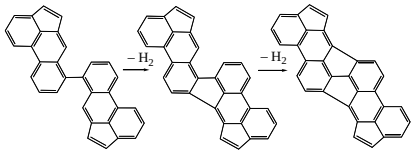

(1)

1 **2** **3**

Fullerene modelers have often invoked the Stone-Wales (SW) rearrangement[2,3] to explain annealing in aromatic compounds. In the simplest example of the SW reaction the 5-membered rings in pyracyclene, **4**, are shifted as shown in eq. 2. This mechanism can be used to isolate 5-membered rings in polycyclic aromatic compounds.

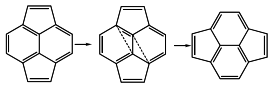

(2)

4

Another interesting annealing reaction is the isomerization of azulene, **5**, to naphthalene, **6**. This reaction may also be important in the zipper mechanism.

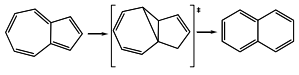

(3)

5 **6**

The calculated barriers for these reactions are fairly high [120 to 130 kcal mol^{-1} for reaction (2) and > 83 kcal mol^{-1} for reaction (3)] which might limit their extent during combustion. We have found that addition of a hydrogen atom to **4** and **5** dramatically reduces the barrier for these reactions and since hydrogen atom is fairly abundant in flames, this catalytic effect may increase the likelihood of these isomerization reactions.

Computational Techniques

The calculations in this study were carried out using the Gaussian 98 suite of programs at the following level: B3LYP/6-31+G(d,p) Local minima and transitions states were found using Berny optimizations. Starting geometries for the transition state optimizations were often located using a potential energy scan, where one internal coordinate was systematically changed while all other coordinates where allowed to relax. The geometry at the calculated maximum of this scan was used as a starting geometry for a TS optimization. Stable structures had only positive vibrational frequencies while transition states had one imaginary frequency. The transition states were confirmed by visual inspection of the imaginary frequency using the Molden visualization package. The transition states were also confirmed using IRC calculations.

Results and Discussion

Stone-Wales

We have considered two mechanisms for the SW reaction in pyracyclene; a two-step mechanism involving cyclopropyl transition states and a cyclobutyl intermediate and one-step mechanism[5] with an sp^3 carbon atom in the transition state. The calculated potential energies for the transition states of these mechanisms are shown in **Figure 1**. Since the product and reactant are the same for this molecule, the two cyclopropyl transition states are necessarily equivalent. As can be seen, the barriers for both of these processes are high (129.8 kcal mol^{-1} for the sp^3 mechanism and 119.3 kcal mol^{-1} for the cyclopropyl mechanism). Furthermore, the level of theory used often underpredicts barrier energies by up to 5 kcal mol^{-1}. These barriers are high enough that other processes, such as C-H bond scissions (*DH* ~ 110 kcal mol^{-1}) will be more likely.

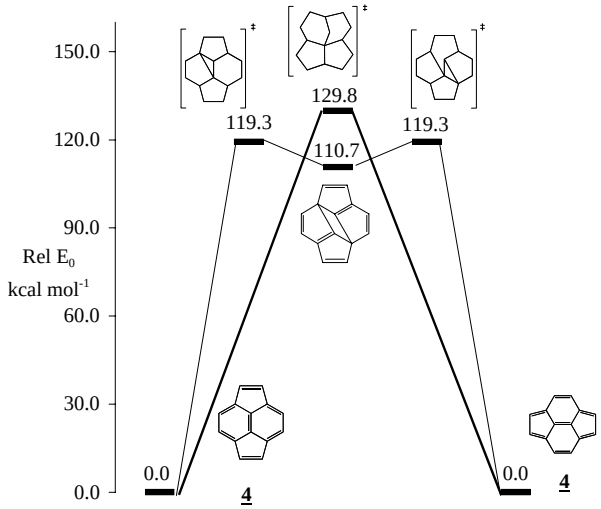

Figure 1. A potential energy plot of the calculated relative energies for the SW reaction in pyracyclene. The energies include the zero point energy.

The addition of a hydrogen atom to the central atom of pyracyclene significantly reduces the reaction barriers for the SW reaction. This is shown in **Figure 2**. As can be seen the relative energy of the cyclopropyl transition state drops from 119.3 kcal mol^{-1} for neat pyracyclene to 66.9 kcal mol^{-1} for H+pyracyclene and the sp^3 transition state dropped from 129.8 kcal mol^{-1} for the neat pyracyclene to 73.3 kcal mol^{-1} for H+pyracyclene. In addition to the lower energy barrier, there is a chemical activation energy that would be available when hydrogen atom adds to pyracyclene. For the molecule shown in **Figure 2** the chemical activation energy is 20.4 kcal mol^{-1}. We have calculated the reaction energetics when a hydrogen atom is added to the external bridge carbon atoms on pyracyclene. The results are shown in Table I. As can be seen,

hydrogen atoms attached to these carbon atoms have a larger chemical activation energy, but have a smaller reduction in the reaction barrier relative to the neat pyracyclene

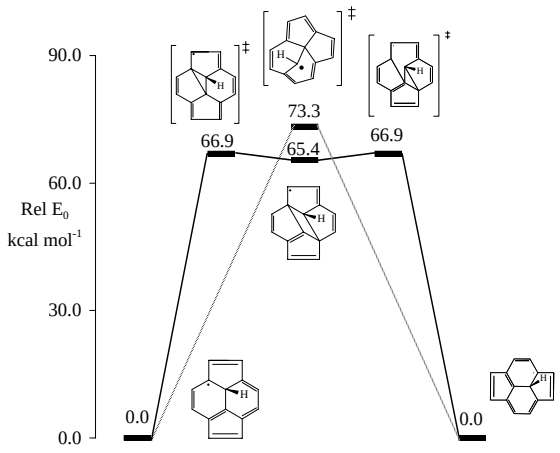

Figure 2. A potential energy plot of the calculated energies for the SW reaction in pyracyclene

Table I Calculated relative energies[a] for SW for pyracyclene and pyracyclene + H atom. (kcal mol^{-1})

	chem act.[b]	sp^3 mech.	cyclopropyl mech.			
React[c]		TS	TS1	c-C4	TS2	Prod.
neat		129.8	119.3	110.7	119.3	0.0
H-C13	20.4	73.3	66.9	65.4	66.9	0.0
H-C9	34.5		105.3	97.4	105.3	0.0
H-C1	54.4		128.0	118.8	125.9	14.6

[a]Includes zero point energy [b]The energy of the adduct relative to the energy of H atom + pyracyclene [c]This shows where the H atom is attached on the pyracyclene. See carbon numbering scheme below:

Azulene/Naphtalene Isomerization

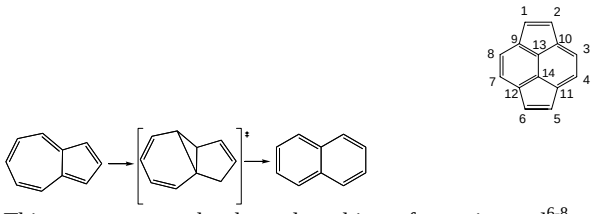

This rearrangement has been the subject of experimental[6-8] and theoretical studies[11]. We find a single transition for the neat molecule with a barrier energy of E_0 = 83.4 kcal mol^{-1}. With the addition of a hydrogen atom to a bridge carbon atom, the energetics changes considerably. **Figure 3** shows a plot of the calculated energies of the intermediates relative to the energy of azulene + H atom. As can be seen, the adduct formed from the addition of H atom to the bridge carbon is –30.9 kcal mol^{-1} lower in energy than the reactants. This chemical activation energy is sufficient to surmount the barriers to naphthalene formation. In this case H atom catalysis makes the isomerization facile.

This mechanism also has an interesting consequence on aromatic formation from the recombination of cyclopentadienyl radical (C_5H_5). It has been proposed that in combustion two cyclopentadienyl radicals can react to form naphthalene by a mechanism which involves two cyclopropyl intermediates. 9,10

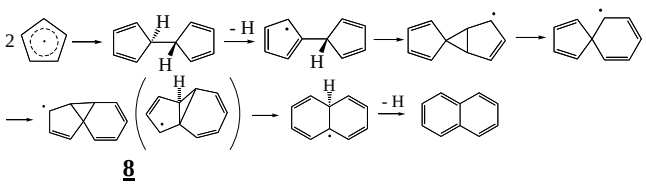

8

The intermediate, **8**, in this mechanism is identical to the cyclopropyl intermediate in the H atom catalyzed transformation of azulene to naphthalene shown in **Figure 3**. Thus, it is possible that the recombination of cyclopentadienyl radicals could lead to the formation of azulene in addition to naphthalene.

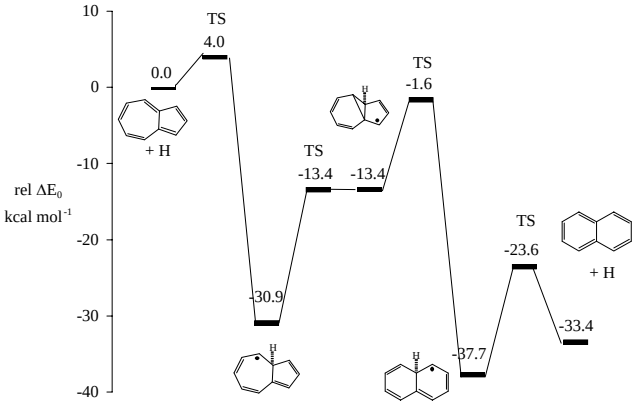

Figure 3. Relative energies of intermediates in the H atom catalyzed isomerization of azulene to naphthalene.

In summary, we have found that rearrangements of 5,6-rings and 5,7-rings in simple compounds that are designed to model more complex rearrangements in fullerenes have barriers that are significantly lowered by the addition of an H-atom to the rearranging framework. The resulting radicals, which are likely to exist in relatively high concentrations due to the high concentrations of H-atoms in flame environments, represent a possible low energy catalytic pathway for the SW and related rearrangements in fullerenes.

Acknowledgment

We would like to acknowledge the National Center for Supercomputer Applications (NCSA Grant # CHE-980028n) for computer time.

References

1. Richter, H.; Howard, J.B. *Prog. Energy Comb. Sci*. **2000**, *26*, 565.
2. Homann, K.H. *Ang. Chem. Int. Ed*. **1998**, *37*, 2435.
3. Stone, A.J.; Wales, D.J. *Chem. Phys. Lett.* **1986**, *128*, 501.
4. Walsh, T.R.; Wales, D.J. *J. Chem. Phys.* **1998**, *109*, 6691.
5. Murry, R.L.; Strout, D.L.; Odom, G.K.; Scuseria, G.E. *Nature* **1993**, *366*, 665**.**
6. Scott, L. T.; Kirms, M. A. *J. Am. Chem. Soc.* **1981**, *103*, 5875-5879.
7. Scott, L. T. *Acc. Chem. Res.* **1982**, *15*, 53-58**.**
8. Alder, R. W.; Whiteside, R. W.; Wittaker, G.; Wilshire, C. *J. Am. Chem. Soc.* **1979**, *101*, 629-632.
9. Melius, C. F.; Colvin, M. E.; Marinov, N. M.; Pitz, W. J.; Senkan, S. M. *26th Symposium on Combustion* 1996, 685-692.
10. Filley J.; McKinnon J.T. *Combust, Flame* **2001**, *124*, 721-723.
11. Alder, R. W.; East, S. P.; Harvey, J. N.; Oakley, M. T. *J. Am. Chem. Soc.* **2003**, *125*, 5375.

COMBINATION AND DISPROPORTIONATION REACTIONS OF ALKYL RADICALS: AN AB INITIO KINETICS STUDY FOR $CH_3 + C_2H_5$

*R. S. Zhu, Z. F. Xu and M. C. Lin**

Department of Chemistry
Emory University
Atlanta, GA 30322

I. Introduction

The kinetically competitive combination and disproportionation of alkyl radicals are important to the global chemistry of hydrocarbon decomposition and combustion processes. The mechanism responsible for these reactions was a subject of much discussions[1-4] after their kinetic data had been measured extensively with the advent of the gas chromatographic technique in the 1950's.

Despite the great advance in ab intio molecular orbital and statistical rate constant calculations in recent years, reliable prediction of the product branching probabilities for the two competitive processes has not been achieved. For example, in a latest paper by Mousavipour and Homayoon[5] published in the course of our preparation for publication of this work, the critical disproportionation process has not been clearly elucidated, the corresponding barrier for this path was predicted to lie between 0.05 and 6.2 kcal/mol by different methods and its rate constant was fitted to experimental data with different energy barriers.

In this work we employed the state-of-the-art computational techniques for both electronic structure and rate constant prediction. Most significantly, the disproportionation reaction, for example, for $CH_3 + C_2H_5$ takes place via a H-bonded CH_3---H--C_2H_4 intermediate, instead of a direct transition state as reported by Mousavipour and Homayoon.[5] This mechanism is expected to be universal for the alkyl-alkyl disproportationation processes as will be demonstrated in the future for the series of the R + R' reactions (where, R = H, CH_3, …; R' = CH_3, C_2H_5,…).

II. Computational Methods

The potential energy surface (PES) was calculated at the G2M (CC2)//B3LYP/6-311+G(3df, 2p) level[6]. Some critical points are also calculated at the CCSD(T)/6-311+G(3df, 2p)//B3LYp/6-311+G(3df, 2p) level. For all the molecular orbital calculations the Gaussian 03[7] and Molpro2002.3[8] programs were used.

The rate constants were computed with microcanonical variational RRKM (Variflex)[9] and ChemRate codes.[10]

III. Results and discuss

A. Potential energy surface (PES) and mechanism

a. Abstraction reactions

$CH_4 + {}^1C_2H_4$ formation. For the direct abstract process, a relatively loose transition state was located at the B3LYP/6-311+G(3df, 2p) level. Because of the importance of the transition state barrier for the prediction of disproportionation rate constant, the barrier height of this transition state was also calculated by other methods. The results show that the barrier is around -1.6 ± 0.5 kcal/mol relative to the reactants. A loose hydrogen-bonding precursor was found to be involved in this process.

Abstraction reactions can also happen on the triplet surfaces to produce $CH_4 + {}^3C_2H_4$, $CH_4 + {}^3CH_3CH$ and ${}^3CH_2 + C_2H_6$ with higher barriers, 15.4, 15.8 and 18.4 kcal/mol, respectively.

b. Association reaction

The interaction of the two unsaturated carbon atoms in CH_3 and C_2H_5 forms association product, C_3H_8. The association energy was predicted to be 89.0 kcal/mol at the G2M (CC2) level.

c. Decomposition of chemically activated C_3H_8

H_2-elimination. The interaction of the two H atoms from the same group of CH_3 or CH_2 and from different groups in $CH_3CH_2CH_3$ will result in H_2 elimination to produce the following different products.

$H_2 + CH_3CCH_3$. The interaction of the two H atoms from the CH_2 group in C_3H_8 eliminates H_2 via a three-member-ring transition state wit a barrier above the reactants by 12.0 kcal/mol and this process has endothermicity by 5.1 kcal/mol.

$H_2 + CH_3CHCH_2$. The are two possibilities to form the products. In the first case, two H atoms, each from the CH_3 and CH_2 groups in $CH_3CH_2CH_3$, form a HHCC four-member-ring transition state with barrier above the reactants by 20.6 kcal/mol. For the second case, H_2 eliminates from one of the CH_3 groups, with simultaneously, one of the H atoms in the CH_2 group migrating to the terminal C to form $H_2 + CH_3CHCH_2$. This process has 14.8 kcal/mol barrier. The exothermicity for the reaction is 61.3 kcal/mol.

$H_2 + cyc\text{-}C_3H_6$. In this channel, the two C-H bonds in CH_3 groups of $CH_3CH_2CH_3$ intermediate are lengthening to form a H-H bond, meanwhile, the two C atoms from the CH_3 groups are connecting to form a C-C bond. Although this is an exothermic process with exothermicity of 52.7 kcal/mol, it has a much higher barrier, 58.9 kcal/mol above the reactants, it will not be kinetically important.

CH_2 elimination. In this channel, one of the H atoms in the CH_3 group of $CH_3CH_2CH_3$ can migrate to the CH_2 group via a three-member-ring transition state to form a loose complex with a barrier of 14.5 kcal/mol above the reactants. The complex lies above the reactants by 11.7 kcal/mol, which further dissociates to produce ${}^1CH_2 + C_2H_6$ with endothermicity of 15.1 kcal/mol.

CH_4-elimination. There are two possible ways to eliminate CH_4 from $CH_3CH_2CH_3$.

$CH_4 + CH_2CH_2$. In this channel, one H atom migrates from one CH_3 groups to the other CH_3 group, simultaneously, one of the C-C bond is breaking via a four-member-ring transition state to form the products with a barrier lying above the reactants by 23.7 kcal/mol. Apparently, this channel is not competitive with the direct abstraction one as discussed in the previous section.

CH_4 + CH_3CH. This path involves one H atom in the CH_2 group transferring to one of the CH_3 group via a three-center transition state to form a loose complex which dissociates to produce products $CH_4 + CH_3CH$. The transition state, complex and products lie above the reactants by 5.7, 2.4 and 2.8 kcal/mol, respectively.

B. Rate constant calculations

The rate constants for those channels with barriers less than 15.0 kcal have been calculated. The results show that the dominant channel in the temperature range of 200 – 3000 K is C_3H_8 formation. The predicated rate constants for association, dissociation processes and the ratio of combination/disproportionation are in reasonable agreement with available values.

IV. Conclusions

Complete potential energy surface (PES) for the reaction of $CH_3 + C_2H_5$ has been calculated at the G2M (CC2)//B3LYP/6-311+G(3df, 2p) level. Rate constant calculations show that formation of C_3H_8 is dominant in the temperature range of 200 ~ 3000 K. Predicted rates reasonably agree with experimental data.

Acknowledgement

This work is sponsored by DOE. Acknowledgment is also made to the Cherry L. Emerson Center of Emory University for the use of its resources, which are in part supported by a National Science Foundation grant (CHE-0079627) and an IBM Shared University Research Award.

References

(1) Konar, R. S. *Int. J. Chem. Kinet.* **1970**, *2 (5)*, 419.
(2) Laidler, K. J. *Int. J. Chem. Kinet.* **1971**, *3*, 377.
(3) Konar, R. S. *Int. J. Chem. Kinet.* **1971**, *3*, 379.
(4) Dannenberg, J. J. and Baer, B., *J. Am. Chem. Soc.* **1987**, *109*, 292.
(5) Mousavipour, S. H.; Homayoon, Z. *J. Phys. Chem. A* **2003**, *107*, 8566.
(6) Mebel, A. M.; Morokuma, K.; Lin, M. C. *J. Chem. Phys.* **1995**, *103*,7414.
(7) M. J. Frisch, M. J. et al., *GAUSSIAN 03, REVISION B.0*1; Gaussian, Inc., Pittsburgh PA, **2003**.
(8) MOLPRO is a package of *ab initio* programs written by H.-J. Werner et al.
(9) Klippenstein, S. J. ; Wagner, A. F.; Dunbar, R. C. ; Wardlaw, D. M. and Robertson, S. H. VARIFLEX: VERSION **1.00**, **1999**.
(10) Mokrushin, V.; Bedanov, V.; Tsang, W.; Zachariah, M. R.; Knyazev, V. D. *ChemRate, Version 1.19*; National Institute of Standards and Technology: Gaithersburg, MD 20899, **2002.**

Ab Initio quantum chemical studies of hydrogen abstraction reactions of hydrocarbons

David W. Ewing and Michael J. Manka

Department of Chemistry, John Carroll University
Cleveland, OH 44118 E-mail: ewing@jcu.edu

Alchemy Software, 1610 Clearglades Drive
Wesley Chapel, FL 33543-5759
E-mail: mjmanka@chemicalsoft.com

Introduction

The accurate prediction of kinetic parameters of hydrogen abstraction reactions of hydrocarbons is of fundamental importance to the kinetic modeling of the commercial processing of natural gas, petroleum, and its derivatives[1], as well as their combustion reactions.[2,3] Results of *ab initio* calculations will be reported here for the reactions $C_2H_6 + H\bullet \rightarrow C_2H_5\bullet + H_2$ and $C_2H_6 + CH_3\bullet \rightarrow C_2H_5\bullet + CH_4$. Reactions of propane will be also discussed in the talk.

Methods

Structures and vibrational frequencies were calculated at the HF/DZP level of theory. Activation energies were obtained at various levels of theory, the highest being MP4/pVTZ//HF/DZP. Morokuma's ONIOM method[4] was also used to find activation energies, using a two layer strategy. The abstracting species, the carbon from which the hydrogen atom was being abstracted, and the other hydrogens attached to that carbon were in the high level layer; all other atoms were in the low level layer. Calculations were done using Gaussian 98[5] running on PC workstations.

Results and Discussion

Previous calculations have shown that accurate activation energies can be obtained for reactions of this type from structures calculated at the HF/DZP level, as long as correlated calculations are done, preferably with a large basis set, for the energetics.[6] Figure 1 gives the calculated HF/DZP structures. Subsequent vibrational frequency calculations yielded only one imaginary frequency for each reaction, the normal modes of which were along the reaction coordinate.

Table 1 gives activation energies at various levels of theory and compares these to experiment. The ONIOM results are seen to give activation energies within 1-2 kcal/mol. For comparison the MP4/pVTZ//HF/DZP activation energy for the reaction of $C_2H_6 + H\bullet$ (without using ONIOM) was found to be 11.2 kcal/mol, less than one kcal/mol closer to the experimental value. This latter calculation took nearly 7 hours on a Pentium II PC and used 900 mbytes of scratch disk, whereas the ONIOM calculation only took 19 minutes and 200 Mbytes.

Table 1. Activation Energies (kcal/mol)

Level of Theory	$C_2H_6 + H\bullet$	$C_2H_6 + CH_3\bullet$
HF/DZP	20.0	29.6
MP2/DZP//HF/DZP	15.1	16.7
MP4/DZP//HF/DZP	13.8	17.2
ONIOM*	11.8	16.4
Experiment[7]	10.8	14-15

*MP4/pVTZ for the high level; HF/DZP for the low level

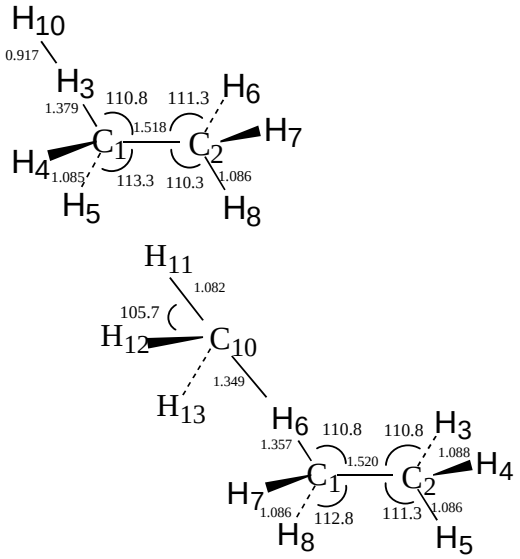

Figure 1. HF/DZP transition state structures for $C_2H_6 + H\bullet \rightarrow C_2H_5\bullet + H_2$ and $C_2H_6 + CH_3\bullet \rightarrow C_2H_5\bullet + CH_4$. Bond lengths are in Å and bond angles are in degrees.

Transition State Theory Calculations

Reaction rate coefficients were calculated using transition state theory (TST) and results from the *ab initio* calculations shown in Table 1. Corrections for barrier tunneling were determined using parabola and the Eckart potential approximations. These calculations were performed using the TS Rate program. The evaluated rate several approximations, including Wigner's, Bell's truncated coefficients for the two hydrogen abstraction reactions are presented in Figures 2 and 3, respectively. The calculated rate coefficient increases with the application of the barrier tunneling corrections. The Wigner approximation, which is applicable for small tunneling corrections near the top of the barrier and does not depend directly on the barrier height, yields the smallest correction and is considered to be inadequate where significant tunneling occurs. Similarly, the truncated parabola, which approximates the barrier as a symmetric parabola, also may only adequately describes the barrier near its top. This correction method is also only applicable for small tunneling corrections. It also appears to grossly over-estimate the tunneling correction where significant tunneling is likely to occur, i.e. at lower temperatures. The Eckart potential function provides a better description of the barrier and the tunneling correction factors are intermediate between the Wigner and Bell approximation corrections.

The calculated results were fitted to the three parameter modified Arrhenius equation to obtain a better fit of the results. The rate coefficient expression has the form

$$\log(k, \mathrm{M^{-1}s^{-1}}) = A - \frac{B}{T} + C\log(T) \qquad (1)$$

where T is the temperature in K. The parameters for the rate expressions for the reactions $C_2H_6 + H\bullet$ and $C_2H_6 + CH_3\bullet$ are given below in Tables 2 and 3, respectively.

These rate coefficient results, except for results obtained using the Bell correction method, were compared to available data from the literature. This comparison is shown in Figures 4 and 5 for the reactions $C_2H_6 + H\bullet$ and $C_2H_6 + CH_3\bullet$, respectively. The calculated results are in better agreement with literature data for the reaction $H\bullet + C_2H_6$ than for $CH_3\bullet + C_2H_6$.

Table 2. Rate Expression Parameters for C_2H_6 + H•

Correction Method	A	B	C
Uncorrected	5.161	2341	1.96
Wigner	5.250	2090	1.90
Bell	-13.920	-556	7.37
Eckart Potential	-7.269	413	5.49

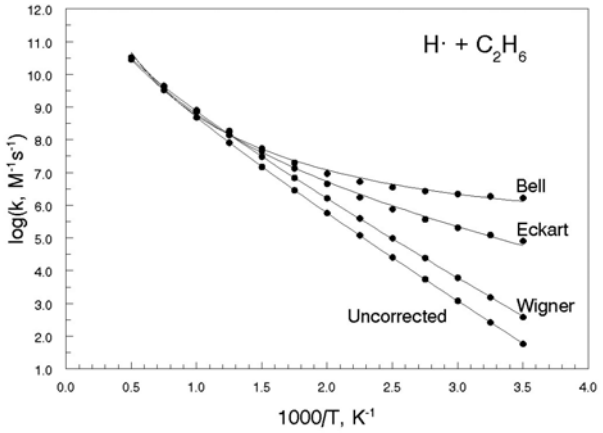

Figure 2. Plot of calculated transition state theory rate coefficients versus temperature for H• + C_2H_6. Corrections for barrier tunneling employing the Wigner, Bell and Eckart approximation methods applied to the uncorrected results.

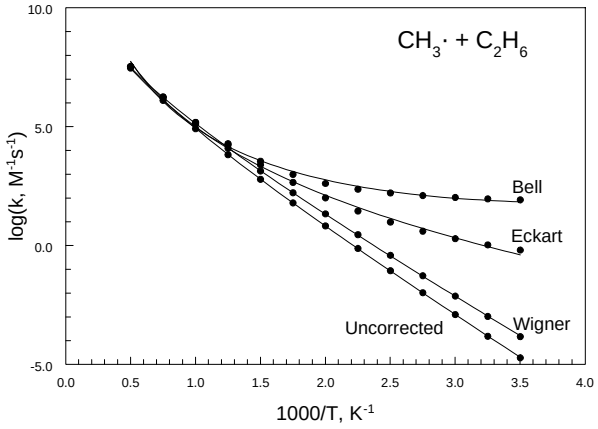

Figure 3. Plot of calculated transition state theory rate coefficients versus temperature for CH_3• + C_2H_6. Corrections for barrier tunneling employing the Wigner, Bell and Eckart approximation methods applied to the uncorrected results.

Table 3. Rate Expression Parameters for C_2H_6 + CH_3•

Correction Method	A	B	C
Uncorrected	-1.173	3178	3.09
Wigner	-0.819	2927	2.96
Bell	-30.205	-1217	11.31
Eckart Potential	-20.703	270	8.66

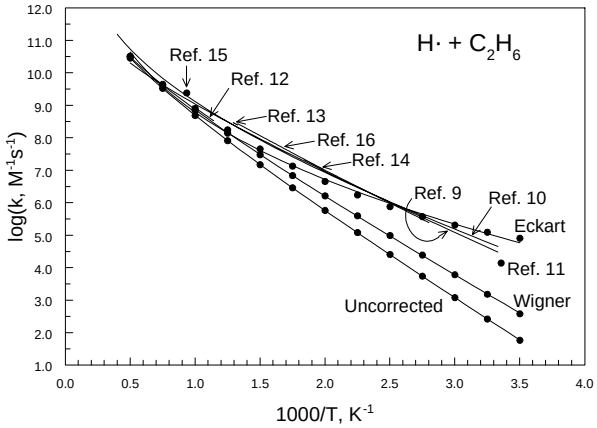

Figure 4. Comparison of calculated transition state theory rate coefficients versus temperature for H• + C_2H_6 and literature data.

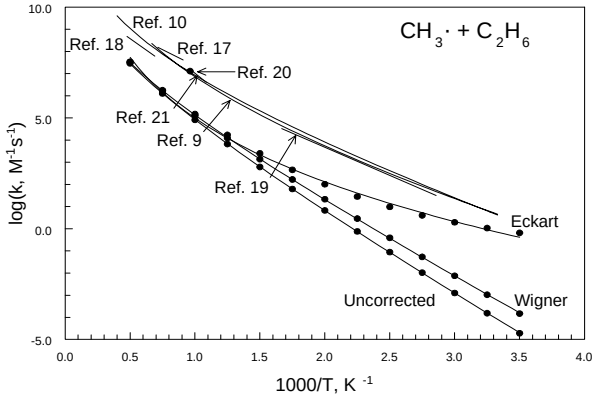

Figure 5. Comparison of calculated transition state theory rate coefficients versus temperature for CH_3• + C_2H_6 and literature data.

References

(1) *Pyrolysis: Theory and Industrial Practice*; Albright, L.F., Crynes, B.L, Corcoran, W.H., Eds.; Academic Press: New York, 1982.

(2) Hucknall,D.J. Chemistry of Hydrocarbon Combustion; Chapman and Hall: London, 1985.

(3) Warnatz, J. In Combustion Chemistry; Gradiner, W.C., Ed.; Springer-Verlag: NewYork, 1984.

(4) Svensson, M.; Humbel, S.; Morokuma, K. *J. Chem. Phys.* **1996**, *105*, 3654.

(5) Gaussian 98 (Rev. A.9), Gaussian, Inc.: Pittsburgh PA, 1998.

(6) Litwinowicz, J.A.; Ewing, D.W.; Jurisevic, S.; Manka M.J. *J. Phys. Chem.* ***1995***, *99*, 9709.

(7) Baulch, D.L.; Cobos, C.J.; Cox, R.A.; Esser, C.; Frank P.; Just, Th.; Kerr, J.A.; Piling, M.J.; Troe, J.; Walker, R.W.; Warnatz, J., *J. Phys. Chem.Ref. Data*, **1992**, *21*, 411.

Methyl Radical and Shift Reactions with Aliphatic and Aromatic Hydrocarbons: Thermochemical Properties, Reaction Paths and Kinetic Parameters

L. Rutz[1] and H. Bockhorn[1] and J. W. Bozzelli[2]

[1]Institute for Chemical Technology, University of Karlsruhe, Karlsruhe, Germany
[2]Department of Chemistry, New Jersey Institute of Technology, Newark, USA

Introduction

The study of soot formation under moderate to low (ca. 1100K), temperatures and pyrolytic conditions, no oxygen, with small hydrocarbons like acetylene, ethylene, methane, propane or propene in flow reactors is of interest for nanotube formation, and for many solid carbon products such as brake pads and carbon black, … etc. A fundamental understanding of soot formation chemistry is important to reducing soot emissions from vehicles and other combustion sources.

Our attempts to model the experimental data in such systems and in our laboratories utilized soot formation models from well established combustion mechanisms. We quickly realized that there are no mechanisms in the literature that serve to model the soot formation experiment data at the lower temperature conditions. Kinetic and sensitivity analysis on the mechanisms shows that the first step - that to break the first carbon - hydrogen or carbon - carbon bond is the limiting in these literature mechanisms.

We have, therefore started a search for alternative ways to generate / initiate radicals to improve the mechanisms. In this symposium we present two new initiation mechanisms and this paper focuses on one of these reactions - that of methyl radical addition to π bonds and substitution in SP^3 Bonds of carbon to form C2 adducts which further initiate the chain and undergo further reaction to molecular weight growth.

Methyl radical, CH_3 is an active species that is well known in combustion research. New results show that it can also play a role in CVD and CVI processes. We have investigated literature and performed computational chemistry calculations on addition and substitution reactions of methyl radical. Two substitution reactions are evaluated: one on aromatic and one on aliphatic systems. One reaction, addition to a p bond of an aromatic or olefin system, occurs via a relatively low energy barrier of only 15 kcal/mole. The second reaction, substitution in an aliphatic at a moderate energy barrier of only 50 kcal/mole, compared to bond cleavage reactions that require energies of about 100 kcal/mole. While both of these reactions are well known in gas phase kinetics, it is not clear that they have been implemented in mechanisms for evaluation of their effects. Soot formation in pyrolysis and combustion conditions occurs at sufficiently high temperatures that the substitution reaction could play a role.

Calculation Methods

Thermodynamic Properties. Geometry optimizations and frequency calculations for reactants, intermediates, and transition states from vinylidene insertion reactions are performed using several Density Functional (DFT) Methods (B3LYP/6-31G(d,p), B3LYP/6-311G(d,p), B3LYP/6-311+G(d,p), B3LYP/6-311++g(3df,2p), B3LYP/SVP and B3LYP/TZV) levels of theory in the Gaussian 98 program suite. The ab initio calculations, MP2/fc-6-311G(d,p), MP2/full-6-311G(d,p) and G3MP2, are also used to improve our calculation level and validate the DFT results. The optimized geometry parameters with B3LYP/6-31G(d,p) level are used to obtain total electronic energies in B3LYP/6-31G(d,p), CBS-lq//B3LYP/6-31G(d,p) single point calculations and the CBSQ//B3LYP/6-31G(d,p) composite method.

Potential Barriers for intramolecular rotation about the carbon-carbon bonds in unsaturated and polycyclic aromatic hydrocarbons are analyzed versus torsional angle using B3LYP/6-31G(d,p). Total energies are corrected by ZPVE, which are scaled by the recommended values by Scott et al.[1] Thermal correction is taken into account using structures and vibrations determined at several of the calculation levels. Transition state geometries are identified by the existence of only one imaginary frequency in the normal mode coordinate analysis, evaluation of the TS geometry, the reaction coordinate vibrational motion and an intrinsic reaction coordinate analyses.

Enthalpies of formation ($\Delta H_f^\circ{}_{298}$) are estimated using total energies and calculated $\Delta H_{rxn}^\circ{}_{298}$ with several isodesmic, or group balance working reactions on each species. The calculated $\Delta H_{rxn}^\circ{}_{298}$ and known $\Delta H_f^\circ{}_{298}$ of reference species are utilized to estimate $\Delta H_f^\circ{}_{298}$ of the target molecules in each of the reaction schemes. $\Delta H_f^\circ{}_{298}$ for the reference species comes from literature thermodynamic properties.

Contributions of vibration, translation, and external rotation to entropies and heat capacities are calculated by statistical mechanics based on the scaled vibrational frequencies and moments of inertia from the DFT optimized structures.

The torsion frequencies are omitted in calculation of $S^\circ{}_{298}$ and Cp(T)'s, and their contributions are replaced with values from analysis of the internal rotations. Contributions from hindered rotors to $S^\circ{}_{298}$ and Cp(T)'s are determined by solving the Schrödinger equation with free rotor wave functions and direct integration over energy levels of the intramolecular rotation potential curves which are represented by a truncated Fourier series expansion. The contributions from optical isomers and spin degeneracy of unpaired electrons are incorporated in S values.

Results - Thermochemical Data. The ($\Delta H_f^\circ{}_{298}$ for reactants, intermediate and products are calculated using total energies and isodesmic reactions with group balance if possible. The ($\Delta H_f^\circ{}_{298}$ values for transition states are calculated from the ($\Delta H_f^\circ{}_{298}$ values of reactants plus reaction enthalpy. Thermodynamic parameters ($\Delta H_f^\circ{}_{298}$, $S^\circ{}_{298}$ and Cp(300) to Cp (1500) for species in the reaction schemes are listed.

Kinetic Properties. Unimolecular dissociation and isomerization reactions of the chemically activated and stabilized adducts resulting from addition or combination reactions are analyzed by first constructing potential energy diagrams for the reaction system. DFT and ab initio calculations are used to calculate transition state structures and energy for isomerization, beta scission, and dissociation reactions. The enthalpies and entropies are used with conventional transition state theory to obtain high pressure limit rate constants (k_∞) as function of temperature. Nonlinear Arrhenius effects resulting from changes in the thermochemical properties of the respective transition state relative to adduct with temperature are incorporated using a two parameter Arrhenius preexponential factor (A, n) in AT^n. Branching ratios of the energized adduct to stabilization or various product channels are then calculated using multifrequency QRRK analysis for k(E)[2,3] with the steady-state assumption on the energized adduct(s). The QRRK calculation are used to evaluate energy dependent rate constants, k(E), of the energized adduct to the various channels for bimolecular chemical activation reaction systems; they include equilibrium in isomerization reactions. The QRRK / Master equation analysis described by Gilbert[4], Chang et al.[5] and Sheng et al.[6] is shown to yield reasonable results and provides a framework by which the effects of temperature

and pressure can be evaluated in complex reaction systems. The QRRK code utilizes a reduced set of three vibration frequencies which accurately reproduce the adduct heat capacity and include one external rotation in calculation of density of states F(E)/Q. The master equation analysis for falloff uses a 0.3 to 0.5 kcal energy grain to obtain rate constants as a function of temperature and pressure for chemical activation and dissociation reactions. (ΔE)°down of 630 cal/mol is used for master equation analysis as argon is the third body.

Results and Discussion - Reaction Paths, Barriers

One of our objectives is to show a direct reaction path that leads from methyl radicals, CH_3, over aliphatic hydrocarbons to aromatic systems. Therefore we observe some partly well know reactions and there transition states to build up a reaction path for the molecular weight growth[7].

Incipient with a substitution reaction of methyl radical with methane ethane and hydrogen will be formed. This transition state has a barrier of 51.24 kcal/mol and is lower than the bond dissociation in methane with 104 kcal/mol. In the next step CH_3 interacts with ethane to abstract a hydrogen and C_2H_5 and CH_4 is build over an activation barrier of ca. 14 kcal/mol.

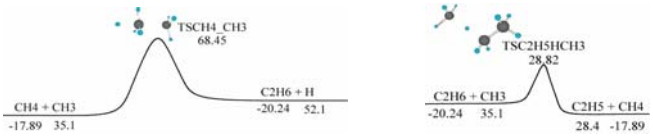

The ethyl radical now can loose second hydrogen and our first unsaturated species is form. This takes 37,77 kcal/mol.

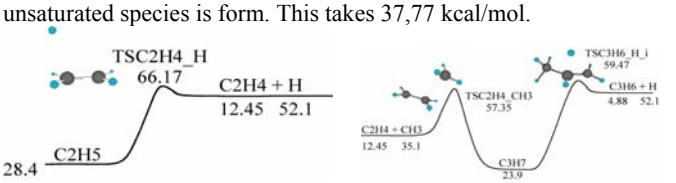

An additional methyl radical reacts now with ethylene and produce n-propyl radical which directly can loose a hydrogen atom and forms propene. The barrier for these are 9.8 respectively 35,57 kcal/mol. Furthermore C_3H_6 can interact with methyl in two different possibilities. One is to generate 1-butene over a H-atom substitution with a barrier of 52,24 kcal/mol. A second route leads over a quite low transition state with 1,59 kcal/mol to the allyl radical while CH_4 is produced.

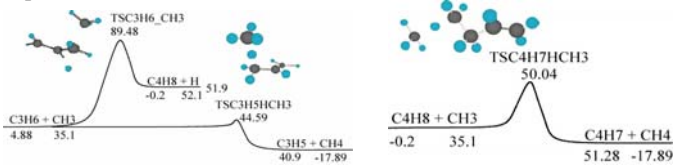

1-butene can follow these recur process and the production of but-3-en-1-yl radical is conceivable. The necessary activation energy will be 15,14 kcal/mol. The abstraction of a hydrogen atom from C_4H_7 take us to next higher homolog unsaturated hydrocarbon, 1,3-Butadiene.

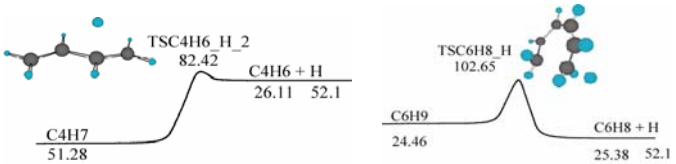

Just as in the previous TST we found a 31,14 kcal/mol barrier. The following transition state shows the internal substitution of a hydrogen in z,z-2,4-Hexadien-1-yl. The barrier is with 78,19 kcal/mol lower than the methane bond energy with 104 kcal/mol.

After the formation of this cyclical hydrocarbon it is an easy exercise to make use of the introduced reaction pattern. 1,3-Cyclhexadiene will be attacked by CH_3 and loose one H atom (8.56 kcal/mol barrier).

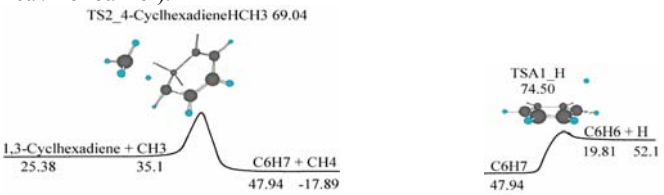

The activation energy to loose the second hydrogen and generate the first aromatic ring is 26.56 kcal/mol. Additional CH_3 form with benzene 2-Methyl-1,4-cyclohexadienyl a subsequently toluene (12.4/43.47 kcal/mol).

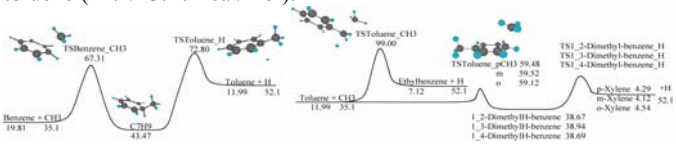

The next methyl radicals can react in the following with the aliphatic or the aromatic part of toluene, which lead to a molecular weight growth on an aliphatic chain or a multi substitution of the ring.

In our study of CH_3 reactions we also analysis shift reactions to explain the formation of big graphite layers and the selective growth on the edge. In a similar pattern we start to look for 1,2-CH_3-shift reactions on small molecules till we end up with a shift reaction on top of an unsaturated ring system.

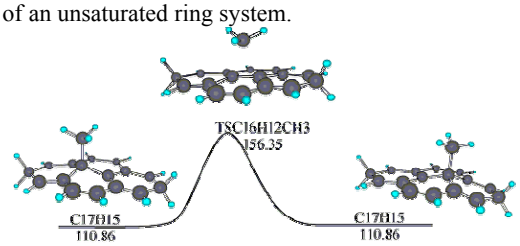

The transition states of this position change are as well investigated as the previous addition of methyl on the surface.

Conclusions

Thermodynamic properties of addition, elimination, substitution and shift reactions in the methyl system were determined by ab initio and density functional calculations. Entropies ($S°_{298}$) and heat capacities (Cp(T)) are also determined, with inclusion of internal rotor contributions. Reaction paths and kinetics are analyzed on methyl reaction system using QRRK for k(E) and master equation for falloff.

Acknowledgement. This work was financially supported by the Deutsche Forschungsgemeinschaft (SFB 551, 'Kohlenstoff aus der Gasphase: Elementarreaktionen, Strukturen, Werkstoffe').

References

[1] Scott, A. P.; Radom, L. *J. Phys. Chem.* **1996**, *100*, 16502
[2] Ritter, E. R.; Bozzelli, J. W. *International Journal of Chemical Kinetics* **1991**, *23*, 767.
[3] Lay, T. H.; Bozzelli, J. W.; Dean, A. M.; Ritter, E. R. *J. Phys. Chem.* **1995**, *99*, 14514.
[4] Gilbert, R. G.; Luther, K.; Troe, J. *Ber. Bunsen. Phys. Chem.* **1983**, *87*, 169.
[5] Chang, A. Y.; Bozzelli, J. W.; Dean, A. M. *Zeitschrift für Physikalische Chemie (München)* **2000**, *214*, 1533.
[6] Sheng, C. Y.; Bozzelli, J. W.; Dean, A. M.; Chang, A. Y. *Journal of Physical Chemistry A* **2002**, *106*, 7276.
[7] Tokmakov, I. V.; Lin M.C., *Int. J. Chem. Kinet*. **2001** 33, 633-653.

Theoretical Study on the Mechanism of $Ni(d^{10}\,{}^1S)+CO_2+3H_2 \rightarrow NiO+CH_4+H_2O$ Reaction

Changwei Hu[1], *Song Qin*[1], *Anmin Tian*[1], *Ning-Bew Wong*[2]

[1]Sichuan Key Laboratory of Green Chemistry and Technology, College of Chemistry, Sichuan University, Chengdu, 610064, China
[2]Department of Biology and Chemistry, City University of Hong Kong, Kowloon, HK

Introduction

Ni-based catalyst is very effective in CO_2 hydrogenation, and its reaction mechanism therefore represents a research topic of great interest[1-3]. Some experimental investigations provide evidences for the formation of adsorbed surface acid species in CO_2 hydrogenation on Ni-based catalysts[4,5]. However, no theoretical study regarding co-interaction of H_2 molecule and CO_2 molecule with Ni atom is available so far to our knowledge. It is shown recently, density functional methods yield reasonable molecular geometries at a relatively low computational cost for transition metal system[6-8]. In present work, the co-interaction of H_2 and CO_2 with Ni is studied by using DTF method in order to find possible reaction intermediates and reaction path in CO_2 hydrogenation on Ni-based catalyst.

Computational Details

Full geometry optimizations and ZPE corrected energies of all intermediates and transition states in the above reaction were performed at B3LYP/6-311+G(2d,2p) level using Gaussian 98 programs. The intrinsic reaction coordination (IRC) method is used to track and verify the minimum energy paths from intermediates to intermediates via transition states.

Results and Discussion

The optimized geometries of various species along the predicted reaction path of the titled reaction and their corresponding ZPE corrected relative energies are shown in **Figure 1**.

Our predicted reaction path can be divided into three stages as the following:

1. $CO_2 + H_2 + Ni(d^{101}S) \rightarrow H_2\text{-}NiCO_2 \rightarrow TS1 \rightarrow HNiCOOH \rightarrow TS3 \rightarrow O\text{-}NiCHOH$
2. $O\text{-}NiCHOH + H_2 \rightarrow H_2\text{-}NiOCHOH \rightarrow TS4 \rightarrow HO\text{-}HNiCHOH \rightarrow TS5 \rightarrow H_2O\text{-}NiCHOH \rightarrow NiCHOH + H_2O$
3. $NiCHOH + H_2 \rightarrow H_2\text{-}NiCHOH \rightarrow TS6 \rightarrow H_2\text{-}NiCHOH' \rightarrow TS7 \rightarrow HNiCH_2OH \rightarrow TS8 \rightarrow HNiCH_2OH' \rightarrow TS9 \rightarrow HONiCH_3 \rightarrow TS10 \rightarrow ONiHCH_3 \rightarrow TS11 \rightarrow ONi\text{-}CH_4 \rightarrow CH_4 + NiO$

In stage 1, reactants H_2 and CO_2 molecules first co-interact with the Ni center with formation the precursor complex H_2-$NiCO_2$ before proceeding to transition state. The calculation shows that, for H_2-$NiCO_2$ species, H_2 is undissotiatively interacted with Ni atom and Ni-CO_2 moiety is very close to the singlet η^2_{co} complex which have been found to be the most stable form in four possible different $Ni(CO_2)$ complex modes[9]. The calculated energies place this species 51.0kJ mol^{-1} lower than that of the free H_2 and η^2_{co} mode of $NiCO_2$ complex, which means that the H_2-$NiCO_2$ complex may be a possible intermediate in CO_2 hydrogenation involving Ni atom. From H_2-$NiCO_2$ complex, the reaction proceeds to form intermediate HNiCOOH in which -COOH fragment is much similar to carboxyl. From intermediate HNiCOOH the reaction continues to form intermediate Ni-HCOOH whose HCOOH moiety were very close to formic acid molecule. The above results indicate that the predicted reaction stage 1 involves the formation of adsorbed formic acid intermediates and leads to the cleavage of C-O bond of CO_2 molecule. This is in accordance with previous experimental investigations which provided evidences that the CO_2 hydrogenation on Ni catalyst involves the formation of adsorbed formic acid.[10]

In stage 2, another H_2 molecule attaches the O-NiCHOH species with formation of the H_2-NiOCHOH complex. For this species, H_2 is undissotiatively interacted with Ni. From this complex, the reaction is predicted to the formation of intermediate HO-HNiCHOH in which H-H bond of H_2 molecule is broken. From intermediate HO-HNiCHOH, the reaction continues to proceed and forms intermediate H_2O-NiCHOH in which the adsorbed water molecule forms. The H_2O-NiCHOH may lose one water molecule and completes this reaction stage with the formation of NiCHOH species.

In stage 3, another H_2 molecule continues to attach the NiCHOH species and forms H_2-NiCHOH complex. In this complex, H_2 molecule is still undissotiatively interacted with Ni atom. From this species, the reaction proceeds via a series of transition states and corresponding intermediates to form the intermediates $HNiCH_2OH$ in which the H-H bond of H_2 molecule is broken and the CH_2OH moiety forms. From this species, the reaction continues to proceed and eventually forms the $ONi\text{-}CH_4$ complex which contains an adsorbed methane molecule. This intermediate may lose the adsorbed methane molecule and completes the whole reaction with formation of NiO and CH_4 products.

The overall exothermicity of this reaction is calculated to be 61.1kJmol^{-1}. B3LYP/6-311+G(2d,2p) level gives the energy between intermediate Ni-HCOOH and transition state TS3 is 246.0kJ mol^{-1} which is the largerest in the whole predicted reaction path, the rate-controlling step therefore may be considered to be from intermediate Ni-HCOOH to intermediate O-NiCHOH via TS3.

Conclusion

A detailed reaction mechanism of CO_2 hydrogenation on Ni atom is carried out at B3LYP/6-311+G(2d,2p) level. The calculation predicts that this reaction involves the formation of some sorts of adsorbed formic acid complex, the exothermicity of overall reaction is calculated to be about 61.1kJ mol^{-1}, and the activation energy is calculated to be about 246.0kJ mol^{-1}. The rate-controlling step is predicted to be the step from intermediate Ni-HCOOH to intermediate O-NiCHOH via TS3.

Acknowledgments. This work is financially supported by the Key Project of National Fundamental Research and Development of China (973) (*No.* G1999022407), NNSF (*No.* 20243006), the Special Research Foundation of Doctoral Education of China (*No.* 2000061028), the Foundation of Science and Technology of Sichuan Province (*No.* 200018-16) and TRAPOYT(2002).

References

1. Nerlov J.; Chorkendorff I., *J. Catal*. **1999**, *181*, 271.
2. Tsuji M.; Kodama T.; Yoshida T.; Kitayama Y.; Tamaura Y., *J. Catal.* **1996**, *164,* 315.
3. Alexander M. M.; Hwang D.-Y., *J. Phys Chem.* **2000**, *104,* 11622.
4. Schild C.; Wokaun A.; Kaepper R. A.; Bauker A., *J. Phys.Chem*. **1991**, *95*, 6341
5. Fujita S.-I.; Nakamura M.; Doi T., *Appl Cata.l A: General.* **1993**, *104*, 87
6. Luis R.-S.; Mariona S.; Vicenc B., *J. Chem. Phys.* **1996**, *22*, 105.
7. Fornier R., *J Chem. Phys*. **1993**, *98*, 8041.
8. Barone V.; Adamo C., *J. Phys. Chem*. **1996**, *100*, 2094
9. Wang J.; Johnson B. G.; Boyd R. J., Eriksson L. A., *J. Phys. Chem*. **1996**, *100*, 63
10. Schild C.; Wokaun A., *J. Phys. Chem.,* **1991** *95*(16) *6341*

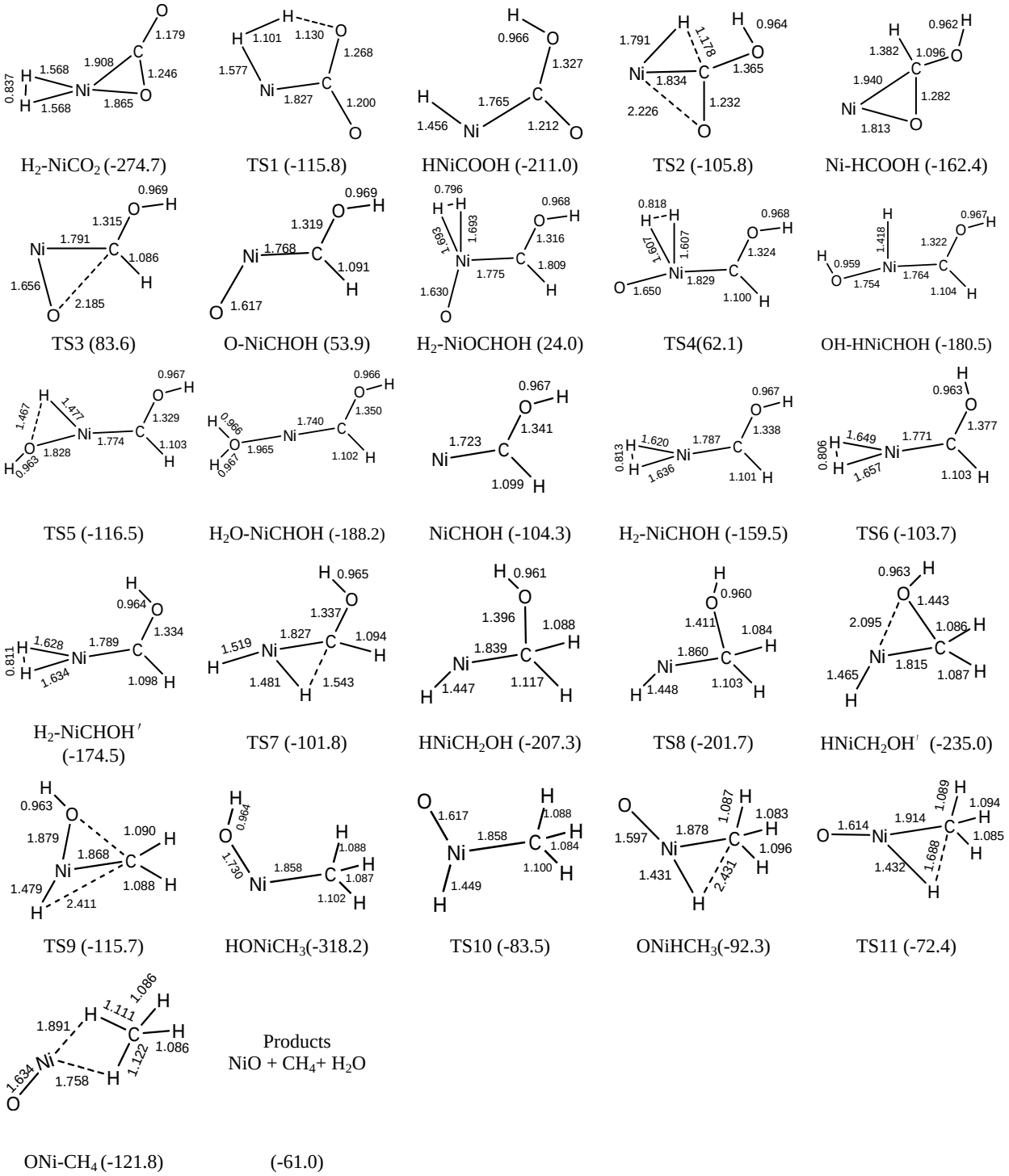

Figure 1. Geometries of all species obtained at B3LYP/6-311+G(2d,2p) level along the Ni(d^{10} ^{1}S)+CO_2+3H_2→ NiO+CH_4+H_2O reaction. Bond lengths are in Å, and the ZPE corrected relative energies with respected to reactant [Ni(d^{10} ^{1}S)+CO_2+3H_2] given in kJ mol^{-1} are in parentheses.